
# Asymptotic analysis of the damping response of a structure

Postgraduate Program: Computational Mechanics

Anastasios Vafeidis

Advisor: Prof. Dimitris Goussis

Mechanics Section
School of Applied Mathematical and Physical Science
National Technical University of Athens

Athens
October 2016

# Abstract

To building model is consisted of damped harmonic oscillation equations which are second order ordinary differential equation. The study and model reduction of building models is important because buildings is the most popular structure and their accurate simulation of their response requires dense discretization and leads to large-scale systems. Here, the fast/slow dynamics of the building models will be analysed, by employing the *Computational Singular Perturbation (CSP)* algorithm to an 8 floor building. Given a multi-scale (stiff) $N$-dimension system of ordinary differential equations which exhibits $M$ fast time scales, the solution is attracted quickly on a $N - M$ *Slow Invariant Manifold (SIM)*. On the *SIM* the building response is governed by a system, which is free of the fast time scales, so that the flow there is characterized by the slow time scales. The *CSP* algorithm provides an approximation of the *SIM* and of the slow system. A number of *CSP*-related *diagnostic tools* are employed for the analysis of the building model, which provide all the relevant physical understanding for the different phenomena that appear during building vibrations. The purpose of the present analysis of the building model under various external loadings and excitations is to identify (i) the natural eigenmodes of the buildings that stimulated, (ii) the contribution of each natural eigenmode to the building vibration, (iii) the natural eigenmodes that correspond to the time scales at each instant, (iv) the evolution of the *SIM* under significant changes of the loading case. Finally, the results of the CSP method are compared to other model reduction methods mentioned by *Antoulas et al.*.

# Contents

# Chapter 1

# Introduction

The dynamical behaviours of the buildings are very complex. The last decades, these behaviours have been extensively studied. [8–10, 19, 20, 35, 48]. There are many phenomena that have been observed. Because of the complexity of the dynamical behaviours there is the need to create more accurate models. That led to the increase the number of the degrees of freedom(DoFs). This results to very large systems. It was essential to acquire a reduced system that can give results that simulate the dynamical behaviour sufficiently with respect to an error. The results produced with this approach can be very useful since:

- it is possible to identify the useful eigenmodes of the building,
- the reduced system can be significantly smaller than the ones with the whole Dofs,
- the slow and fast behaviours of the physical phenomenon can be identified,
- the reduction of the order of the system can led to dramatic decrease of the computational power and the computer memory
- it enables to identify the changes in the dynamical behaviour with respect to the changes in the value of the parameters of the physical problem.

There are many difficulties in the simulation of the building dynamical response. One of them is how to determine the values of the damping coefficients. This process is quite hard and ambiguous because the building materials do not have only elastic behaviour. Also the forces that are produced from the deformed shape of a building under maximum loads. That forces are called second order forces [19]. Another one is the inelastic and plastic properties of the materials that are used at building construction. Luckily all the above phenomenons and much more don't have a huge impact except from the case of applying extreme loads in the structure. Structural engineers can calculate the appropriate dimensions of the structural elements such that the structure don't get in inelastic and plastic behaviour. This is not an assumption that is applied on the building codes [20] on the most cases for the sake of safety. In the case study of the building of Los Angeles hospital found in the [3, 4, 15, 16] was selected. This is a building with elastic behaviour

and damping. More information about the theory of the response of buildings under static loads and vibration excitations found in the chapter (3) and in [1, 29, 30].

Building vibrations are modelled with the use of *Ordinal Differential Equation (ODE)* systems [8, 17, 19, 31, 35]. The most common method to construct and solve these Differential Equations is the Finite Element Method(FEM). [7, 37, 48]. Many software had been developed the last decades which solve building vibration problems like Ansys,Abaqus, e.t.c. [7]. These systems are (i) easy to handle due to their well understood mathematical framework, (ii) very fast, because the matrices of these systems are quite sparse and most of the non zero values are close to the diagonal(the matrices have small bandwidth) with a good numbering of the DoFs, (iii) the systems are quite robust. Although in many cases the systems are quite big and there is the need to find systems with significant lower number of unknowns that simulate efficiently the dynamical behaviour of the system. In the next chapters of this dissertation it is shown that exceptional order reduction of the starting systems can be achieved due to the nature of the problem. Therefore, there will be no need of absurd computational power or computer memory to achieve the solution.

Here, the building's dynamical response will be modelled with a system of harmonic damping oscillation ODEs. As a next step an algorithmic method will be applied that performs asymptotic analysis. In this way it will be achieved a better physical understanding of the physical phenomenon and the fast and slow time-scales that co-exist. With the usage of this method called Computational Singular Perturbation (CSP) method a reduction in the order of the system can be achieved as well.

The harmonic damping oscillation is a second order elliptic differential equation that describes the motion of objects (in this case buildings) that is reduced by the time due to damping. This happens mainly due to frictional forces that decrease the velocity in proportion to the acting frictional force. This ODE is the foundation of the mechanics of vibrations [31, 35] and this ODE will be mentioned with greater detail in the chapter 3 of the dissertation.

During this study of the building vibrations, it would be clear that the verification of the results is not possible due to the lack of quantitative experimental data. The only way that it could be checked that the model is efficient is that the results are of similar order as of some experimental data from other buildings [1,20,30] and identify deformation patterns that are similar to the deformation patterns that are known for other buildings. In this case, the numerical results that are produced have been checked and they are normal in every loading case. Also in this dissertation it would be analysed extensively for different loadings and frequency of loadings and it would be observed that the system is robust which is expected.

One of the most important challenges regarding this study is to identify the eigenmodes that are responsible for the deformation of the building during the loading. One goal is to connect the value and the frequency of loading to the response of the building. Another goal is to incorporate in this investigation the determination of the eigenmodes that are activated mostly in each loading case.

The traditional tool for the identification of the fast components of a multi-scale system and of the reduced model that drives its slow evolution is the emphSingular Perturbation Analysis(SPA). SPA is a tool that identifies (i) the fast components that participate in the various equilibrations that develop and (ii) the slow components that finally drive the system [17,21,22,34, 44–46]. The disadvantage of the paper/pencil *SPA* is that it can handle relative simple models because it requires (i) the governing equations of the system to be cast in the proper non-dimensional

form, (ii) the identification of the fast and the slow variables and (iii) the identification of the small parameter $\epsilon$, which is indicative of the gap between the fast and slow time scales. Given the complexity of the systems that are produced to investigate the behaviour of buildings to vibrations, the application of the *SPA* faces significant obstacles, mainly due to the complexity and size of the models that are currently of interest.

The fast/slow dynamics of the Los Angeles hospital [3, 16] to different loading cases will be examined in the chapter (5), by employing the *Computational Singular Perturbation (CSP)* algorithm. *CSP* reproduces the results of the classical SPA in an algorithmic fashion. The methodology is not hindered by the size and complexity of the mathematical model and does not require the system to be cast in a dimensionless form. *CSP* identifies (i) the fast and slow variables, (ii) the way that the fast time scales lead the system to equilibria, (iii) the reduced model that governs the slow evolution under the constraints (i.e., equilibria) generated by the fast time scales, and (iv) the components that contribute to the equilibria and the slow evolution [11, 14, 26, 28, 42]. Also with *CSP* the different types of equilibria with respect the loading cases that are applied in this physical problem can be identified.

To evaluate the CSP method a search of model reduction methods in the bibliography [3, 6, 16, 33, 36] was conducted and the basic categories of all these methods were presented in chapter (4). For each category a characteristic method was presented with further details. Furthermore, there are some methods of model reduction that works specifically for the systems that simulate the dynamic behaviour of the buildings due to some specific properties that are related to the nature of the problem.

First, the *CSP* methodology will be briefly presented and the *CSP* tools will be discussed. Next, the harmonic damping oscillation equation will be introduced and some phenomenon that are observed in buildings during vibrations will be discussed. It follows a bibliographic research of model reduction methods and the further discussion of some important methods. The detailed model of Los Angeles hospital will be then presented, along with its parameters, initial conditions and loading cases that are applied. The results of the *CSP* analysis will be finally presented and discussed in chapter (5).

Finally, i would like to thank professor D.Goussis and Ph.D. student D.Maris for the help and guidance that provide during the completion of this dissertation.

# Chapter 2

# The CSP algorithm

Usually in order to formulate a physical problem there is the need of mathematical models that are approximations of the real problems. In mechanics, in physics, in biology, in computer science e.t.c. there are usually mathematical model of multiple time scales. These models simulate physical problems in which *slow* and *fast* time scales are developed.

A system of ordinary differential equations in which *slow* and *fast* time scales are developed is called *stiff* when :

- the *fast* time scales are *dissipative*
- the area of the vector field of the solution where the *slow* time scales are superior is much bigger than the are where the *fast* time scales are superior

Therefore, the fast time scales characterize the solution of the stiff dynamical systems only for a small time period. Later the slow time scales will dominate the fast ones and the effect of the fast time scales is not important. Although, the existence of fast time scales in time periods where slow time scales characterized the solution, it creates arithmetic difficulties that characterize the stiff problems and led to the use of implicit calculating algorithms. The subspace in which the slow time scales are responsible for the development of the solution and the solution is determined by a non-stiff system is called exponentially attracting *Slow Invariant Manifold* (SIM). [17, 44–46]

The *phase space* of the SIM is called *tangent space* and can also describes by fast and slow subspaces, in which fast or slow time scales are dominant, respectively. For an ordinary differential equation during the movement of the solution inside SIM the two subspaces are rotating. [44]

The SIM is defined by linear independent equations that are determined by the projection of the vector field in the principal directions of the fast subspace of the *tangent space*. The non-stiff system that simulates the movement of the solution on the SIM is determined by the projection of the vector field to the principal direction of the slow subspace of the *tangent space*. [44]

The existence of the SIM allows the creation of simplified and non-stiff models with reduced order. In this way the solution of large-scale stiff problems becomes easy. Also, it is possible to identify the contribution of different physical phenomenon to the creation of the SIM. There are many asymptotic methods from the *Singular Perturbation Analysis* (SPA) that can derive the SIM and the non-stiff model with reduced order. As mentioned in chapter (1) these methods cannot

handle complex and large-scale system. For that reason algorithmic methods have developed that have no limitation for the size and complexity of the mathematical models that can handle. One such method is the *Computational Singular Perturbation* (CSP) and the mathematical background of this methods is presented in [11,14,26,28,32]. In this chapter the algorithm and various important tools of the CSP method were presented.

The success of *CSP* in the analysis of multi-scale systems is based on the existence of a time scale gap among the fastest time scales in the dynamics of the system and the time scale that is characteristic of the system's evolution. When these, say M, fast time scales are of dissipative nature (i.e., they are generated by processes that tend to drive the system to equilibrium) they become quickly exhausted, so that the fastest time scale of the slow ones becomes the characteristic time scale for the system's evolution. The gap between the slowest of the fast ($\tau_M$) and the fastest of the slow ($\tau_{M+1}$) time scales measures the time scale gap that is indicative of the fast/slow separation. This gap is approximated by the ratio:

$$\epsilon = \tau_M / \tau_{M+1} \tag{2.1}$$

which by definition satisfies $\epsilon < 1$.

Consider a physical process which is governed by the N-dimensional system of (*ODE*'s):

$$\frac{d\mathbf{y}}{dt} = \mathbf{g}(\mathbf{y}) \tag{2.2}$$

where $\mathbf{y}$ and $\mathbf{g}(\mathbf{y})$ are the $N$-dimensional column *state vector* and *vector field*, respectively and $\mathbf{g}$ is an algebraic function of $\mathbf{y}$. Let the dynamics of this system exhibit $M$ dissipative time scales, which are much faster than the time scale that characterizes the evolution of the system. Such a system is known as a *stiff* one [2]. According to the *CSP* algorithm, the vector field $\mathbf{g}$ can be decomposed in a fast and a slow part, as:

$$\frac{d\mathbf{y}}{dt} = \mathbf{a}_r \mathbf{f}^r + \mathbf{a}_s \mathbf{f}^s \tag{2.3}$$

where $\mathbf{a}_r \mathbf{f}^r$ and $\mathbf{a}_s \mathbf{f}^s$ are the components of the vector field $\mathbf{g}(\mathbf{y})$ in the $M$-dimensional *fast subspace* and $N - M$ dimensional *slow subspace*, respectively. The fast subspace, where the fast time scales act, is spanned by the $M$ $\mathbf{a}_i$ $(i = 1, ..., M)$ column vectors which form the $(N \times M)$ matrix $\mathbf{a}_r$:

$$\mathbf{a}_r = \Big[\mathbf{a}_1 \ \mathbf{a}_2 \ ... \ \mathbf{a}_M\Big] \tag{2.4}$$

The slow subspace, where the slow time scales act, is spanned by the $N-M$ $\mathbf{a}_j$ $(j = M+1, ..., N)$ column vectors, which form the $N \times (N - M)$ matrix $\mathbf{a}_s$:

$$\mathbf{a}_s = \Big[\mathbf{a}_{M+1} \ \mathbf{a}_{M+2} \ ... \ \mathbf{a}_N\Big] \tag{2.5}$$

The *CSP* amplitudes $\mathbf{f}^r$ and $\mathbf{f}^s$ are the projections of the vector field $\mathbf{g}(\mathbf{y})$ along the $M$ fast and $N-M$ slow directions, respectively, and are defined by the relations:

$$\mathbf{f}^r = \mathbf{b}^r \mathbf{g} \qquad \mathbf{f}^s = \mathbf{b}^s \mathbf{g} \tag{2.6}$$

where

$$\mathbf{b}^r = \begin{bmatrix} \mathbf{b}^1 \\ \mathbf{b}^2 \\ : \\ \mathbf{b}^M \end{bmatrix} \qquad \mathbf{b}^s = \begin{bmatrix} \mathbf{b}^{M+1} \\ \mathbf{b}^{M+2} \\ : \\ \mathbf{b}^N \end{bmatrix} \tag{2.7}$$

The $N$-dimensional row vectors $\mathbf{b}^i$ $(i = 1, ..., N)$ are dual to the $N$-dimensional column vectors $\mathbf{a}_i$ $(i = 1, ..., N)$ and due to orthogonality they satisfy relations (2.8):

$$\mathbf{b}^r \mathbf{a}_r = \mathbf{I}^r_r \qquad \mathbf{b}^r \mathbf{a}_s = \mathbf{0}^r_s \qquad \mathbf{b}^s \mathbf{a}_r = \mathbf{0}^s_r \qquad \mathbf{b}^s \mathbf{a}_s = \mathbf{I}^s_s \qquad \mathbf{a}_r \mathbf{b}^r + \mathbf{a}_s \mathbf{b}^s = \mathbf{I}^N_N \tag{2.8}$$

where $\mathbf{I}^N_N$ and $\mathbf{0}^M_k$ are the unit $(N \times N)$ and zero $(M \times k)$ matrices respectively.

When the trajectory evolves on the $(N-M)$-dimension *Slow Invariant Manifold* (*SIM*) the $M$ fast dissipative time scales $\tau_i$ $(i = 1, \ldots, M)$ are exhausted, so that the flow is characterized by the slow time scale $\tau_{M+1}$. On the *SIM* the vector field $\mathbf{g}(\mathbf{y})$ has no component in the fast subspace; i.e., the amplitudes (2.9) attain negligible values:

$$\mathbf{f}^r = \mathbf{b}^r \bullet \mathbf{g} \approx \mathbf{0}^r_N \tag{2.9}$$

so that the flow on the *SIM* is approximated by the system:

$$\frac{d\mathbf{y}}{dt} \approx \mathbf{a}_s \mathbf{f}^s \tag{2.10}$$

The Eq. (2.10) results from the full system in Eq. (2.3), after neglecting the fast component. Therefore, the reduced system in Eq. (2.10) is non-stiff.

Note that since $\mathbf{a}_s \mathbf{b}^s = \mathbf{I}^N_N - \mathbf{a}_r \mathbf{b}^r$, Eqs. (2.9, 2.10) show that for the construction of both the algebraic equation approximating the manifold and the slow system, it is sufficient to have available the fast basis vectors $\mathbf{a}_r$ and $\mathbf{b}^r$ only.

The *CSP* basis vectors $\mathbf{a}_r$ and $\mathbf{a}_s$, and their duals $\mathbf{b}^s$ and $\mathbf{b}^r$ are approximated with the *CSP* algorithm by two iterative procedures, the "$\mathbf{b}^r$" and the "$\mathbf{a}_r$" *CSP* refinements. The $\mathbf{b}^r$-refinement alters $\mathbf{b}^r$ and $\mathbf{a}_s$, leaving $\mathbf{b}^s$ and $\mathbf{a}_r$ unaffected, and it is related to the accuracy in the description of the manifold [11,25–28,40,47]. The $\mathbf{a}_r$-refinement alters $\mathbf{a}_r$ and $\mathbf{b}^s$, leaving $\mathbf{a}_s$ and $\mathbf{b}^r$ unaffected, and it is related to the non-stiffness of the simplified model [11, 25, 26, 28, 47].

- Assuming that "$k_1$" $\mathbf{b}^r$-refinements and "$m_1$" $\mathbf{a}_r$-refinements have already being made, an additional $\mathbf{b}^r$-refinement that improves the accuracy of $\mathbf{a}_s$ and $\mathbf{b}^r$ vectors is provided by the following relations:

$$\mathbf{b}^r(k_1+1,m_1) = \boldsymbol{\tau}_r^r(k_1,m_1)\left[\frac{d\mathbf{b}^r(k_1,m_1)}{dt} + \mathbf{b}^r(k_1,m_1)\mathbf{J}\right] \tag{2.11}$$

$$\mathbf{a}_r(k_1+1,m_1) = \mathbf{a}_r(k_1,m_1) \tag{2.12}$$

$$\mathbf{b}^s(k_1+1,m_1) = \mathbf{b}^s(k_1,m_1) \tag{2.13}$$

$$\mathbf{a}_s(k_1+1,m_1) = \left[\mathbf{I} - \mathbf{a}_r(k_1+1,m_1)\mathbf{b}^r(k_1+1,m_1)\right]\mathbf{a}_s(k_1,m_1) \tag{2.14}$$

where

$$\boldsymbol{\tau}_r^r(k_1,m_1) = (\boldsymbol{\lambda}_r^r(k_1,m_1))^{-1} = \left[\left(\frac{d\mathbf{b}^r(k_1,m_1)}{dt} + \mathbf{b}^r(k_1,m_1)\mathbf{J}\right)\mathbf{a}_r(k_1+1,m_1)\right]^{-1} \tag{2.15}$$

- Assuming that "$k_2$" $\mathbf{b}^r$-refinements and "$m_2$" $\mathbf{a}_r$-refinements have already being made, an additional $\mathbf{a}_r$-refinement that improves the accuracy of $\mathbf{a}_r$ and $\mathbf{b}^s$ vectors is provided by the following relations:

$$\mathbf{a}_r(k_2,m_2+1) = \left[-\frac{d\mathbf{a}_r(k_2,m_2)}{dt} + \mathbf{J}\mathbf{a}_r(k_2,m_2)\right]\boldsymbol{\tau}_r^r(k_2,m_2) \tag{2.16}$$

$$\mathbf{b}^r(k_2,m_2+1) = \mathbf{b}^r(k_2,m_2) \tag{2.17}$$

$$\mathbf{b}^s(k_2,m_2+1) = \mathbf{b}^s(k_2,m_2)\left[\mathbf{I} - \mathbf{a}_r(k_2,m_2+1)\mathbf{b}^r(k_2,m_2+1)\right] \tag{2.18}$$

$$\mathbf{a}_s(k_2,m_2+1) = \mathbf{a}_s(k_2,m_2) \tag{2.19}$$

where

$$\boldsymbol{\tau}_r^r(k_2,m_2) = (\boldsymbol{\lambda}_r^r(k_2,m_2))^{-1} = \left[\left(\frac{d\mathbf{b}^r(k_2,m_2)}{dt} + \mathbf{b}^r(k_2,m_2)\mathbf{J}\right)\mathbf{a}_r(k_2+1,m_2)\right]^{-1} \tag{2.20}$$

## 2.1 Implementation of the CSP refinements

The implementation of the CSP-refinements starts by assuming an initial guess for the basis vectors $\mathbf{a}_i$ and $\mathbf{b}^i$, $i = 1, \ldots, N$. If these basis vectors are constants, the time derivative terms are ignored in the first implementation of the refinements, which in the following will be referred as "Phase (1)". The time derivative terms will be retained in the following implementations of the refinements, which in the following will be referred as "Phase (2)". Since in the general case of a non linear system the time derivatives contribute to higher order accuracy, the "Phase (1)" of the CSP refinements involves only one set of $\mathbf{b}^r$ and $\mathbf{a}_r$-refinements. On the other hand, "Phase (2)" can involve more than one set of refinements [41]. The only limitation in this case is set by the increasing computational cost, as it will be shown explicitly next.

The goal of the iterative process of $\mathbf{b}^r$ and $\mathbf{a}_r$ refinements is that the $\mathbf{b}^r$and $\mathbf{a}_r$ to converge to their real values at each time step. In can be proved that after infinite number of refinements the $\mathbf{b}^r$and $\mathbf{a}_r$ vectors are equal to the first M vectors of the (fast) right and left eigenvectors respectively. So actually the $\mathbf{b}^r$ and $\mathbf{a}_r$ vectors shows which are the primal directions of the problem where the solution moves fast. A clever selection of the initial guess can lead to significant lower number of iterations in order to achieve a sufficient convergence of the $\mathbf{b}^r$ and $\mathbf{a}_r$ vectors. In detail the way of creating the vectors for the initial guess will be mentioned in the following chapters.

Differentiating Eq.(2.9) with respect to time, along a solution of a trajectory $\mathbf{y}(t)$, yields:

$$\frac{df^i}{dt} = \sum_{j=1}^{N} \lambda_j^i f^j \tag{2.21}$$

where $i$=1,..., N and

$$\lambda_j^i \equiv \left( \frac{d\mathbf{b}^i}{dt} + \mathbf{b}^i \bullet \mathbf{J} \right) \bullet \mathbf{a}_j \tag{2.22}$$

where $i$,$j$ = 1,..., N. In vector form Eq.(2.21) yields:

$$\frac{d}{dt} \begin{bmatrix} \mathbf{f}^r \\ \mathbf{f}^s \end{bmatrix} = \begin{bmatrix} \boldsymbol{\lambda}_r^r & \boldsymbol{\lambda}_s^r \\ \boldsymbol{\lambda}_r^s & \boldsymbol{\lambda}_s^s \end{bmatrix} \begin{bmatrix} \mathbf{f}^r \\ \mathbf{f}^s \end{bmatrix} \tag{2.23}$$

where r=1, ... , M and s=M+1, ... , N. The $\mathbf{b}^r$-refinements tend to reduce the order of $\boldsymbol{\lambda}_s^r$, while the $\mathbf{a}_r$-refinements tend to reduce the order of $\boldsymbol{\lambda}_r^s$. Evidently, these features result to (i) the decoupling of the fast time scales from the slow ones, when $\boldsymbol{\lambda}_s^r \to \mathbf{0}_s^r$ and (ii) the decoupling of the slow time scales from the fast ones, when $\boldsymbol{\lambda}_r^s \to \mathbf{0}_r^s$) [41].

### 2.1.1 Phase (1) of the *CSP* refinements

Consider the case where the first guess for the CSP vectors is the constant vectors $\mathbf{b}^r(0,0)$ and $\mathbf{a}_r(0,0)$, so:

$$\frac{d\mathbf{b}^r(0,0)}{dt} = 0, \qquad \frac{d\mathbf{a}_r(0,0)}{dt} = 0 \tag{2.24}$$

In this case, the CSP algorithm for the first $\mathbf{b}^r$-refinement yields:

$$\mathbf{b}^r(1,0) = \boldsymbol{\lambda}_r^r(0,0)\mathbf{b}^r(0,0)\mathbf{J} \tag{2.25}$$

$$\mathbf{a}_r(1,0) = \mathbf{a}_r(0,0) \tag{2.26}$$

$$\mathbf{b}^s(1,0) = \mathbf{b}^s(0,0) \tag{2.27}$$

$$\mathbf{a}_s(1,0) = [\mathbf{I} - \mathbf{a}_r(1,0)\mathbf{b}^r(1,0)]\mathbf{a}_s(0,0) = [\mathbf{I} - \mathbf{a}_r(0,0)\mathbf{b}^r(1,0)]\mathbf{a}_s(0,0) \tag{2.28}$$

where:

$$\boldsymbol{\lambda}_r^r(0,0) = \mathbf{b}^r(0,0)\mathbf{J}\mathbf{a}_r(0,0) \qquad\qquad \boldsymbol{\tau}_r^r(0,0) = [\boldsymbol{\lambda}_r^r(0,0)]^{-1} \tag{2.29}$$

The effect of the $\mathbf{b}^r$-refinement is to lower the norm of $\boldsymbol{\lambda}_s^r$ (where $(d\mathbf{b}^r(1,0)/dt) \bullet \mathbf{a}_s(1,0) = \mathbf{0}_s^r$):

$$\boldsymbol{\lambda}_s^r(1,0) = \mathbf{b}^r(1,0)\mathbf{J}\mathbf{a}_s(1,0) = \mathcal{O}(\epsilon\boldsymbol{\lambda}_s^r(0,0)) \tag{2.30}$$

by an order of $\epsilon = |\tau_M/\tau_{M+1}| < 1$, making the fast modes "purer", by decoupling them from the slow modes, while the decoupling level of the slow time scales with the fast time scales is left unchanged:

$$\boldsymbol{\lambda}_r^s(1,0) = \mathbf{b}^s(1,0)\mathbf{J}\mathbf{a}_r(1,0) = \mathbf{b}^s(0,0)\mathbf{J}\mathbf{a}_r(0,0) = \boldsymbol{\lambda}_r^s(0,0) \tag{2.31}$$

Given the CSP vectors after one $\mathbf{b}^r$-refinement, the algorithm of the $\mathbf{a}_r$-refinement yields:

$$\mathbf{a}_r(1,1) = \mathbf{J}\mathbf{a}_r(0,0)\boldsymbol{\tau}_r^r(1,0) \tag{2.32}$$

$$\mathbf{b}^r(1,1) = \mathbf{b}^r(1,0) \tag{2.33}$$

$$\mathbf{a}_s(1,1) = \mathbf{a}_s(1,0) \tag{2.34}$$

$$\mathbf{b}^s(1,1) = \mathbf{b}^s(1,0)[\mathbf{I} - \mathbf{a}_r(1,1)\mathbf{b}^r(1,1)] = \mathbf{b}^s(0,0)[\mathbf{I} - \mathbf{a}_r(1,1)\mathbf{b}^r(1,0)] \tag{2.35}$$

where:

$$\boldsymbol{\lambda}_r^r(1,0) = \mathbf{b}^r(1,0)\mathbf{J}\mathbf{a}_r(0,0) \qquad\qquad \boldsymbol{\tau}_r^r(1,0) = [\boldsymbol{\lambda}_r^r(1,0)]^{-1} \tag{2.36}$$

The result of the $\mathbf{a}_r$-refinement is to lower the norm of $\boldsymbol{\lambda}_r^s$:

$$\boldsymbol{\lambda}_r^s(1,1) = \left[\frac{d\mathbf{b}^s(1,1)}{dt} + \mathbf{b}^s(1,1)\mathbf{J}\right]\mathbf{a}_r(1,1) = \mathcal{O}(\epsilon\boldsymbol{\lambda}_r^s(1,0)) = \mathcal{O}(\epsilon\boldsymbol{\lambda}_r^s(0,0)) \tag{2.37}$$

by an order of $\epsilon = |\tau_M/\tau_{M+1}| < 1$, making the slow modes "purer", by decoupling them from the fast modes, while the decoupling level of the fast time scales with the slow time scales is left unchanged:

$$\begin{aligned}\boldsymbol{\lambda}_s^r(1,1) &= \left[\frac{d\mathbf{b}^r(1,1)}{dt} + \mathbf{b}^r(1,1)\mathbf{J}\right]\mathbf{a}_s(1,1) = \left[\frac{d\mathbf{b}^r(1,0)}{dt} + \mathbf{b}^r(1,0)\mathbf{J}\right]\mathbf{a}_s(1,0) \\ &= \boldsymbol{\lambda}_s^r(1,0) = \mathcal{O}(\epsilon\boldsymbol{\lambda}_s^r(0,0))\end{aligned} \tag{2.38}$$

### 2.1.2 Phase (2) of the *CSP* refinements

The CSP vectors are now considered functions of the stated vector $\mathbf{y}$, so they are time dependent. The time derivatives of the basis vectors are taken into account, so that high-order terms are retained which result to a better decoupling between fast and slow modes [41]. Given the *CSP* basis vectors from Phase (1), one additional $\mathbf{b}^r$-refinement yields:

$$\mathbf{b}^r(2,1) = \boldsymbol{\tau}_r^r(1,1)\left[\frac{d\mathbf{b}^r(1,1)}{dt} + \mathbf{b}^r(1,1)\mathbf{J}\right] = \boldsymbol{\tau}_r^r(1,1)\left[\frac{d\mathbf{b}^r(1,0)}{dt} + \mathbf{b}^r(1,0)\mathbf{J}\right] \tag{2.39}$$

$$\mathbf{a}_r(2,1) = \mathbf{a}_r(1,1) \tag{2.40}$$

$$\mathbf{b}^s(2,1) = \mathbf{b}^s(1,1) \tag{2.41}$$

$$\mathbf{a}_s(2,1) = [\mathbf{I} - \mathbf{a}_r(2,1)\mathbf{b}^r(2,1)]\,\mathbf{a}_s(1,1) = [\mathbf{I} - \mathbf{a}_r(1,1)\mathbf{b}^r(2,1)]\,\mathbf{a}_s(1,0) \tag{2.42}$$

where:

$$\boldsymbol{\lambda}_r^r(1,1) = \left[\frac{d\mathbf{b}^r(1,1)}{dt} + \mathbf{b}^r(1,1)\mathbf{J}\right]\mathbf{a}_r(1,1) \qquad\qquad \boldsymbol{\tau}_r^r(1,1) = [\boldsymbol{\lambda}_r^r(1,1)]^{-1} \tag{2.43}$$

The result of the $\mathbf{b}^r$-refinement is to lower even more the norm of $\boldsymbol{\lambda}_s^r$:

$$\begin{aligned}\boldsymbol{\lambda}_s^r(2,1) = &\left[\frac{d\mathbf{b}^r(2,1)}{dt} + \mathbf{b}^r(2,1)\mathbf{J}\right]\mathbf{a}_s(2,1) = \mathcal{O}(\epsilon\boldsymbol{\lambda}_s^r(1,1)) = \mathcal{O}(\epsilon\boldsymbol{\lambda}_s^r(1,0)) \\ &= \mathcal{O}(\epsilon^2\boldsymbol{\lambda}_s^r(0,0))\end{aligned} \tag{2.44}$$

by an additional order of $\epsilon = |\tau_M/\tau_{M+1}| < 1$, making the fast time scales "purer", by decoupling them from the slow ones, while the decoupling level of the slow time scales with the fast ones is left unchanged:

$$\begin{aligned}\boldsymbol{\lambda}_r^s(2,1) &= \left[\frac{d\mathbf{b}^s(2,1)}{dt} + \mathbf{b}^s(2,1)\mathbf{J}\right]\mathbf{a}_r(2,1) = \left[\frac{d\mathbf{b}^s(1,1)}{dt} + \mathbf{b}^s(1,1)\mathbf{J}\right]\mathbf{a}_r(1,1) \\ &= \boldsymbol{\lambda}_r^s(1,1) = \mathcal{O}(\epsilon\boldsymbol{\lambda}_r^s(1,0)) = \mathcal{O}(\epsilon\boldsymbol{\lambda}_r^s(0,0))\end{aligned} \tag{2.45}$$

Given the *CSP* basis vectors after the second $\mathbf{b}^r$-refinement, an additional $\mathbf{a}_r$-refinement yields:

$$\mathbf{a}_r(2,2) = \left[\frac{d\mathbf{a}_r(2,1)}{dt} + \mathbf{b}^r(2,1)\mathbf{J}\right]\boldsymbol{\tau}_r^r(2,1) = \left[\frac{d\mathbf{a}_r(1,1)}{dt} + \mathbf{J}\mathbf{a}_r(1,1)\right]\boldsymbol{\tau}_r^r(2,1) \tag{2.46}$$

$$\mathbf{b}^r(2,2) = \mathbf{b}^r(2,1) \tag{2.47}$$

$$\mathbf{a}_s(2,2) = \mathbf{a}_s(2,1) \tag{2.48}$$

$$\mathbf{b}^s(2,2) = \mathbf{b}^s(2,1)[\mathbf{I} - \mathbf{a}_r(2,2)\mathbf{b}^r(2,2)] = \mathbf{b}^s(1,1)[\mathbf{I} - \mathbf{a}_r(2,2)\mathbf{b}^r(2,1)] \tag{2.49}$$

where:

$$\boldsymbol{\lambda}_r^r(2,1) = \left[\frac{d\mathbf{b}^r(2,1)}{dt} + \mathbf{b}^r(2,1)\mathbf{J}\right]\mathbf{a}_r(2,1) \qquad\qquad \boldsymbol{\tau}_r^r(2,1) = [\boldsymbol{\lambda}_r^r(2,1)]^{-1} \tag{2.50}$$

The result of the second $\mathbf{a}_r$-refinement is to lower even more the norm of $\boldsymbol{\lambda}_r^s$:

$$\boldsymbol{\lambda}_s^r(2,2) = \left[\frac{d\mathbf{b}^s(2,2)}{dt} + \mathbf{b}^s(2,2)\mathbf{J}\right]\mathbf{a}_r(2,2) = \mathcal{O}(\epsilon\boldsymbol{\lambda}_r^s(2,1)) = \mathcal{O}(\epsilon^2\boldsymbol{\lambda}_r^s(1,0)) = \mathcal{O}(\epsilon^2\boldsymbol{\lambda}_r^s(0,0)) \tag{2.51}$$

by an additional order of $\epsilon = |\tau_M/\tau_{M+1}| < 1$, making the slow modes "purer", by decoupling them from the fast modes, while the decoupling of the fast modes from the slow ones is left unchanged:

$$\begin{aligned}\boldsymbol{\lambda}_s^r(2,2) &= \left[\frac{d\mathbf{b}^r(2,2)}{dt} + \mathbf{b}^r(2,2)\mathbf{J}\right]\mathbf{a}_s(2,2) = \left[\frac{d\mathbf{b}^r(2,1)}{dt} + \mathbf{b}^r(2,1)\mathbf{J}\right]\mathbf{a}_s(2,1) \\ &= \boldsymbol{\lambda}_s^r(2,1) = \mathcal{O}(\epsilon\boldsymbol{\lambda}_s^r(1,1)) = \mathcal{O}(\epsilon\boldsymbol{\lambda}_s^r(1,0)) = \mathcal{O}(\epsilon^2\boldsymbol{\lambda}_s^r(0,0))\end{aligned} \tag{2.52}$$

### 2.1.3 Time derivatives of the Jacobian

In order to calculate the *CSP* basis vectors in Phase (2), a number of time derivatives of the CSP vectors must be computed [41]. The main expressions used for this purpose are:

$$\frac{d\mathbf{b}^r(1,1)}{dt} = \frac{d\mathbf{b}^r(1,0)}{dt} = \boldsymbol{\tau}_r^r(0,0)\mathbf{b}^r(0,0)\frac{d\mathbf{J}}{dt}\left[\mathbf{I} - \mathbf{a}_r(0,0)\mathbf{b}^r(1,0)\right] \tag{2.53}$$

$$\begin{aligned}\frac{d\mathbf{a}_r(2,1)}{dt} = \frac{d\mathbf{a}_r(1,1)}{dt} =&[\mathbf{I} - \mathbf{a}_r(1,1)\mathbf{b}^r(1,0)]\frac{d\mathbf{J}}{dt}\mathbf{a}_r(0,0)\boldsymbol{\tau}_r^r(1,0)\\ &- \mathbf{a}_r(1,1)\frac{d\mathbf{b}^r(1,0)}{dt}\mathbf{a}_r(1,1)\end{aligned} \tag{2.54}$$

$$\begin{aligned}\frac{d\mathbf{b}^r(2,1)}{dt} = \boldsymbol{\tau}_r^r(1,1)&\left[\frac{d\mathbf{b}^r(1,0)}{dt}\mathbf{J} + \mathbf{b}^r(1,0)\frac{d\mathbf{J}}{dt} + \frac{d^2\mathbf{b}^r(1,0)}{dt^2}\right]\left[\mathbf{I} - \mathbf{a}_r(1,1)\mathbf{b}^r(2,1)\right]\\ &- \mathbf{b}^r(2,1)\frac{d\mathbf{a}_r(1,1)}{dt}\mathbf{b}^r(2,1)\end{aligned} \tag{2.55}$$

where

$$\begin{aligned}\frac{d^2\mathbf{b}^r(1,0)}{dt^2} = &\left[\frac{d\boldsymbol{\tau}_r^r(0,0)}{dt}\mathbf{b}^r(0,0)\frac{d\mathbf{J}}{dt} + \boldsymbol{\tau}_r^r(0,0)\mathbf{b}^r(0,0)\frac{d^2\mathbf{J}}{dt}\right]\left[\mathbf{I} - \mathbf{a}_r(0,0)\mathbf{a}^r(1,0)\right]\\ &- \boldsymbol{\tau}_r^r(0,0)\mathbf{b}^r(0,0)\frac{d\mathbf{J}}{dt}\mathbf{a}_r(0,0)\frac{d\mathbf{b}^r(1,0)}{dt}\end{aligned} \tag{2.56}$$

The time derivatives involve the evaluation of the time rate change of the Jacobian matrix $d\mathbf{J}/dt$ and the high order rates $d^2\mathbf{J}/dt^2$ as well:

$$\frac{d\mathbf{J}}{dt} = \sum_{i=1,N_s}\frac{\partial\mathbf{J}}{\partial y^i}\frac{d\mathbf{y}^i}{dt} = \sum_{i=1,N_s}\frac{\partial\mathbf{J}}{\partial y^i}\mathbf{g}^i \tag{2.57}$$

$$\frac{d^2\mathbf{J}}{dt^2} = \sum_{i,j=1,N_s}\left[\frac{\partial^2\mathbf{J}}{\partial y^i\partial y^j}\mathbf{g}^i + \frac{\partial\mathbf{J}}{\partial y^i}\mathbf{J}\right]\mathbf{g}^j \tag{2.58}$$

The fact that the time derivatives of the Jacobian are required for the description of the *SIM* and of the slow system only in Phase (2) suggests that the curvature of the *SIM* contributes in high order accuracy terms only [41].

## 2.2 The Criteria to identify the M number of the exhausted modes

The number $M$ of the fast exhausted time scales of the system and the dimensions of the *SIM* $N-M$, might change as a the solution evolves with time. The identification of the number of the exhausted time scales depends on the order of accuracy that is sought. Here, the criteria for leading (first) and second order accuracy will be stated. The measure for the order of accuracy will be the fast/slow time scale ratio $\epsilon = \tau_M/\tau_{M+1}$.

### 2.2.1 First order accuracy

Demanding leading order accuracy, the criterion for declaring the $M$ fast time scales exhausted is:

$$\tau_{M+1}\,|\mathbf{a}_r(1,1)\mathbf{f}^r(1,1)| \;<\; \frac{\tau_M}{\tau_{M+1}}|\mathbf{y}| + \mathbf{AbsErr} \tag{2.59}$$

where $\mathbf{a}^r(1,1)$ is the $(N\times M)$-dim. matrix containing the $M$ fast *CSP* basis vectors (see Eq. (2.4)) computed after performing one $\mathbf{b}^r$- and one $\mathbf{a}_r$-refinements and $\mathbf{f}^r(1,1)$ (see Eq. (2.9)) is the $M$-dim. vector with the $M$ amplitudes of the $M$ fast *CSP* modes computed after performing one $\mathbf{b}^r$- and one $\mathbf{a}_r$-refinements. The first term in the RHS of Eq. (2.59) indicates the relative error allowed when integrating the slow system, while the second term denotes the equivalent absolute error. The results that will be reported next were computed by setting $\text{AbsErr}^i = 10^{-16}$ for all $i = 1,\ldots,N$.

### 2.2.2 Second order accuracy

Seeking second order accuracy, the criterion for declaring the $M$ fast time scales exhausted is:

$$\tau_{M+1}\,|\mathbf{a}_r(2,1)\mathbf{f}^r(2,1)| \;<\; \left(\frac{\tau_M}{\tau_{M+1}}\right)^2|\mathbf{y}| + \mathbf{AbsErr} \tag{2.60}$$

where the $\mathbf{a}^r(2,1)$ $(N\times M)$-dim. matrix contains the $M$ fast *CSP* basis vectors (see Eq. (2.4)) computed after performing two $\mathbf{b}^r$- and one $\mathbf{a}_r$-refinements and $\mathbf{f}^r(2,1)$ (see Eq. (2.9)) is the $M$-dim. vector with the $M$ amplitudes of the $M$ fast *CSP* modes computed after performing two $\mathbf{b}^r$- and one $\mathbf{a}_r$-refinements. As when seeking leading order accuracy, the first term in the RHS of Eq. (2.60) indicates the relative error allowed when integrating the slow system, while the second term denotes the equivalent absolute error. The results that will be reported next were computed by setting $\text{AbsErr}^i = 10^{-16}$ for all $i = 1,\ldots,N$.

## 2.3 The CSP diagnostic tools

*CSP* allows for the development of a number of computational tools by which the meaningful physical understanding for the evolution of the system under examination can be acquired.

It is assumed that the vector field $\mathbf{g}(\mathbf{y})$ can be represented as the sum of the products $\mathbf{S}_k R^k$ $(k = 1, ..., 2K)$:

$$\mathbf{g}(\mathbf{y}) \;=\; \mathbf{S}_1 R^1(\mathbf{y}) + \mathbf{S}_2 R^2(\mathbf{y}) + \ldots \mathbf{S}_{2K} R^{2K}(\mathbf{y}) \tag{2.61}$$

where $\mathbf{S}_k$ in the case of building models is the is $k^{th}$ eigenmode-eigenvector and process and $R^k(\mathbf{y})$ is the corresponding eigenvector-eigenfrequency. Therefore, the amplitude of the $i^{th}$ CSP mode $f^i$ $(i = 1, \ldots, N$; see Eq. (2.6)), can be expressed as:

$$f^i \;=\; f_1^i + ... + f_{2K}^i \tag{2.62}$$

where $f_k^i(\mathbf{y}) = (\mathbf{b}^i \bullet \mathbf{S}_k) R^k(\mathbf{y})$. When $f^m$ represents an exhausted mode $(m = 1, \ldots, M$; see Eq. (2.9)), Eq. (2.62) yields:

$$f^m \;=\; f_1^m + ... + f_{2K}^m \approx 0 \tag{2.63}$$

### 2.3.1 The CSP Pointer

The variables that are affected the most by the $m^{th}$ fast time scale and exhibit a significant influence on the terms participating in the occurring cancelations in the vanishing amplitude of the $m^{th}$ mode, see Eq. (2.63), can be identified by the the *CSP Pointer* for the $m^{th}$ mode:

$$\mathbf{D}^m = diag[\mathbf{a}_m \mathbf{b}^m] = [a_m^1 b_1^m, ..., a_m^N b_N^m]^T \tag{2.64}$$

where due to the orthogonality $\mathbf{b}^m \cdot \mathbf{a}_m = 1$, it follows that $a_m^1 b_1^m + ... + a_m^N b_N^m = 1$, $(m = 1, \ldots, M)$ [11, 13, 23–25, 28]. A value of $a_m^j b_j^m$ $(j = 1, ..., N)$ close to unity denotes the association of the $j^{th}$ variable with the $m^{th}$ *CSP mode* $\mathbf{a}_m f^m$ and the related time scale $\tau_m$.

### 2.3.2 The Participation Index

Eq.(2.63) indicates that the decay to negligible values of the exhausted fast amplitudes is the result of equilibrations emerging among various components in the model. These components are identified with the use of the *Participation Index*:

$$P_k^m = \frac{f_k^m(\mathbf{y})}{\sum_{j=1}^{2K} |f_j^m(\mathbf{y})|} \tag{2.65}$$

where $m$ denotes the fast *CSP* mode ($m = 1, \ldots, M$), $k$ denotes the $k^{th}$ component ($k = 1, ..., 2K$) and by definition $|P_1^m| + ... + |P_k^m| = 1$ [11, 13, 25, 28]. Since only exchausted modes are considered, for which $f^m \approx 0$, the following relation also holds: $P_1^m + ... + P_k^m \approx 0$. As a result, a relatively large value of $P_k^m$ indicates a large contribution of the $k^{th}$ term of Eq. (2.61) to the constraint developed along the $m^{th}$ *CSP* basis vector $\mathbf{a}_m$, imposed by the $m^{th}$ fast time scale, when becomes exhausted.

### 2.3.3 The Importance Index

The flow on the *SIM* is governed by the slow system in Eq. (2.10):

$$\frac{d\mathbf{y}}{dt} \approx \mathbf{a}_s \mathbf{f}^s = \mathbf{g}_{slow} \tag{2.66}$$

The contribution of the $k^{th}$ term of Eq. (2.61) to the evolution on the *SIM* of the $n^{th}$ variable in $\mathbf{y}$, according to the slow system, can be evaluated with the *CSP Importance Index*, which is defined as follows. Each element of $\mathbf{g}_{slow}(\mathbf{y})$ can be expressed with $2K$ terms as:

$$g_{slow}^n(\mathbf{y}) = g_{slow}^{n,1}(\mathbf{y}) + g_{slow}^{n,2}(\mathbf{y}) + ... + g_{slow}^{n,2K}(\mathbf{y}) \tag{2.67}$$

where $g_{slow}^{n,2K}(\mathbf{y}) = \sum_{j=M+1}^{N} a_j^n (\mathbf{b}^j \bullet \mathbf{S}_k) R^k(\mathbf{y})$, $(k = 1, ..., 2K)$ and $a_j^n$ denoted the $n^{th}$-th element of the column vector $\mathbf{a}_j$ $(j = M+1, \ldots, N)$ in $\mathbf{a}_s$; see Eq.(2.5). The Importance Index is defined as:

$$I_k^n = \frac{g_{slow}^{n,k}(\mathbf{y})}{\sum_{j=1}^{2K} |g_{slow}^{n,j}(\mathbf{y})|} \tag{2.68}$$

where by definition $|I_1^n| + |I_2^n| + ... + |I_{2K}^n| = 1$ [11, 13, 25]. A relatively large value of $|I_k^n|$ indicates that the $k^{th}$ term of Eq. (2.61) provides a significant contribution to the evolution of $y^n$ on the *SIM*, while a relatively small value of $|I_k^n|$ indicates a negligible contribution.

### 2.3.4 The Eigenvalue Participation Index

In general, all terms represented in the vector field $\mathbf{g}(\mathbf{y})$, see Eq. (2.61), contribute to the emergence of the $M$-fast dissipative time scales. The exact contribution of each term can be identified by the *Eigenvalue Participation Index (EPI)*, which provides the contibution of the $k^{th}$ term of Eq. (2.61) to the development of the $m^{th}$ eigenvalue $\lambda_m$. For a real eigenvalue $\lambda_m$ it holds that:

$$\lambda_m = \mathbf{q}^m \mathbf{J} \mathbf{p}_m \tag{2.69}$$

where $\mathbf{q}_m$ and $\mathbf{p}_m$ are the corresponding left (row) and right (column) eigenvectors of the Jacobian $\mathbf{J}$. Substituting from Eq. (2.61) yields the following partition of the eigenvalue $\lambda_m$ with respect to the $2K$ processes:

$$\lambda_m = \lambda_m^1 + \lambda_m^2 + ... + \lambda_m^{2K} \tag{2.70}$$

where

$$\lambda_m^k = \mathbf{q}^m \mathbf{S}_k \nabla R^k \mathbf{p}_m, \quad (k = 1, ..., 2K) \tag{2.71}$$

The EPI is defined as:

$$\Lambda_k^m = \frac{\lambda_m^k}{\sum_{j=1}^{2K} |\lambda_m^j|} \tag{2.72}$$

By definition $|\Lambda_1^n| + |\Lambda_2^n| + ... + |\Lambda_{2K}^n| = 1$ and the value of $\Lambda_k^n$ provides a measure of the influence of the $k^{th}$ term of Eq. (2.61) to the value of the $n^{th}$ eigenvalue $\lambda_n$. [12–14] Negative values of $\Lambda_k^n$ indicate a trend to of the $k^{th}$ term of Eq. (2.61) to move the $n^{th}$ *CSP* mode towards equilibrium, i.e., $f^n(\mathbf{y}) \to 0$. These terms will be called dissipative ones. On the other hand, positive values of $\Lambda_k^n$ indicate a trend away from equilibrium. Naturally, such terms will be declared as explosive ones. Regarding the exhausted time scales $\tau_m (m = 1, ..., M)$, in which the dissipative processes dominate, a non-negligible negative $\Lambda_k^m$ indicates that the rate of the $k^{th}$ term of Eq. (2.61) will act appropriately in order to restore, within a period of $O(\tau_m)$, the equilibration denoted by the $m^{th}$ *CSP* mode $f^m(\mathbf{y}) \approx 0$. A positive $\Lambda_k^m$ will oppose such action.

# Chapter 3

# The harmonic damping Oscillation

The *damped harmonic oscillation* is a second order differential equation that is used to calculate the response of an object (building in this case) under structural loads. Before analysing the complex case, the theory for the simple case will be analysed to get a better grasp of the problem before achieving the general system of equations. A great book that presents the theory of building vibrations in an easy and understanding way is the [8]. Many figures in this chapter are taken from there so the readers will understand better the mathematical background of the dynamical response of the buildings under various external forces and excitations.

## 3.1 Dynamical problem in simple case

In the first part of this chapter a simple structure such as a single storey building will be modelled as a system with concentrated mass with weightless columns. The dynamical response of those structures under static loads and earthquake excitations will be observed. Furthermore, the differential equations for some simple structures will be shown. Afterwards those differential equation will be solved analytically for the simple cases.

### 3.1.1 Simple Structures

The main focus of this dissertation is the understanding of the oscillation of those structures under a horizontal force applied on the concentrated mass or a ground movement caused by an earthquake. Those cases are similar and it was proved that in the section (3.1.6).

Those structures are called simple because they could be modeled by using a concentrated mass m which is supported on weightless columns with stiffness k in the horizontal direction. This assumption can be valid only in structures that one part of the structure is a lot stiffer than the other and can be modelled as a concentrated mass. This system can be shown in Fig. (3.1 a,b). The mass m equals to the total mass of the structure and the stiffness k is equal to the sum of all the lateral stiffness of the structural elements. So the one storey structures have only one unknown, the displacement $u$ in the horizontal direction.

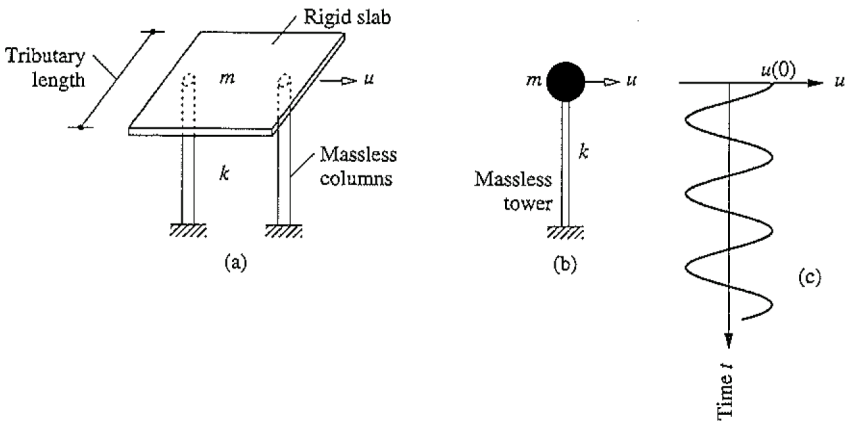


**Figure 3.1:** (a) idealized pergola, (b) idealized water tank, (c) free vibration due to initial displacement, adopted from [8]

The differential equation that describes the dynamical behaviour of such structures [8, 10, 19] with mass $m$, damping $c$ and stiffness $k$ is the following :

$$m\ddot{u} + c\dot{u} + ku = p \tag{3.1}$$

where $u$ is the horizontal displacement if the mass, $\dot{u}$ is the velocity, $\ddot{u}$ is the acceleration and $p$ is the external forces. The specific case when the system is moved from its initial equilibrium and it left alone to oscillate freely without any external loads or earthquake excitations and with an initial displacement $u(0)$ and initial velocity $\dot{u}(0)$ is given by :

$$m\ddot{u} + c\dot{u} + ku = 0 \tag{3.2}$$

This motion is called *free vibration*. When the damping is ignored the movement of the mass is similar to the Fig. (3.1 c). Then the object will oscillate for ever. This is not a realistic assumption. Denote the *amplitude* as the maximum displacement reached in every oscillation cycle. In reality the amplitude of the oscillation is decreased over time due to the damping. In Fig. (3.2) two different experiments conducted by the university of Berkeley are presented. [8]

There are numerous mechanisms that are responsible for the decrease of the amplitude over time. All those mechanisms consume energy during the movement of the system. The effect of those damping mechanisms is shown in the Fig. (3.2). Consequently, the damping is related to material and the damping of plexiglass is much greater than the one of the aluminium. Damping is a very complex phenomenon that is analysed in section (3.1.4) and in [1, 29, 30].

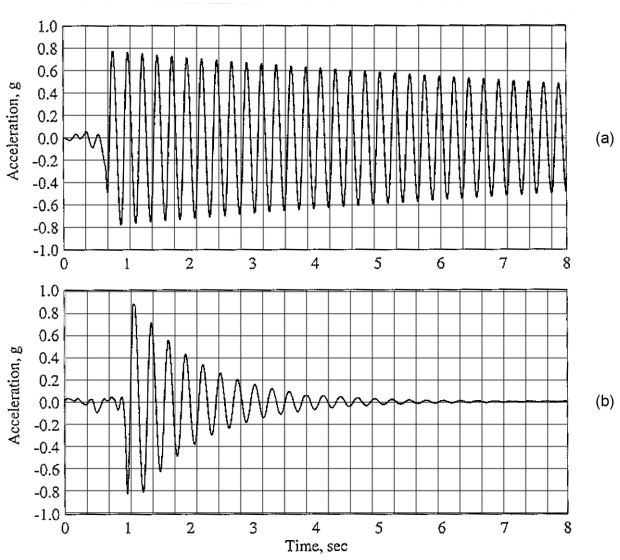


**Figure 3.2:** (a) free vibration of aluminum model, (b) free vibration of plexiglass model, adopted from [8]

### 3.1.2 Single degree of freedom systems

The system that is studied in this section is shown in Fig. (3.3 a). This system consisting of a concentrated mass $m$ in the ceiling, a weightless supporting structure with stiffness $k$ and a viscous damper $c$. The axial deformation of the beam and the columns are neglected.

These assumptions are reasonable for a single-storey building. In real constructions every part (beam,column,wall,etc.) contribute to the inertia (mass), elastic forces (stiffness) and damping. In the idealised system every characteristic is concentrated in the separate elements: mass , stiffness and damping.

The number of independent displacements that are required to define the movement of all the masses in respect with their initial position is called the number of degrees of freedom(DOFs). In this particular case the system has only one degree of freedom which is the horizontal displacement of the mass. Accordingly, this system has a single degree of freedom (SDF).

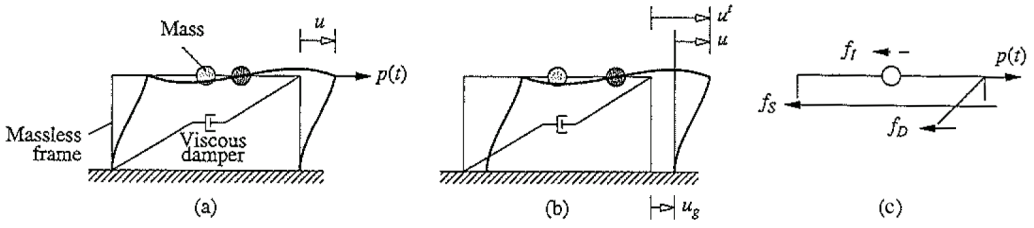


**Figure 3.3:** (a) single storey frame structure and its deformed state, (b) single storey frame structure and its deformed state when ground motion $u_g$ is applied to the structure, (c) free body diagram, adopted from [8]

### 3.1.3 Force-Displacement relation

In the single degree of freedom system shown in Fig. (3.3 a) a static force $p(t)$ is applied in the direction of the degree of freedom $u$. The internal force $f_s$ that resists the displacement $u$ and is equal and opposite from the force $p(t)$. The goal is to determine the relation between the force $f_s$ and the relative deformation $u = u^t - u_g$. This relation will be linear for small deformations but it will become non linear for larger deformations as shown in the Fig. (3.4 a,b).

#### 3.1.3.1 Linear elastic systems

For a linear elastic system the relation between the horizontal force $f_s$ and the deformation $u$ is linear:

$$f_s = ku \tag{3.3}$$

where $k$ is the resistance of the system to the horizontal force (stiffness in the case of the bending deformation). In the Eq. (3.3) it is claimed that the hypothesis of the linear equation between $f_s$ and $u$ which is destined for the small deformations of the structure is also valid for large deformation too. A system like this is called elastic.

For the structure in Fig. (3.3 a) denote the height $h$, Young's modulus $E$ and moment of inertia (in the direction of the deformation) $I$. The stiffness of the whole system is the sum of the stiffness of every column. For the case where the slab is rigid (its deformation is very small and it is considered zero) the stiffness is given by :

$$k = \sum_{columns} \frac{12EI_c}{h^3} = 24\frac{EI_c}{h^3} \tag{3.4}$$

For all the different cases where the slab can be deformed the formulas are given in [7, 10, 19].

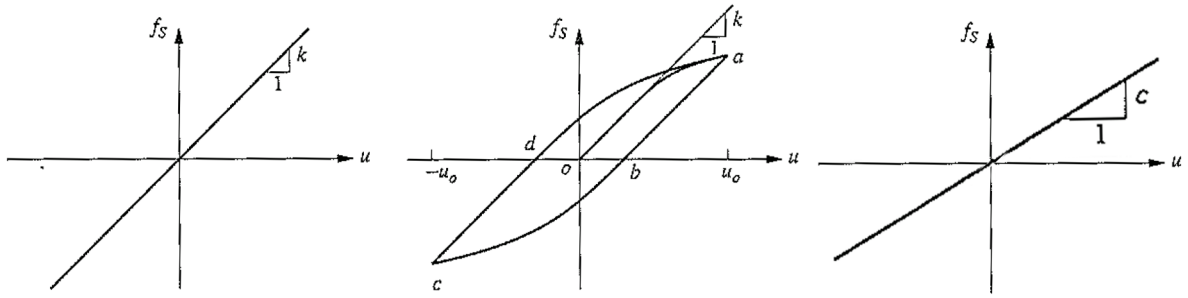


**Figure 3.4:** (a) force-displacements relation for linear systems, (b) force-displacements relation for non linear systems, (c) damping forces - velocities diagram, adopted from [8]

#### 3.1.3.2 Inelastic systems

The procedure to calculate the relation between the horizontal force $f_s$ and the deformation $u$ is more complicated. It involves periods of applying and removal of forces in a cycle manner.

$$f_s = f_s(u, \dot{u}) \tag{3.5}$$

The force-displacement diagram produced is not linear and the behaviour of the material is different every time the forces are applied. This behaviour is shown in Fig. (3.4 b). This is a more realistic assumption but it requires actual information about the material to form the system of the differential equations. The focus of this dissertation is the linear case. More information can be found in [7, 9, 20].

### 3.1.4 Damping Forces

As mentioned earlier, the mechanisms that are responsible for the reduction of the the amplitude during an oscillation is called *damping*. The energy of an oscillated system is consumed through different mechanisms that may work simultaneously on the structure. Such mechanisms in a simple case can be the thermal effects through repeated elastic staining of the material and from the internal friction when a solid is deformed. Although, in real buildings the mechanisms are much more complex. During an oscillation in a building there is friction in the metal connections, opening and closing of micro cracks in the concrete and the friction between structural and non structural elements like the brick walls. The detailed calculation of all this mechanisms is nearly impossible and for that reason in most cases the damping is simulated in a very simplified way. [1, 8, 20, 29, 30]

The real damping in a single degree system can be simulated with a *linear viscous damper*. The *damping coefficient* is selected such as the vibrational energy to be equal with the energy consumed by all the damping mechanisms. This idealization is called *equivalent viscous damping* and more information can be found in [1, 8, 20, 29, 30].

In the Fig. (3.3 a) there is a construction with a *linear viscous damper*. In this case a force $p(t)$ is applied in the direction of the degree of freedom $u$. The internal force of the damper $f_D$ is equal to the external force $p(t)$. The relation between the damping force $f_D$ and the velocity $\dot{u}$ is linear is shown in Fig. (3.4 c) and is given by the equation :

$$f_D = c\dot{u} \tag{3.6}$$

where the constant $c$ is the coefficient of the viscous damping.

In contrast with the stiffness, the coefficient of the viscous damping cannot be calculated by the dimensions of the structural elements. This is not surprising because the damping mechanisms are very complex in real structures.

For that reason the *equivalent viscous damper* is used in order to simulate the loss of the energy for values of deformation inside the width of linear elastic behaviour. Outside of this width the damping coefficient can vary due to inelastic behaviour. [8, 20] The non linearity of the damping behaviour is usually neglected. When it is included there is a change in the selection of the value of the damping coefficient suitable for the width of the deformation, similar to the relation of the deformation to the relation of the linear elastic limit of the structure in Eq. (3.5).

### 3.1.5 Equation of motion: External force

In the simple case of the idealized single storey building that mentioned before an external force $p(t)$ is applied dynamically in the direction of the degree of freedom (see Fig. (3.3 a)). This symbolism shows that the force $p$ can change over time $t$. Also the displacement of the mass changes over time $t$ so the symbol $u(t)$ is used for every instant there is a differential equation (see Eq. (3.8)).

#### 3.1.5.1 Application of Newton's second law

The forces that are applied in the mass at each instant presented in the Fig. (3.3 c). Those include the external force $p(t)$, the elastic (or inelastic) force of resistance $f_s$ and the the damping force $f_D$. The resulted force in the direction of the degree of freedom is $p - f_s - f_D$ and the Newton's second law gives:

$$p - f_s - f_D = m\ddot{u} \qquad \Leftrightarrow \qquad m\ddot{u} + f_D + f_s = p(t) \tag{3.7}$$

With substitution of the Eq. (3.3) and Eq. (3.6) this equation becomes:

$$m\ddot{u} + c\dot{u} + ku = p(t) \tag{3.8}$$

That is the proof of the general equation of motion for linear systems that describes the deformation or the displacement $u(t)$ of the idealized structure shown in Fig. (3.3 a), in which an external dynamical force $p(t)$ is applied. In similar way by substituting the Eq. (3.5) and Eq. (3.6) to the Eq. (3.7) the equation of motion for inelastic systems becomes:

$$m\ddot{u} + c\dot{u} + f_s(u, \dot{u}) = p(t) \tag{3.9}$$

### 3.1.6 Equation of motion: Earthquake excitation

In earthquake-prone areas, the main problem of structural dynamics that concern the structural engineers is the behaviour of structures subjected to earthquake induced motion of the base of the structure. The displacement of the ground is denoted by $u_g$, the total displacement of the mass with $u^t$ and the *relative displacement* of the mass to the ground with $u$ (see Fig. (3.3 b)). At each instance these deformation are related to:

$$u^t(t) = u(t) + u_g(t) \tag{3.10}$$

The $u^t$ and $u_g$ are referred to the same system and their positive directions are the same as shown in Fig. (3.3 b).

The equation of motion for the idealized one storey building in Fig. (3.3 b) when it is subjected to earthquake excitation can be derived with the *dynamic equilibrium*. From the free-body diagram shown in Fig. (3.3 c), that contains the *inertia force* $f_I$, the dynamical equillibrium equation is:

$$f_I + f_D + f_s = 0 \tag{3.11}$$

Only the relative displacement $u$ between the mass and the base produces elastic and damping forces due to structural deformation. The rigid-body component of the displacement $u_g$ of the structure produces no internal forces. Thus for a linear system the Eq. (3.3) and Eq. (3.6) are still valid. The inertia force $f_I$ is related to the acceleration $\ddot{u}^t$ of the mass by :

$$f_I = m\ddot{u}^t \tag{3.12}$$

Substituting the Eq. (3.3), Eq. (3.6) and Eq. (3.12) to Eq. (3.11) and using the Eq. (3.10) gives :

$$m\ddot{u} + c\dot{u} + ku = -m\ddot{u}_g(t) \tag{3.13}$$

This is the equation of motion with respect the relative displacement or deformation u(t) of the linear system of the picture that is subjected to ground acceleration $\ddot{u}_g(t)$.

In a similar way the equation for the inelastic systems can be derived by using the Eq. (3.11), but replace the Eq. (3.3) with the Eq. (3.5):

$$m\ddot{u} + c\dot{u} + f_s(u, \dot{u}) = -m\ddot{u}_g(t) \tag{3.14}$$

The equation of motion of the structure is the same in two different excitations by comparing the Eq. (3.8) and the Eq. (3.13) or the (3.9) and the Eq. (3.14). These two are the ground acceleration $\ddot{u}_g(t)$ and the external force $= -m\ddot{u}_g(t)$. So the displacement $u(t)$ of the structure will be the same in those two cases as shown in Fig. (3.5). In that manner, the effective force $p_{eff}$ that can be applied to a structure with stationary base in order to simulate the ground acceleration $\ddot{u}_g(t)$ is :

$$p_{eff}(t) = -m\ddot{u}_g(t) \tag{3.15}$$

The force $p_{eff}(t)$ is called *effective earthquake force* in [8, 10, 20]. One important conclusion is that the relation between the *effective earthquake force* and the mass of the structure is linear. So if the structural designer increases the mass of the structure it increases the *effective earthquake force* .

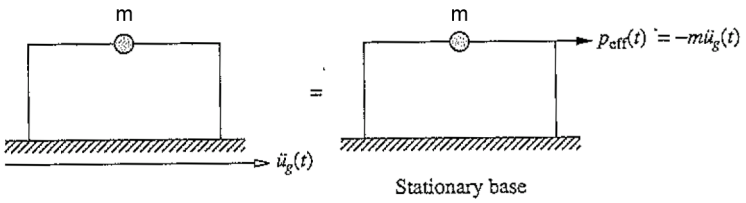


**Figure 3.5:** Effective earthquake force: horizontal ground motion, adopted from [8]

### 3.1.7 Methods of solving the differential equation

The equation of motion for a linear single degree of freedom system which is subjected to external force $p(t)$ is the second order differential equation from earlier on this chapter:

$$m\ddot{u} + c\dot{u} + ku = p(t) \tag{3.16}$$

The goal is to determine the solution for the initial displacement $u(0)$ and the initial velocity $\dot{u}(0)$. Usually the structure is in equilibrium state so $u(0) = \dot{u}(0) = 0$

#### 3.1.7.1 Classic Solution

The total solution of the linear differential equation consisted of the complementary solution $u_c(t)$ and the particular solution $u_p(t)$ so $u(t) = u_c(t) + u_p(t)$. So in the solution there will be two constants that will be determined by the initial values of the problem.

For the idealized building shown in Fig. (3.3 a) without damping an analytic expression of the solution can be derived using the following method.

Lets consider the static force $p(t) = p_0, t \geq 0$. The Eq. (3.16) with no damping ($c = 0$) is :

$$m\ddot{u} + ku = p_0 \tag{3.17}$$

The particular solution of the Eq. (3.17) is :

$$u_p(t) = \frac{p_0}{k} \tag{3.18}$$

and the complementary solution is :

$$u_c(t) = A\cos\omega_n t + B\sin\omega_n t \tag{3.19}$$

where $A$ and $B$ are constants of integration and $\omega_n = \sqrt{\frac{k}{m}}$

The complete solution is the sum of the Eq. (3.18) and the Eq. (3.19) :

$$u(t) = A\cos\omega_n t + B\sin\omega_n t + \frac{p_0}{k} \tag{3.20}$$

If the system is initially at equilibrium state, $u(0) = \dot{u} = 0$ at $t = 0$. For these initial conditions the constants $A$ and $B$ are :

$$A = -\frac{p_0}{k} \qquad B = 0 \tag{3.21}$$

The complete solution is given by substituting Eq. (3.21) in Eq. (3.20) :

$$u(t) = \frac{p_0}{k}(1 - \cos\omega_n t) \tag{3.22}$$

The classic solution is the basic method that is used to derive analytic solutions for this problem. Similarly,the analytic solutions can be derived when damping is included, for free vibration and for excitations that can be described analytically, such as harmonic, step and pulse forces.

#### 3.1.7.2 Other analytic methods

There are two more methods in [8] to derive analytic solution of this differential equation :

- Duhamel's Integral
- Frequency-Domain Method

The above methods won't be described in this dissertation. The method that was presented before can derive all the analytic solution needed to get a better grasp of the problem and the shape of the solutions. This way the reader can judge better the solution of the systems with multiple DOFs that are derived with computational ways in the following chapters of this dissertation.

## 3.2 Free Vibration

A structure is said to be undergoing free vibration when it is disturbed from its static equilibrium position and then allowed to vibrate without any external dynamic excitation. The free vibration problem is described by the notions of *natural vibration frequency* and *damping ration* of an SDF system. It will be shown that the rate at which the motion decays in free vibration is controlled by the *damping ratio*. Thus the Fig. (3.7) will be better explained. Even if the damping in real structures is complex as mentioned in section (3.1.4),it is shown in [1, 8, 20, 29, 30] that a practical mathematical approach is to idealize it with *equivalent viscous damping*.

### 3.2.1 Undamped free vibration

The motion of linear SDF systems is described by the Eq. (3.16). In the case of the undamped free vibration the $p(t) = 0$ and $c = 0$ and the Eq. (3.16) becomes :

$$m\ddot{u} + ku = 0 \tag{3.23}$$

The free vibration starts when the system is disturbed from its static equilibrium position by changing the initial displacement $u(0)$ and initial velocity $\dot{u}(0)$ at time zero, which is defined as the instant the motion is initiated :

$$u = u(0) \qquad \dot{u} = \dot{u}(0) \tag{3.24}$$

The solution of the differential equation has already been obtained in the Eq. (3.20) and by finding $A$ and $B$ suitable to fulfil the initial conditions the solution becomes :

$$u(t) = u(0)\cos\omega_n t + \frac{\dot{u}(0)}{\omega_n}\sin\omega_n t \tag{3.25}$$

where :

$$\omega_n = \sqrt{\frac{k}{m}} \tag{3.26}$$

The Eq. (3.25) is shown in the Fig. (3.6). It is obvious that the motion is *periodic*. The time required for the undamped system to complete one cycle of free vibration is the natural period of vibration of the system, which is denoted as $T_n$. It is related to the *natural circular frequency* of vibration $\omega_n$ with the formula :

$$T_n = \frac{2\pi}{\omega_n} \tag{3.27}$$

The system executes $\frac{1}{T_n}$ cycles in 1 sec. This *natural cyclic frequency* of vibration is denoted by

$$f_n = \frac{1}{T_n} \tag{3.28}$$

The units of $f_n$ are hertz (Hz) and $f_n$ is related to $\omega_n$ with :

$$f_n = \frac{\omega_n}{2\pi} \tag{3.29}$$

The term *natural frequency of vibration* applies to both $\omega_n$ and $f_n$.

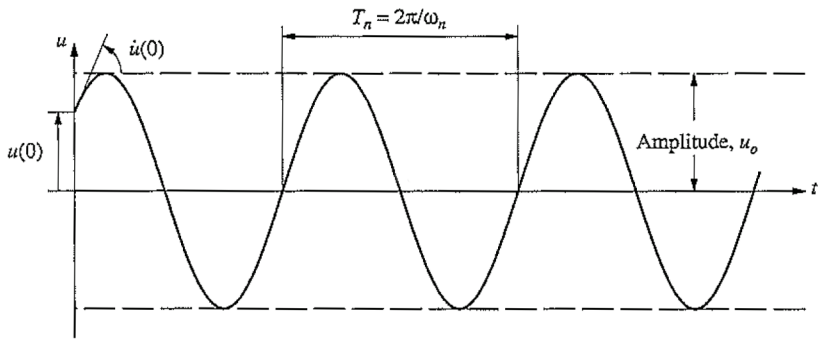


**Figure 3.6:** Free vibration of a system without damping, adopted from [8]

The natural vibration properties of an undamped system $\omega_n$, $T_n$, and $f_n$ depend only on the mass and stiffness of the structure from Eq. (3.26), Eq. (3.27) and Eq. (3.28). Even for the cases where the damping is not neglected, the stiffer of two SDF systems having the same mass will have the higher natural frequency and the shorter natural period [8,10,19]. The qualifier natural is used in defining $T_n$,$\omega_n$ and $f_n$ to emphasize the fact that these are natural properties of the system when

it is allowed to vibrate freely without any external excitation. Because the system is linear, these vibrations are independent of the initial displacement and velocity.

The amplitude of the undamped free vibration system is denoted by $u_0$ and is denoted by the formula :

$$u_0 = \sqrt{[u(0)]^2 + \left[\frac{\dot{u}(0)}{\omega_n}\right]^2} \tag{3.30}$$

It was shown in Fig. (3.6) that in the undamped case the amplitude $u_0$ stay constant and it depends only to the initial displacement and velocity.

### 3.2.2 Damped free vibration

By setting $p(t) = 0$ in the Eq. (3.16) the differential equation of free vibration SDF systems with damping becomes:

$$m\ddot{u} + c\dot{u} + ku = 0 \tag{3.31}$$

Lets denote the *critical damping coefficient* $c_{cr}$ and the *damping ratio* $\zeta$ as follows:

$$c_{cr} = 2m\omega_n = 2\sqrt{km} = \frac{2k}{\omega_n} \tag{3.32}$$

$$\zeta = \frac{c}{2m\omega_n} = \frac{c}{c_{cr}} \tag{3.33}$$

By dividing the Eq. (3.31) with $m$ :

$$\ddot{u} + 2\zeta\omega_n\dot{u} + \omega_n^2 u = 0 \tag{3.34}$$

#### 3.2.2.1 Types of motion

In the Fig. (3.7) the displacement $u(t)$ due to the initial displacement $u(0)$ is shown for three cases:

- $c = c_{cr}$ $(\zeta = 1)$ where the system returns to the equilibrium position without oscillation,
- $c > c_{cr}$ $(\zeta > 1)$ where the system returns to the equilibrium position without oscillation as with the case where $\zeta$ but at a slower rate,
- $c < c_{cr}$ $(\zeta < 1)$ where the system oscillates about its equilibrium position with a progressively decreasing amplitude.

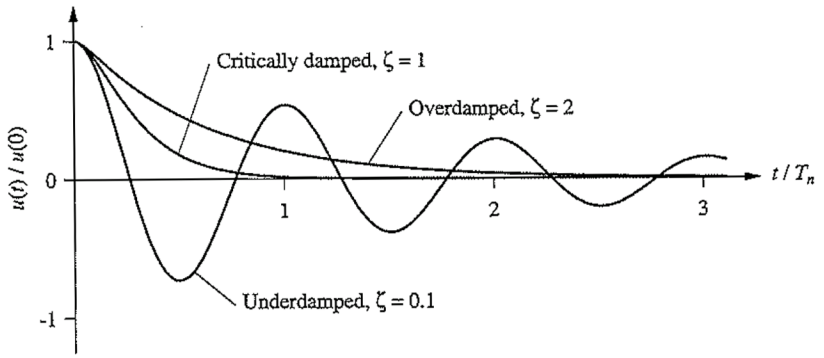


**Figure 3.7:** Free vibration of underdamped, critically damped, and overdamped systems, adopted from [8]

The *damping coefficient* $c_{cr}$ is *called critical damping coefficient* due to is the limit of $c$ that divides the systems that to those which are oscillate and not.

All of the structures falls in the third category and specifically where the damping ratio $\zeta < 0.10$. [8, 20, 29, 30] In this dissertation it was assumed that $\zeta = 0.05$ or 5% which is the most common case for building shown in [8,20,29,30],ghali2003structural, filiatrault2013elements. The other cases are analysed deeper at [30].

#### 3.2.2.2 Underdamped Systems

In this chapter the Eq. (3.31) will be solved with the initial conditions of the Eq. (3.24) for a system with $c < c_{cr}$ and $\zeta < 1$. The solution of the Eq. (3.34) is of the form of :

$$u = e^{st} \tag{3.35}$$

Substituting to the Eq. (3.34) :

$$(s^2 + 2\zeta\omega_n s + \omega_n^2)e^{st} = 0 \tag{3.36}$$

which is true for every value of t so :

$$s^2 + 2\zeta\omega_n s + \omega_n^2 = 0 \tag{3.37}$$

The Eq. (3.37) is known as the characteristic equation of this differential equation and it has two solutions :

$$s_{1,2} = \omega_n(-\zeta \pm i\sqrt{1-\zeta^2}) \tag{3.38}$$

So the general solution could be written :

$$u(t) = A_1 e^{s_1 t} + A_2 e^{s_2 t} \tag{3.39}$$

By substituting the Eq. (3.38) to the Eq. (3.39) the displacement is given by the following formula :

$$u(t) = e^{-\zeta\omega_n t}(A_1 e^{i\omega_D t} + A_2 e^{-i\omega_D t}) \tag{3.40}$$

where :

$$\omega_D = \omega_n\sqrt{1-\zeta^2} \tag{3.41}$$

The parenthesis term of the Eq. (3.40) can be written using trigonometric functions and calculate the integration constants $A$ and $B$ to fulfil the initial conditions.

$$u(t) = e^{-\zeta\omega_n t}(A\cos\omega_D t + B\sin\omega_D t) \tag{3.42}$$

$$A = 0 \qquad B = \frac{\dot{u}(0) + \zeta\omega_n u(0)}{\omega_D} \tag{3.43}$$

By substituting the Eq. (3.43) to the Eq. (3.42) the final solution is obtained :

$$u(t) = e^{-\zeta\omega_n t}\left[u(0)\cos\omega_D t + \frac{\dot{u}(0) + \zeta\omega_n u(0)}{\omega_D}\sin\omega_D t)\right] \tag{3.44}$$

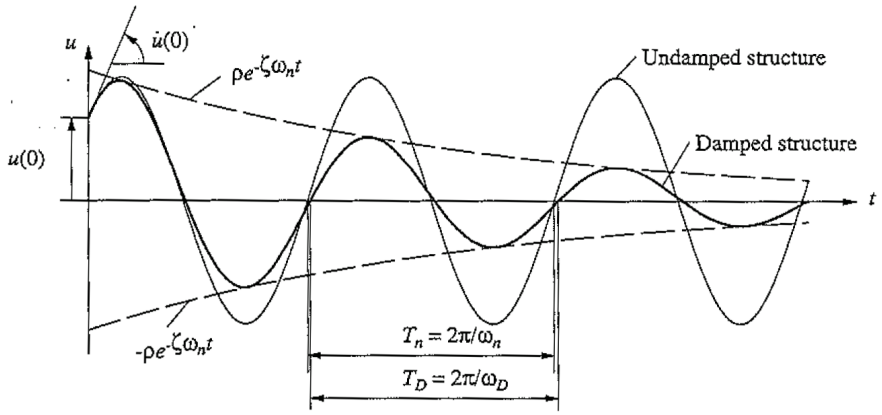


**Figure 3.8:** Effects of damping on free vibration, adopted from [8]

The above solution can be shown in the Fig. (3.8) and the natural period of the damped vibration $T_D = \frac{2\pi}{\omega_D}$ is related to the natural period without damping with:

$$T_D = \frac{T_n}{\sqrt{1-\zeta^2}} \tag{3.45}$$

It was shown in the Fig. (3.8) that the amplitude decays exponentially over time. The envelope curves are $\pm\rho e^{-\zeta\omega_n t}$, where

$$\rho = \sqrt{[u(0)]^2 + \left[\frac{\dot{u}(0) + \zeta\omega_n u(0)}{\omega_D}\right]^2} \tag{3.46}$$

By observing the Fig. (3.9) from [8] it could be concluded that the most important effect of the damping is the rate at which the amplitude decays. For $\zeta = 5\%$ the oscillations after 10-15 natural periods $T_n$ become insignificant.

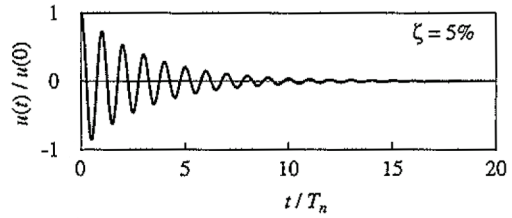


**Figure 3.9:** Free vibration of systems with damping level $\zeta = 5\%$, adopted from [8]

### 3.2.3 Harmonic vibration with viscous damping

In the problem that the CSP method is applied there are external harmonic forces. Harmonic or cosine forces is an alternative approach to simulate earthquake excitation. The differential equation of an SDF system with these type of forces are :

$$m\ddot{u} + c\dot{u} + ku = p_0 \sin\omega t \tag{3.47}$$

$$m\ddot{u} + c\dot{u} + ku = p_0 \cos\omega t \tag{3.48}$$

For both Eq. (3.47) and Eq. (3.48) the particular solution is given by the form :

$$u_p(t) = C\sin\omega t + D\cos\omega t \tag{3.49}$$

where the formulas of the constants $C$ and $D$ are given in [8, 30] for both cases.

The complementary solution of the Eq. (3.47) and Eq. (3.48) is given by the Eq. (3.47). So the complete solution of the Eq. (3.47) and Eq. (3.48) is :

$$u(t) = \underbrace{e^{-\zeta\omega_n t}(A\cos\omega_D t + B\sin\omega_D t)}_{transient} + \underbrace{C\sin\omega t + D\cos\omega t}_{steady\ state} \tag{3.50}$$

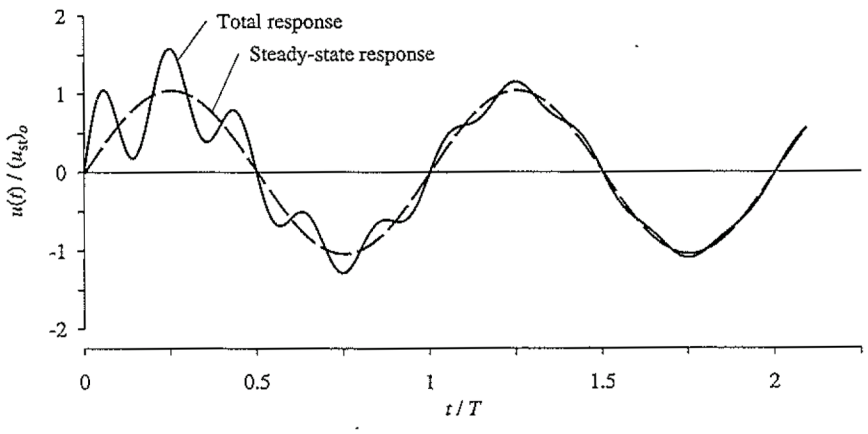


**Figure 3.10:** Response of damped system to harmonic force; $\frac{\omega}{\omega_n} = 0.2$, $\zeta = 0.05$, $u(0) = 0$, and $u(0) = \frac{\omega_n p_0}{k}$, adopted from [8]

The integral constants $A$ and $B$ can be calculated from the initial conditions $u = u(0)$ and $\dot{u} = \dot{u}(0)$. For the case of the harmonic force the Fig. (3.10) from [8] shows how the transient part of the solution steadily tends to 0.

## 3.3 Multiple Degree of Freedom systems

In this section, the general method of creating the system of equations to simulate a whole building will be described. The method is similar with the case of the SDF system. By using the same approach of the equillibrium between external forces and three types of internal forces the Eq. (3.11) can be written as :

$$\mathbf{f}_I + \mathbf{f}_D + \mathbf{f}_s = \mathbf{p}(t) \tag{3.51}$$

where the forces are :

- $\mathbf{f}_I$ are the *inertia forces* related to the displacements $\mathbf{u}$
- $\mathbf{f}_D$ are the *damping forces* related to the velocities $\dot{\mathbf{u}}$
- $\mathbf{f}_s$ are the *elastic forces* related to the accelerations $\ddot{\mathbf{u}}$
- $\mathbf{p}(t)$ are the *external forces*

Because the system is linear the effect of those forces can be added as shown in the Fig. (3.11). The only difference in the case of multiple degrees of freedom(DOF) is that the $\mathbf{f}_I$, $\mathbf{f}_D$, $\mathbf{f}_s$ and $\mathbf{p}(t)$ are vectors of length equal to the number of DOFs. In the following pages of this chapter the method to calculate all the internal forces is presented. Before defining the forces the structure needs to be discretized and the DOFs to be defined.

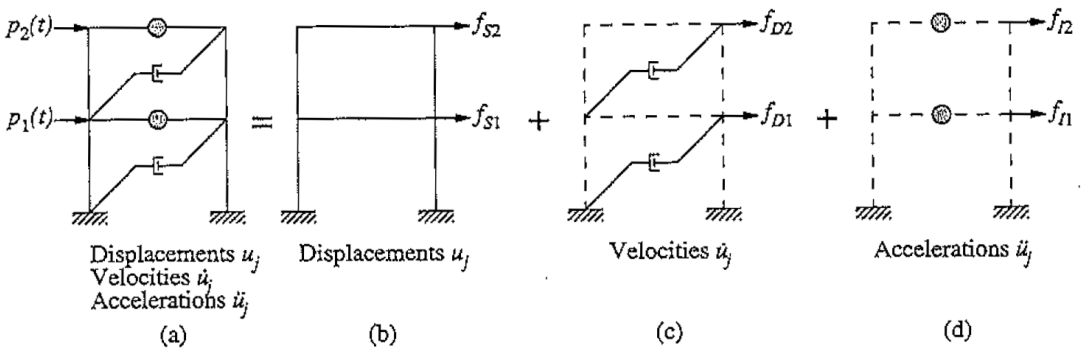


**Figure 3.11:** (a) System, (b) stiffness component, (c) damping components, (d) inertia components, adopted from [8]

### 3.3.1 Discretization

A frame structure can be simulated as an assemblage of beams and columns connected at nodes. The displacements of the nodes are the degrees of freedom. In general, a node in a planar two dimensional frame has three DOFs (two translation and one rotation) as shown in the Fig. (3.12 a). The two storey frame structure of the Fig. (3.12 a) has 6 nodes and 18 DOFs. One reasonable assumption that can reduce the number of DOFs in the frame structure is that the axial deformations can be neglected. So the two storey has finally 8 DOFs shown in the Fig. (3.12 b). The external dynamical loads that are applied shown in the Fig. (3.13). Usually the external moments $p_3(t)$ to $p_8(t)$ are equal to zero.

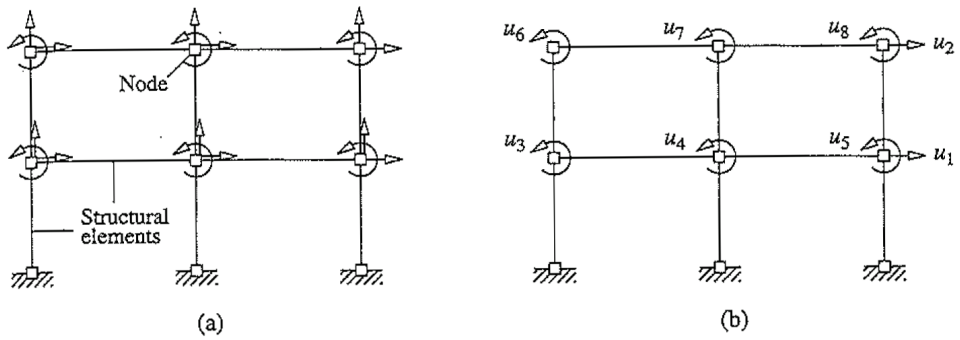


**Figure 3.12:** Degrees of freedom (a) axial deformation included: 18 DOFs, (b) axial deformation neglected: 8 DOFs, adopted from [8]

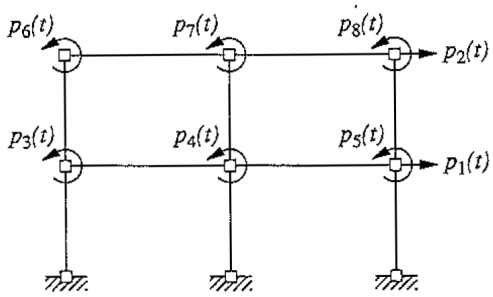


**Figure 3.13:** External dynamic forces, p(t), adopted from [8]

### 3.3.2 Elastic Forces

The external forces $f_{sj}$ will be related on the stiffness component of the structure to the resulting displacements $u_j$ in the Fig. (3.14 a). For linear systems this relationship can be obtained by the method of *superposition* and the concept of *stiffness influence coefficients*.

A unit displacements along DOF $j$ is applied, holding all other DOFs equal to zero as shown in the Fig. (3.14 b,c). The *stiffness influence coefficient* $k_{ij}$ is the force along DOF $i$ due to the unit displacement at DOF $j$ when all the other DOFs are equal to 0. In the Fig. (3.14 b,c) there are the schemes from which the $k_{i1}$ and $k_{i4}$ can be calculated for $(i = 1, 2, ..., 8)$. The calculation of these forces is a structural problem that won't be analysed here. To calculate the elastic force $f_{sj}$ at DOF $i$ the formula is used:

$$f_{si} = \sum_{j=1}^{N} k_{ij} u_j \tag{3.52}$$

where $N$ is the number of the DOFs.

The Eq. (3.52) exists for every $i = 1$ to $N$. The systems of those $N$ equations can be written in matrix form :

$$\begin{bmatrix} f_{s1} \\ f_{s2} \\ \vdots \\ f_{sN} \end{bmatrix} = \begin{bmatrix} k_{11} & k_{12} & \dots & k_{1N} \\ k_{21} & k_{22} & \dots & k_{2N} \\ \vdots & \vdots & \ddots & \vdots \\ k_{N1} & k_{N2} & \dots & k_{NN} \end{bmatrix} \begin{Bmatrix} u_1 \\ u_2 \\ \vdots \\ u_N \end{Bmatrix} \tag{3.53}$$

or

$$\mathbf{f}_s = \mathbf{k}\mathbf{u} \tag{3.54}$$

where $\mathbf{k}$ is the stiffness matrix of the building and is a symmetric matrix $(k_{ij} = k_{ji})$ [8].

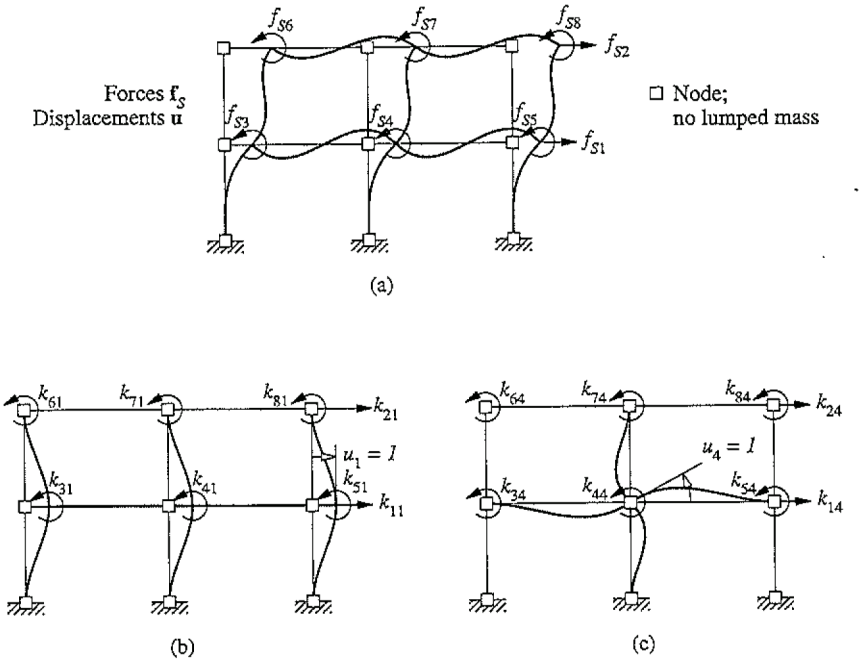


**Figure 3.14:** (a) Stiffness component of frame, (b) stiffness influence coefficients for $u_1 = 1$, (c) stiffness coefficients for $u_4 = 1$, adopted from [8]

The stiffness matrix **k** for a discretized system is a structural problem and can be solved by many methods. [7,10,19,35] The most commonly used method is the *direct stiffness method* wherein the stiffness matrices of individual elements are assembled to obtain the structural stiffness matrix. Therefore, this method will not be developed in this dissertation but can be found in [7, 10, 19, 35].

### 3.3.3 Damping Forces

As mentioned in the section (3.1.4) there are mechanics that consume the system energy and can be simulated with *equivalent viscous damping*. With this assumption the external forces $f_{Dj}$ acting on the damping components of the structure are related to the velocities $\dot{u}_j$ in Fig. (3.15). A unit velocity along DOF j is applied while the velocities on all the other DOFs are kept zero. The *damping influence coefficient* $c_{ij}$ is the external force in DOF $i$ due to unit velocity in DOF $j$. In similar way as the elastic forces were calculated, here the damping forces $f_{Di}$ that resist to those velocities can be calculated using the following formula :

$$f_{Di} = \sum_{j=1}^{N} c_{ij}\dot{u}_j \tag{3.55}$$

where $N$ is the number of the DOFs.

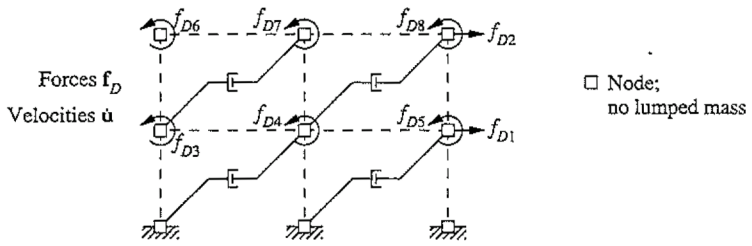


**Figure 3.15:** Damping component of frame structure, adopted from [8]

The Eq. (3.55) exists for every $i = 1$ to $N$. The systems of those $N$ equations can be written in matrix form :

$$\begin{bmatrix} f_{D1} \\ f_{D2} \\ \vdots \\ f_{DN} \end{bmatrix} = \begin{bmatrix} c_{11} & c_{12} & \dots & c_{1N} \\ c_{21} & c_{22} & \dots & c_{2N} \\ \vdots & \vdots & \ddots & \vdots \\ c_{N1} & c_{N2} & \dots & c_{NN} \end{bmatrix} \begin{Bmatrix} \dot{u}_1 \\ \dot{u}_2 \\ \vdots \\ \dot{u}_N \end{Bmatrix} \tag{3.56}$$

or

$$\mathbf{f}_D = \mathbf{c}\dot{\mathbf{u}} \tag{3.57}$$

where $\mathbf{c}$ is the damping matrix of the building.

The damping matrix $\mathbf{c}$ is impractical to calculate for systems with multiple degrees of freedom (MDF). Therefore, damping for MDF systems is generally specified by numerical values for the damping rations, as for SDF systems. There are methods in [8, 29, 30] that are trying to construct the damping matrix from known *damping ratios*.

### 3.3.4 Inertia Forces

The external forces $f_{Ij}$ acting on the mass component of the structure are related to the accelerations $\ddot{u}_j$. A unit acceleration along DOF $j$ is applied, while the accelerations in all other DOFs are kept zero. According to *D'Alembert's principle* [7, 10, 19, 35], inertia forces oppose these accelerations. The mass influence coefficient $m_{ij}$ is the external force in DOF $i$ due to unit acceleration in DOF $j$. In similar way as the elastic forces and the damping forces were calculated, here the inertia forces $f_{Ii}$ that resist to those accelerations can be calculated using the following formula :

$$f_{Ii} = \sum_{j=1}^{N} m_{ij}\ddot{u}_j \tag{3.58}$$

where $N$ is the number of the DOFs.

The Eq. (3.58) exists for every $i = 1$ to $N$. The systems of those $N$ equations can be written in matrix form :

$$\begin{bmatrix} f_{I1} \\ f_{I2} \\ \vdots \\ f_{IN} \end{bmatrix} = \begin{bmatrix} m_{11} & m_{12} & \dots & m_{1N} \\ m_{21} & m_{22} & \dots & m_{2N} \\ \vdots & \vdots & \ddots & \vdots \\ m_{N1} & m_{N2} & \dots & m_{NN} \end{bmatrix} \begin{Bmatrix} \ddot{u}_1 \\ \ddot{u}_2 \\ \vdots \\ \ddot{u}_N \end{Bmatrix} \tag{3.59}$$

or

$$\mathbf{f}_I = \mathbf{m}\ddot{\mathbf{u}} \tag{3.60}$$

where $\mathbf{m}$ is the mass matrix of the building and is a symmetric matrix ($m_{ij} = m_{ji}$) [7,8,10,19,35].

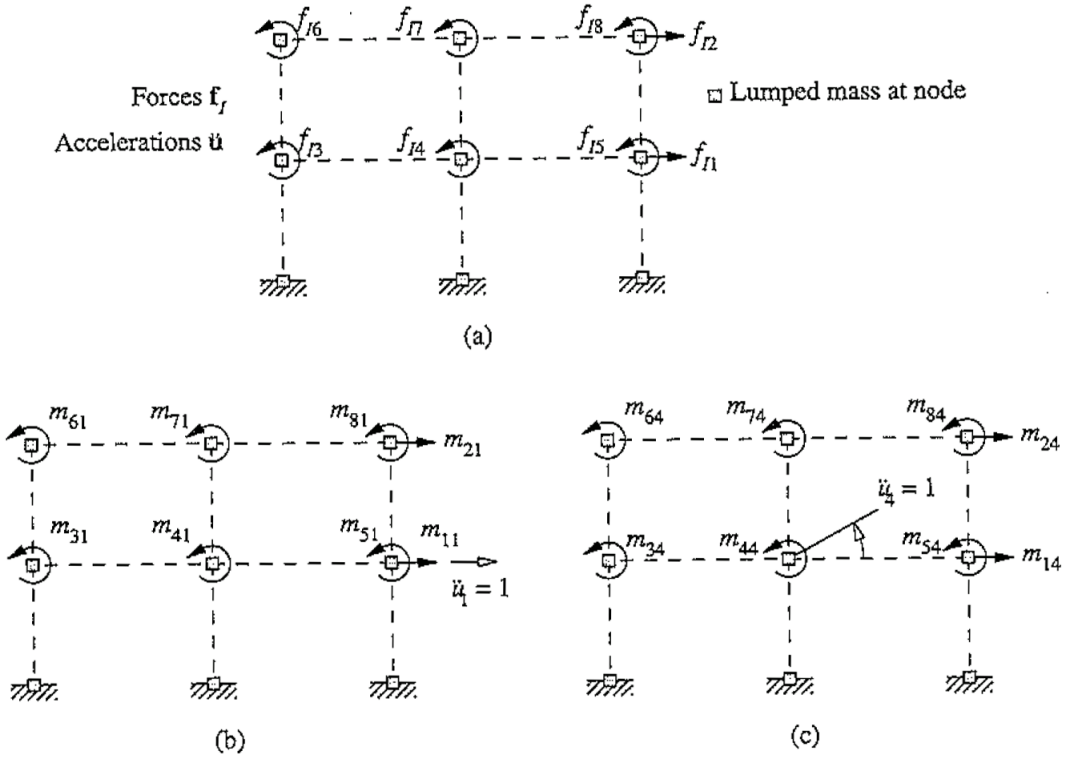


**Figure 3.16:** (a) Mass component of frame, (b) mass influence coefficients for $\ddot{u}_1 = 1$, (c) mass influence coefficients for $\ddot{u}_4 = 1$, adopted from [8]

The mass is distributed throughout actual stuctures but it can be simulated with conscentrated masses on the nodes of the discretized structure. As shown in the Fig. (3.16 a) in a frame structure the masses of each structural element are divided to the closest nodes. In this frame structure the masses of the nodes don't interact with each other for the 8 DOFs of the structure. Also the unit accelerations $\ddot{u}_1 = 1$ and $\ddot{u}_2 = 1$ activate the masses $a, b, c$ and $d, e, f$ respectively. But the unit accelerations $\ddot{u}_j = 1$ for $j = 3, 4, ..., 8$ don't activate any mass movements as shown in the Fig. (3.16 c) for $\ddot{u}_4 = 1$. All the above can be written as :

$$m_{11} = m_a + m_b + m_c \qquad m_{22} = m_d + m_e + m_f \qquad m_{jj} = 0 \quad for \quad j = 3, 4, ..., 8 \tag{3.61}$$

$$m_{ij} = 0 \qquad i \neq j \tag{3.62}$$

By using the Eq. (3.51), Eq. (3.54), Eq. (3.57) and the Eq. (3.60) the system of equations for the MDF system was derived :

$$\mathbf{m\ddot{u} + c\dot{u} + ku} = \mathbf{p}(t) \tag{3.63}$$

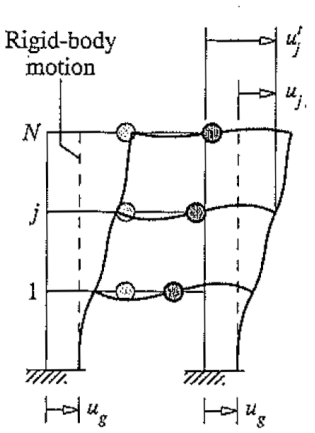


**Figure 3.17:** Building frame, adopted from [8]

### 3.3.5 Equation of motion:Earthquake excitation

Many building have slabs that are very stiff with respect to the other structural elements. In this case a valid assumption can be that the mass is concentrated in every slab as shown in the Fig. (3.17). Then the dynamical equation before the earthquake excitation is the Eq. (3.63) with $\mathbf{p}(t) = \mathbf{0}$ :

$$\mathbf{m\ddot{u} + c\dot{u} + ku} = \mathbf{0} \tag{3.64}$$

By using the same method from the section (3.1.6) a vector of effective earthquake forces $\mathbf{p}_{eff}(t)$ [8, 10, 19, 20] can be created that is consisted from the forces shown in the Fig. (3.18). By creating a vector $\mathbf{m}_{eff}$ that is equal to the masses of each slab in the DOFs that correspond to the horizontal DOFs of theses masses and is equal to 0 for all other DOFs :

$$\mathbf{p}_{eff}(t) = -\mathbf{m}_{eff}\ddot{u}_g(t) \tag{3.65}$$

$$\mathbf{m}\ddot{\mathbf{u}} + \mathbf{c}\dot{\mathbf{u}} + \mathbf{k}\mathbf{u} = -\mathbf{m}_{eff}\ddot{u}_g(t) \tag{3.66}$$

The above equation is the generalization of the Eq. (3.13) for MDF system like the one in the Fig. (3.18).

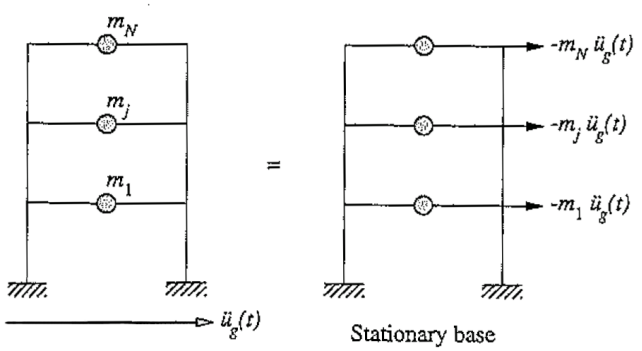


**Figure 3.18:** Effective earthquake forces, adopted from [8]

# Chapter 4

# Model reduction methods of large-scale systems

From the theory of the problem that presented in chapter (3) it was shown that the system of differential equations that simulate the behaviour of a structure is :

$$\mathbf{m\ddot{u}} + \mathbf{c\dot{u}} + \mathbf{ku} = \mathbf{p}(t) \tag{4.1}$$

This equation is a system of second order *elliptic differential equation* that are extensively studied in [7, 8, 19, 20, 35]. There are numerous methods to solve the system of the Eq. (4.1). The problem that appears in many applications, is the number of equations $n$ can get quite large. Direct numerical simulations can be difficult due to :

- memory
- time limitation
- ill-conditioning

In [38, 39] there are techniques to moderate the above problems (e.g. like skyline storage integration, clever new algorithms that require less time, preconditioning e.t.c.). Although those techniques can be very efficient, for really large-scale problems they are still not enough. This is the reason *model reduction* methods are needed.

This dissertation will focus on the *Computational Singular Perturbation* (CSP) method that is a multi time scale method. As mentioned in chapter (2) this method can decouple the fast time scales from the slow ones. In this way a system that is much smaller than the starting one is achieved. Therefore the time needed to get a solution can drastically decreased. Alongside with that much less computational power and computer memory are needed.

In this chapter some methods that achieve model reduction will be mentioned. By searching the bibliography many different methods were found and most of them can be distinguished in the following categories [4, 16] :

- Singural value decomposition (SVD) gramian based methods
- Krylov moment matching based methods
- SVD gramian - Krylov moment matching based methods

Specifically, for solving a large-scale system that describes the behaviour of a building there are methods that can use useful information about this type of systems to achieve model reduction, such as the building slabs work as rigid diaphragms and the seismic forces are applied horizontally in every slab of the structure as shown in Fig (3.18). Those methods are based on the *modal analysis* of the general system. They can reduce the number of DOFs and use and calculate only the important *natural frequencies* and *natural nodes* and approximate the others. One such method is *Rayleigh-Ritz* method.

## 4.1 State space form

In [16] in order to study those systems they rewrite them in the *state space form*. The *state space form* of *single-input-single-output*(SISO) systems that are *linear time invariant* (LTI) is :

$$\mathbf{\Sigma}: \begin{cases} \sigma \mathbf{x}(t) = \mathbf{A}\mathbf{x}(t) + \mathbf{b}u(t) \\ y(t) = \mathbf{c}\mathbf{x}(t) + du(t) \end{cases} \Leftrightarrow \mathbf{\Sigma} := \left[\begin{array}{c|c} \mathbf{A} & \mathbf{b} \\ \hline \mathbf{c} & d \end{array}\right] \tag{4.2}$$

where $\mathbf{A} \in \mathbb{R}^{n\times n}$, $\mathbf{b} \in \mathbb{R}^n$, $\mathbf{c}^T \in \mathbb{R}^n$, $d \in \mathbb{R}$ and $\sigma$ denotes the derivative operator for the continuous time systems. In Eq. (4.2) the $\mathbf{x}(t) \in \mathbb{R}^n$ is the *state*, $u(t) \in \mathbb{R}$ is the input and $y(t) \in \mathbb{R}$ is the *output* of the system $\mathbf{\Sigma}$. The above formulation can be easily generalised for multiple inputs of outputs. These problems can be named as *single-input-multi-output* (SIMO) or *multi-input-multi-output* (MIMO) in [43]. Below there are some important properties about LTI systems.

The *transfer function* $G(s)$ of $\mathbf{\Sigma}$ is given by :

$$G(s) = \mathbf{c}(s\mathbf{I} - \mathbf{A})^{-1}\mathbf{b} + d \tag{4.3}$$

The *transfer function* $G(s)$ can be derived by applying a Laplace transform to the first part of the Eq. (4.2):

$$\dot{\mathbf{x}}(t) = \mathbf{A}\mathbf{x}(t) + \mathbf{b}u(t) \tag{4.4}$$

which yields :

$$s\mathbf{x}(s) - \mathbf{x}(0) = \mathbf{A}\mathbf{x}(s) + \mathbf{b}u(s) \tag{4.5}$$

Then by solving the Eq. (4.5) for $x(s)$ follows :

$$\mathbf{x}(s) = (s\mathbf{I} - \mathbf{A})^{-1}\mathbf{x}(0) + (s\mathbf{I} - \mathbf{A})^{-1}\mathbf{b}u(s) \tag{4.6}$$

By substituting the Eq. (4.5) with assuming with the initial condition $x(0) = 0$ to the second part of the Eq. (4.2):

$$y(s) = \mathbf{c}\mathbf{x}(s) + du(s) = \mathbf{c}(s\mathbf{I} - \mathbf{A})^{-1}\mathbf{b}u(s) + du(s) = (\mathbf{c}(s\mathbf{I} - \mathbf{A})^{-1}\mathbf{b} + d)u(s) = G(s)u(s) \tag{4.7}$$

The Eq. (4.7) shows that there is a map from $u$ to $y$ with the *transfer function* $G(s)$ of the Eq. (4.3). For the system $\mathbf{\Sigma}$ in the Eq. (4.2) there are tests for *controllability* and *observability* in [43].

### 4.1.1 Controllability

*Controllability* is an important property of a control system, and the *controllability* property plays a crucial role in many control problems, such as stabilization of unstable systems by feedback, or optimal control.

*State controllability condition* implies that it is possible by admissible inputs to steer the states from any initial value to any final value within some finite time window [43]. A continuous time-invariant linear state-space model Eq. (4.2) is *controllable* if and only if :

$$rank \begin{bmatrix} \mathbf{b} & \mathbf{A}\mathbf{b} & \dots & \mathbf{A}^{n-1}\mathbf{b} \end{bmatrix} = n \tag{4.8}$$

### 4.1.2 Observability

*Observability* is a measure for how well internal states of a system can be inferred by knowledge of its external outputs. The *observability* and *controllability* of a system are mathematical duals [43] (i.e., as *controllability* provides that an input is available that brings any initial state to any desired final state, *observability* provides that knowing an output trajectory provides enough information to predict the initial state of the system) [43].

A continuous time-invariant linear state-space model Eq. (4.2) is *observable* if and only if :

$$rank \begin{bmatrix} \mathbf{c} \\ \mathbf{c}\mathbf{A} \\ \vdots \\ \mathbf{c}\mathbf{A}^{n-1} \end{bmatrix} = n \tag{4.9}$$

### 4.1.3 Reduced order models

The goal of *model reduction* is to produce a lower dimensional system , with reduced storage requirements and evaluation time. The *reduced system* will be used instead of the original one for the simulations or even help to develop a low dimensional controller suitable for real time applications.

The *reduced order system* $\mathbf{\Sigma}_r$ of the LTI dynamical system $\mathbf{\Sigma}$ is given by :

$$\mathbf{\Sigma}_r : \begin{cases} \dot{\mathbf{x}}_r(t) = \mathbf{A}_r\mathbf{x}_r(t) + \mathbf{b}_r u(t) \\ y_r(t) = \mathbf{c}_r\mathbf{x}_r(t) + d_r u(t) \end{cases} \Leftrightarrow \mathbf{\Sigma}_r := \left[\begin{array}{c|c} \mathbf{A}_r & \mathbf{b}_r \\ \hline \mathbf{c}_r & d_r \end{array}\right] \tag{4.10}$$

where $\mathbf{A}_r \in \mathbb{R}^{r\times r}$, $\mathbf{b}_r \in \mathbb{R}^r$, $\mathbf{c}_r^T \in \mathbb{R}^r$, $d_r \in \mathbb{R}$ where the order of the reduced system is $r \ll n$ such the following properties are satisfied [4, 16] :

- The approximation error $\|y - y_r\|$ is small, and the global error is bounded
- Stability and other system properties are preserved
- The procedure is computationally stable and efficient

The system $\mathbf{\Sigma}_r$ is constructed by *oblique projection*. The method include the construction of the matrices $\mathbf{V} \in \mathbb{R}^{n\times r}$ and $\mathbf{Z} \in \mathbb{R}^{n\times r}$ with $\mathbf{Z}^T\mathbf{V} = \mathbf{I}_r$

$$\mathbf{\Sigma}_r : \mathbf{A}_r = \mathbf{Z}^T\mathbf{A}\mathbf{V}, \qquad \mathbf{b}_r = \mathbf{Z}^T\mathbf{b}, \qquad \mathbf{c}_r = \mathbf{c}\mathbf{V}, \qquad d_r = d \tag{4.11}$$

By proving that $(\mathbf{V}\mathbf{Z}^T)^2 = \mathbf{V}\mathbf{Z}^T$ shows that $\mathbf{V}\mathbf{Z}^T$ is an *oblique projector* due to the definition in [4, 16, 43] :

$$(\mathbf{V}\mathbf{Z}^T)^2 = \mathbf{V}\mathbf{Z}^T\mathbf{V}\mathbf{Z}^T = \mathbf{V}\mathbf{I}_r\mathbf{Z}^T = \mathbf{V}\mathbf{Z}^T \tag{4.12}$$

### 4.1.4 Dynamical equations in state-space form

The dynamical equation shown in the Eq. (3.63) can be written as follows :

$$\ddot{\mathbf{u}}(t) = \mathbf{m}^{-1}\mathbf{p}(t) - \mathbf{m}^{-1}\mathbf{c}\dot{\mathbf{u}}(t) - \mathbf{m}^{-1}\mathbf{k}\mathbf{u}(t) \tag{4.13}$$

This system of equation can be written in the form of the LTI system $\mathbf{\Sigma}$ of the Eq. (4.2) in the following manner :

$$\begin{bmatrix} \dot{\mathbf{x}}_1(t) \\ \dot{\mathbf{x}}_2(t) \end{bmatrix} = \begin{bmatrix} \mathbf{0}_{n,n} & \mathbf{I}_{n,n} \\ -\mathbf{m}^{-1}\mathbf{k} & -\mathbf{m}^{-1}\mathbf{c} \end{bmatrix} \begin{bmatrix} \mathbf{x}_1(t) \\ \mathbf{x}_2(t) \end{bmatrix} + \begin{bmatrix} \mathbf{0}_{n,n} \\ \mathbf{m}^{-1} \end{bmatrix} \mathbf{u}(t) \tag{4.14}$$

$$\mathbf{y}(t) = \begin{bmatrix} \mathbf{I}_{n,n} & \mathbf{0}_{n,n} \end{bmatrix} \begin{bmatrix} \mathbf{x}_1(t) \\ \mathbf{x}_2(t) \end{bmatrix} \tag{4.15}$$

where the $\mathbf{x}_1(t)$ is the displacement vector, the $\mathbf{x}_2(t)$ is the velocities vector and $\mathbf{y}(t)$ is a vector that contains the $n$ displacements of $\mathbf{x}_1(t)$ and $n$ zeros. This is a SIMO system. The SISO case of the problem can be found in [16]. Below it was proved that the above system is *observable* and *controllable*.
The *observability test* for the above system :

$$rank \begin{bmatrix} \mathbf{b} & \mathbf{A}\mathbf{b} \end{bmatrix} = rank \begin{bmatrix} \begin{bmatrix} \mathbf{0}_{n,n} \\ \mathbf{m}^{-1} \end{bmatrix} & \begin{bmatrix} \mathbf{0}_{n,n} & \mathbf{I}_{n,n} \\ -\mathbf{m}^{-1}\mathbf{k} & -\mathbf{m}^{-1}\mathbf{c} \end{bmatrix} \begin{bmatrix} \mathbf{0}_{n,n} \\ \mathbf{m}^{-1} \end{bmatrix} \end{bmatrix} = rank \begin{bmatrix} \mathbf{0}_{n,n} & \mathbf{m}^{-1} \\ \mathbf{m}^{-1} & -\mathbf{m}^{-2}\mathbf{c} \end{bmatrix} \tag{4.16}$$

which is full rank for all $\mathbf{c}$ and all $\mathbf{m}$ that are damping and mass matrices respectively.
The *controllability test* for the above system :

$$rank \begin{bmatrix} \mathbf{c} \\ \mathbf{c}\mathbf{A} \end{bmatrix} = rank \begin{bmatrix} \begin{bmatrix} \mathbf{I}_{n,n} & \mathbf{0}_{n,n} \end{bmatrix} \\ \begin{bmatrix} \mathbf{I}_{n,n} & \mathbf{0}_{n,n} \end{bmatrix} \begin{bmatrix} \mathbf{0}_{n,n} & \mathbf{I}_{n,n} \\ -\mathbf{m}^{-1}\mathbf{k} & -\mathbf{m}^{-1}\mathbf{c} \end{bmatrix} \end{bmatrix} = rank \begin{bmatrix} \mathbf{0}_{n,n} & \mathbf{I}_{n,n} \\ \mathbf{I}_{n,n} & \mathbf{0}_{n,n} \end{bmatrix} \tag{4.17}$$

which is full rank for all $\mathbf{c}$ and all $\mathbf{m}$ that are damping and mass matrices respectively.

## 4.2 SVD gramians based methods

The *SVD gramians* based methods are using the following mathematical knowledge to achieve order reduction of the system $\mathbf{\Sigma}$ in Eq. (4.2):

- Singular Value Decomposition (SVD)
- Hankel singular values
- Gramians of Lyapunov equations

One common SVD methods in [3,4,16] is *Balanced Model Reduction*. Other methods are *Hankel Norm Approximation* and *Balanced Singular Perturbation Approximation* [3, 4, 16]. The *Balanced Model Reduction* methods diagonalises the system *gramians* that correspond to some particular *Lyapunov equations* and then transforms the system to a basis [3, 4, 16, 43]. Afterwards, the states that are difficult to reach are truncated. This is the reason why the method maintains *system stability* and provides approximation error bounds. The disadvantage of the *SVD gramians* based methods is that for large-scale problems requires high computer power and memory because the *SVD factorization* creates dense matrices. Applications of the *balancing model reduction* appear in [3, 4, 16].

### 4.2.1 Singular Value Decomposition (SVD)

*Singular value decomposition* takes a rectangular matrix $\mathbf{A}$ ($\mathbf{A}$ is a $n \times p$ matrix) and can decompose it in the following way [33, 43]:

$$\mathbf{A}_{n\times p} = \mathbf{U}_{n\times n}\mathbf{S}_{n\times p}\mathbf{V}^T_{p\times p} \tag{4.18}$$

where $\mathbf{U}$ and $\mathbf{V}$ are *orthogonal* matrices such that $\mathbf{U}^T\mathbf{U} = \mathbf{I}_{n\times n}$ and $\mathbf{V}^T\mathbf{V} = \mathbf{I}_{p\times p}$

The columns of $\mathbf{U}$ are the *left singular vectors*, the $\mathbf{S}$ contains the *singular values* and is a diagonal matrix and the rows of $\mathbf{V}^T$ are the *right singular vectors*.

Calculating the SVD of a matrix $\mathbf{A}$ consists of finding the *eigenvalues* and *eigenvectors* of $\mathbf{A}\mathbf{A}^T$ and $\mathbf{A}^T\mathbf{A}$. The *eigenvectors* of $\mathbf{A}^T\mathbf{A}$ make up the columns of $\mathbf{V}$ and the *eigenvectors* of $\mathbf{A}\mathbf{A}^T$ make up the columns of $\mathbf{U}$. Also, the *singular values* in $\mathbf{S}$ are square roots of *eigenvalues* from $\mathbf{A}\mathbf{A}^T$ or $\mathbf{A}^T\mathbf{A}$ . The *singular values* are the diagonal entries of the $\mathbf{S}$ matrix and are arranged in descending order. The *singular values* are always real and nonegative numbers because the matrices $\mathbf{A}\mathbf{A}^T$ and $\mathbf{A}^T\mathbf{A}$ are *Hermitian* and *positive semidefinite* . If the matrix $\mathbf{A}$ is a real matrix, then $\mathbf{U}$ and $\mathbf{V}$ are also real.

The proof of the SVD is :

$$\left.\begin{aligned}\mathbf{A} &= \mathbf{U}\mathbf{S}\mathbf{V}^T\\ \mathbf{A}^T &= \mathbf{V}\mathbf{S}\mathbf{U}^T\end{aligned}\right\} \Leftrightarrow \mathbf{A}^T\mathbf{A} = \mathbf{V}\mathbf{S}\mathbf{U}^T\mathbf{U}\mathbf{S}\mathbf{V}^T = \mathbf{V}\mathbf{S}^2\mathbf{V}^T \Leftrightarrow \mathbf{A}^T\mathbf{A}\mathbf{V} = \mathbf{V}\mathbf{S}^2 \tag{4.19}$$

The *Singular Value Decomposition* of a matrix $\mathbf{A}$ helps by simplifying various equations because the transpose $\mathbf{A}^T$ and inverse $\mathbf{A}^{-1}$ matrices can be described by :

$$\mathbf{A}^T = \mathbf{V}\mathbf{S}\mathbf{U}^T \qquad and \qquad \mathbf{A}^{-1} = \mathbf{V}\mathbf{S}^{-1}\mathbf{U}^T \tag{4.20}$$

where $\mathbf{S}^T = \mathbf{S}$ and $\mathbf{S}^{-1}$ can be calculated easily because $\mathbf{S}$ is diagonal and $\mathbf{V}^{-T} = \mathbf{V}$ and $\mathbf{U}^{-1} = \mathbf{U}^T$ because $\mathbf{U}$ and $\mathbf{V}$ are *orthogonal* matrices.

### 4.2.2 Gramians and Hankel singular values

For the LTI continuous time system $\mathbf{\Sigma}$ in Eq. (4.2) there are the corresponding continuous time *Lyapunov Equations* [3, 4, 15, 16, 33, 43] :

$$\mathbf{A}\boldsymbol{\mathcal{P}} + \boldsymbol{\mathcal{P}}\mathbf{A}^T + \mathbf{b}\mathbf{b}^T = 0 \qquad and \qquad \mathbf{A}^T\boldsymbol{\mathcal{L}} + \boldsymbol{\mathcal{L}}\mathbf{A} + \mathbf{c}^T\mathbf{c} = 0 \tag{4.21}$$

where $\boldsymbol{\mathcal{P}}, \boldsymbol{\mathcal{L}} \in \mathbb{R}^{n\times n}$. If the system $\mathbf{\Sigma}$ in Eq. (4.2) is *asymptotically stable* and *minimal* it is known from [3, 4, 15, 16, 33, 43] that the solutions to the Eqs. (4.21) give the *reachability* and *observability gramians* respectively, and are *unique symmetric positive definite*.

The *Hankel singular values* $\sigma_i(\mathbf{\Sigma})$ that correspond to the system $\mathbf{\Sigma}$ are the square roots of the eigenvalues of the product $\boldsymbol{\mathcal{P}}\boldsymbol{\mathcal{L}}$ :

$$\sigma_i(\mathbf{\Sigma}) = \sqrt{\lambda_i(\boldsymbol{\mathcal{P}}\boldsymbol{\mathcal{L}})} \tag{4.22}$$

### 4.2.3 Balanced Reduction method

The minimal and asymptotically stable system $\mathbf{\Sigma}$ is *balanced* when the *reachability* and *observability gramians* are :

$$\boldsymbol{\mathcal{P}} = \boldsymbol{\mathcal{L}} = \mathbf{\Sigma} = diag(\sigma_1\mathbf{I}_{m_1}, \sigma_2\mathbf{I}_{m_2}, \ldots, \sigma_q\mathbf{I}_{m_q}) \tag{4.23}$$

where $q$ is the number of distinct *Hankel singular values* that are putted in descending order and the $m_i$ are the *multiplicities* of $\sigma_i$ and obviously $\sum_{i=1}^{q} m_i = n$. The *gramians* $\boldsymbol{\mathcal{P}}$ and $\boldsymbol{\mathcal{L}}$ are positive definite matrices so by diagonalizing them the Eq. (4.23) can be achieved. By truncating from the system the states that correspond to the smaller *Hanker values*, the parts that are less reachable and observable are removed since the system is *balanced* [16]. But this method can be computationally demanding for large-scale systems and can be unsuccessful due to *ill -condition*. The solution to those problems is actually balancing the reduced order system instead of the initial one.

The *gramians* $\boldsymbol{\mathcal{P}}$ and $\boldsymbol{\mathcal{L}}$ are symmetric positive definite matrices. For every symmetric positive definite matrix $\mathbf{A}$ it is true that $\mathbf{A} = \mathbf{A}^T$ and using the *eigen decomposition* method it can be written as $\mathbf{A} = \mathbf{Q}\Lambda\mathbf{Q}^T$ where $\mathbf{Q}$ is orthogonal and $\mathbf{\Lambda}$ is a diagonal matrix contains all the eigenvalues which are real. By letting $\mathbf{B} = \mathbf{Q}\mathbf{\Lambda}^{\frac{1}{2}}$ its easy to see that the matrix $\mathbf{A}$ can be written as $\mathbf{A} = \mathbf{B}\mathbf{B}^T$. Let

$\mathbf{U}$ and $\mathbf{L}$ such as $\boldsymbol{\mathcal{P}} = \mathbf{U}\mathbf{U}^T$ and $\boldsymbol{\mathcal{L}} = \mathbf{L}\mathbf{L}^T$. In [16] is shown that the SVD repsesentation of $\mathbf{U}_T\mathbf{L}$ is $\mathbf{U}_T\mathbf{L} = \mathbf{X}\boldsymbol{\Sigma}\mathbf{Y}^T$ where $\boldsymbol{\Sigma}$ is given in the Eq. (4.23). By selecting the first $r$ important states such that $r = \sum_{i=1}^{k} m_i$ the matrix $\boldsymbol{\Sigma}_1$ is defined as follows :

$$\boldsymbol{\Sigma}_1 = diag(\sigma_1\mathbf{I}_{m_1}, \sigma_2\mathbf{I}_{m_2}, \ldots, \sigma_k\mathbf{I}_{m_k}) \tag{4.24}$$

Similarly, the $\mathbf{X}_1$ and $\mathbf{Y}_1$ are defined the matrices with the first $r$ columns of $\mathbf{X}$ and $\mathbf{Y}$ respectively. The *reduced order system* $\boldsymbol{\Sigma}_r$ of the Eq. (4.11) is derived by the use of two suitable matrices $\mathbf{V} \in \mathbb{R}^{n\times r}$ and $\mathbf{Z} \in \mathbb{R}^{n\times r}$ with $\mathbf{Z}^T\mathbf{V} = \mathbf{I}_r$ and they are defined as follows:

$$\mathbf{V} = \mathbf{U}\mathbf{X}_1\boldsymbol{\Sigma}_1^{-\frac{1}{2}} \qquad and \qquad \mathbf{Z} = \mathbf{L}\mathbf{Y}_1\boldsymbol{\Sigma}_1^{-\frac{1}{2}} \tag{4.25}$$

The resulted system $\boldsymbol{\Sigma}_r$ is shown in [3, 16] that is *balanced* and *asymptotically stable* with the use of the *Lyapunov equations* shown in Eq. (4.21).

## 4.3 Krylov moment matching based methods

The key ingredient of those methods are the *moments* of the *transfer function* $G(s)$ of the system $\boldsymbol{\Sigma}$ shown in the Eq. (4.3). Below the *transfer function* $G(s)$ is expanded around a point $\sigma \in \mathbb{C}$. The $k^{th}$ *moment* of the system is the $k^{th}$ derivative of the *transfer function* $G(s)$. One method that is based on the *moments* [3, 4, 16] is *rational Krylov method*. The expansion of G(s) around a point $\sigma \in \mathbb{C}$ which is not a *pole* of the system $\boldsymbol{\Sigma}$ is:

$$\begin{aligned} G(s) &= \mathbf{c}(\sigma\mathbf{I} - \mathbf{A} - (\sigma - s)\mathbf{I})^{-1}\mathbf{b} + d \\ &= \mathbf{c}(\mathbf{I} - \sigma\mathbf{I} - \mathbf{A})^{-1}(\sigma - s))^{-1}(\sigma\mathbf{I} - \mathbf{A})^{-1}\mathbf{b} + d \\ &= \eta_\sigma^{(0)} + \eta_\sigma^{(1)}(\sigma - s) + \eta_\sigma^{(2)}(\sigma - s)^2 + \ldots \\ &= \sum_{j=0}^{\infty} \eta_\sigma^{(j)}(\sigma - s)^j \end{aligned} \tag{4.26}$$

where $\eta_\sigma^{(j)}$ is the $j^{th}$ *moment* of system $\boldsymbol{\Sigma}$ about $\sigma$ for $j \geq 0$ and is given by the following formulas [3, 4, 16, 33, 43] :

$$\eta_\sigma^{(0)} = \mathbf{c}(\sigma\mathbf{I} - \mathbf{A})^{-1}\mathbf{b} + d \qquad and \qquad \eta_\sigma^{(j)} = \mathbf{c}(\sigma\mathbf{I} - \mathbf{A})^{-(j+1)}\mathbf{b} \tag{4.27}$$

for $j = 1, 2, \ldots$ if $\sigma \neq \infty$.

$$\eta^{(0)} = d \qquad and \qquad \eta^{(j)} = \mathbf{c}(\mathbf{A})^{j-1}\mathbf{b} \tag{4.28}$$

for $j = 1, 2, \ldots$ if $\sigma = \infty$.

The goal in this method is to find a *reduced order system* $\mathbf{\Sigma}_r$ with *transfer function* $G_r(s)$ :

$$G_r(s) = \hat{\eta}_\sigma^{(0)} + \hat{\eta}_\sigma^{(1)}(\sigma - s) + \hat{\eta}_\sigma^{(2)}(\sigma - s)^2 + \dots \tag{4.29}$$

such that for an appropriate $k$,the first $k$ *moments* of the *reduced system* $\mathbf{\Sigma}_r$ are matching the first $k$ *moments* of the system $\mathbf{\Sigma}$ :

$$\eta_\sigma^{(j)} = \hat{\eta}_\sigma^{(j)} \quad for \quad j = 0, 1, 2, \dots, k \tag{4.30}$$

For the special case where $\sigma = \infty$ the moments are called *Markov parameters* and the moment matching problem is called *partial realization* [3,4,16]. The general moment matching problem can be solved in a recursive and numerical stable way, by the *Lanczos* or *Arnoldi* procedures [38,39]. If the $\sigma \in \mathbb{C}$ is an arbitary frequency then the problem becomes the *rational interpolation problem* [3,4,16] . There are numerous methods to solve the moment matching problems and some of them try to get interpolation for many $\sigma$ [3,4,16]. Although there is no guarantee of a bound of the local and the global error. The advantage of the methods is that they are numerically reliable close to $\sigma$ because it is an iterative method and it requires much less memory and computational power that the *SVD gramians* based methods because they don't require the factorization and storage of dense matrices.

## 4.4 SVD gramians - Krylov moment matching based methods

There are methods in [3,4,16] that use a combination of a *SVD gramian* based method and a *Krylov moment matching* based methods to achieve model reduction. In this way these hybrid methods try to exploit the advantages of each method while trying to minimize the disadvantages. Such methods exist in [3,4,16] and some of them are *least squares* method and *Prony* method. Both of these methods are analysed in [16]. Here, the *least squares* method will be mentioned briefly.

### 4.4.1 Continuous time least squares method

To achieve model reduction for the continuous time case with the *least squares* method there must be a transition to the discrete time case, where a solution is possible and then transition back to the continuous time case. This transformation happen via *Bilinear Transformation* and is explained below. The general method can be described better as an algorithm :

- Transition from the system $\mathbf{\Sigma}$ in Eq. (4.2) to the discrete time system $\mathbf{\Sigma}_d$
- Apply the rational least squares method shown in section (4.4.2)to the discrete time system $\mathbf{\Sigma}_d$ at the interpolation points $\zeta_k = \frac{1+\sigma_k}{1-\sigma_k}$ with the multiplicities $\beta_k$ for $k = 1, \dots, L$. The reduced model from the rational least squares method is denoted as $\mathbf{\Sigma}_{RL}$
- Apply an inverse bilinear transformation to the system $\mathbf{\Sigma}_{RL}$ to obtain the desired continuous time reduced model $\mathbf{\Sigma}_r$

One big disadvantage of the *SVD gramians* based method is that they have higher computational complexity. This can be avoided by avoiding the explicit computation of the matrices $\mathbf{A}_d, \mathbf{b}_d, \mathbf{c}_d, d_d$. Afterwards triangular solvers or *LU decomposition* will be used when they are needed. Since A is sparse in many real life problems one can deal with the problem with a *sparse direct factorization*. Another difficulty that have high computational complexity is the calculation of the *gramian* $\boldsymbol{\mathcal{L}}$ which could be surpassed by applying *Smith iteration* [3,16]. In order not to increase the numerical complexity all the calculation have to be done implicitly during the application of the bilinear transformation.

One more issue is the selection of the *interpolation points*. As shown in [16] an appropriate selection of the *interpolation points* can lead to low errors that are actually comparable to the *SVD gramians* based methods. One such approach is selecting the *interpolation points* as the mirror images of the poles of the system $\boldsymbol{\Sigma}$.

By following the above recommendations the *hybrid methods* satisfy all three qualities that mentioned is section (4.1.3). Global information is related to the usage of the system *gramians* $\boldsymbol{\mathcal{P}}$ and $\boldsymbol{\mathcal{L}}$. A significant characteristic of the *SVD gramian* based methods is the high quality global information. Also, the local information can be extracted through *moment matching* around the chosen *interpolation points* which is a characteristic of the *Krylov moment matching* based methods. Finally, at the cost of reducing the number of moments matched by half and global information missing due to the removing of *gramian* $\boldsymbol{\mathcal{P}}$, the result is between the other two approaches.

### 4.4.2 Discrete time rational least squares method

First some matrices are denoted. The *Hankel matrix* $\boldsymbol{\mathcal{H}}$, the *infinite reachability matrix* $\boldsymbol{\mathcal{R}}$ and the *infinite observability matrix* $\boldsymbol{\mathcal{O}}$ that correspond to the system $\boldsymbol{\Sigma}$ in Eq. (4.2) are :

$$\boldsymbol{\mathcal{H}} := \begin{bmatrix} \eta_1 & \eta_2 & \eta_3 & \dots \\ \eta_2 & \eta_3 & \eta_4 & \dots \\ \eta_3 & \eta_4 & \eta_5 & \dots \\ \vdots & \vdots & \vdots & \ddots \end{bmatrix} \qquad \begin{aligned} \boldsymbol{\mathcal{R}} &:= \begin{bmatrix} \mathbf{b} & \mathbf{Ab} & \dots & \mathbf{A}^{r-1}\mathbf{b} & \dots \end{bmatrix} \\ \boldsymbol{\mathcal{O}} &:= \begin{bmatrix} \mathbf{c}^T & \mathbf{A}^T\mathbf{c}^T & \dots & (\mathbf{A}^T)^{r-1}\mathbf{c}^T & \dots \end{bmatrix}^T \end{aligned} \tag{4.31}$$

where $\eta_i = \mathbf{cA}^{i-1}\mathbf{b}$ is the $i^{th}$ *Markov parameter*. It is easy to see that :

$$\boldsymbol{\mathcal{H}} = \boldsymbol{\mathcal{O}}\boldsymbol{\mathcal{R}} \tag{4.32}$$

This method matches the first $r$ *Markov parameters* exactly and all the remaining ones approximately in a (weighted) least square way. So a good match is expected for the higher order *Markov parameters*.

Let $\boldsymbol{\mathcal{H}}_r$ and $\mathbf{h}_{r+1}$ be the first $r$ columns and the $(r+1)^{th}$ column of *Hankel matrix* $\boldsymbol{\mathcal{H}}$ respectively :

$$\boldsymbol{\mathcal{H}}_r = \begin{bmatrix} \eta_1 & \eta_2 & \eta_3 & \eta_r \\ \eta_1 & \eta_2 & \eta_3 & \eta_{r+1} \\ \vdots & \vdots & \ddots & \vdots \\ \eta_r & \eta_{r+1} & \dots & \eta_{2r-1} \\ \vdots & \vdots & \vdots & \vdots \end{bmatrix} \qquad \mathbf{h}_{r+1} = \begin{bmatrix} \eta_{r+1} \\ \eta_{r+2} \\ \vdots \\ \eta_{2r} \\ \vdots \end{bmatrix} \tag{4.33}$$

The *reachability matrix* $\boldsymbol{\mathcal{R}}_r$ is denoted by leaving the first $r$ terms of $\boldsymbol{\mathcal{R}}$ as follow :

$$\boldsymbol{\mathcal{R}}_r := \begin{bmatrix} \mathbf{b} & \mathbf{Ab} & \dots & \mathbf{A}^{r-1}\mathbf{b} \end{bmatrix} \tag{4.34}$$

It follows that :

$$\boldsymbol{\mathcal{H}}_r = \boldsymbol{\mathcal{H}} \begin{bmatrix} \mathbf{I}_r \\ \mathbf{0} \end{bmatrix} = \boldsymbol{\mathcal{O}}\boldsymbol{\mathcal{R}} \begin{bmatrix} \mathbf{I}_r \\ \mathbf{0} \end{bmatrix} \Leftrightarrow \boldsymbol{\mathcal{H}}_r = \boldsymbol{\mathcal{O}}\boldsymbol{\mathcal{R}}_r \tag{4.35}$$

and

$$\mathbf{h}_{r+1} = \boldsymbol{\mathcal{H}}\mathbf{e}_{r+1} = \boldsymbol{\mathcal{O}}\boldsymbol{\mathcal{R}}\mathbf{e}_{r+1} \Leftrightarrow \mathbf{h}_{r+1} = \boldsymbol{\mathcal{O}}\mathbf{A}^r\mathbf{b} \tag{4.36}$$

where $\mathbf{e}_{r+1}$ is the unit vector so that the above equation will be true. Then by computing the *least squares fit* of the $(r+1)^{th}$ column $\mathbf{h}_{r+1}$ of $\boldsymbol{\mathcal{H}}$ to the columns of $\boldsymbol{\mathcal{H}}_r$ follows :

$$\boldsymbol{\mathcal{H}}_r\mathbf{x}_{LS} = \mathbf{h}_{r+1} + \mathbf{e}_{LS} \tag{4.37}$$

where $\mathbf{e}_{LS}$ is the least squares error.
For the discrete time case, the *gramian* $\boldsymbol{\mathcal{L}}$ is given by the *Stein equation* in the following way :

$$\mathbf{A}^T\boldsymbol{\mathcal{L}}\mathbf{A} + \mathbf{c}^T\mathbf{c} = \boldsymbol{\mathcal{L}} \qquad where \qquad \boldsymbol{\mathcal{L}} = \boldsymbol{\mathcal{O}}^T\boldsymbol{\mathcal{O}} \tag{4.38}$$

The *Stein equation* is the equivalent of the *Lyapunov equation* in Eq.(4.21) for the discrete time case. Then by using the Eq.(4.36),Eq.(4.37) and Eq.(4.38) follows :

$$\mathbf{x}_{LS} = \boldsymbol{\mathcal{H}}_r^{-1}\mathbf{h}_{r+1} = (\boldsymbol{\mathcal{H}}_r^T\boldsymbol{\mathcal{H}}_r)^{-1}\boldsymbol{\mathcal{H}}_r^T\mathbf{h}_{r+1} = (\boldsymbol{\mathcal{R}}_r^T\boldsymbol{\mathcal{L}}\boldsymbol{\mathcal{R}}_r)^{-1}\boldsymbol{\mathcal{R}}_r^T\boldsymbol{\mathcal{O}}^T\mathbf{h}_{r+1} = (\boldsymbol{\mathcal{R}}_r^T\boldsymbol{\mathcal{L}}\boldsymbol{\mathcal{R}}_r)^{-1}\boldsymbol{\mathcal{R}}_r^T\boldsymbol{\mathcal{L}}\mathbf{A}^r\mathbf{b} \tag{4.39}$$

By seeing the reduced order system $\boldsymbol{\Sigma}_r$ of the Eq. (4.11) it is derived by the use of two suitable matrices $\mathbf{V} \in \mathbb{R}^{n\times r}$ and $\mathbf{Z} \in \mathbb{R}^{n\times r}$ with $\mathbf{Z}^T\mathbf{V} = \mathbf{I}_r$ which are defined :

$$\mathbf{V} = \boldsymbol{\mathcal{R}}_r \qquad and \qquad \mathbf{Z} = (\boldsymbol{\mathcal{R}}_r^T\boldsymbol{\mathcal{L}}\boldsymbol{\mathcal{R}}_r)^{-1}\boldsymbol{\mathcal{R}}_r^T\boldsymbol{\mathcal{L}} \tag{4.40}$$

The resulted system $\boldsymbol{\Sigma}_r$ is shown in [3, 16] that is *minimal* and *asymptotically stable*. The *moment matching* around the $L$ *interpolation points* $\zeta_k = \frac{1+\sigma_k}{1-\sigma_k}$ with the *multiplicities* $\beta_k$ for $k = 1, \dots, L$ is shown by noticing that the $Im(\mathbf{V}) = \mathcal{K}_r(\mathbf{A}, \mathbf{b})$ is the $r^{th}$ *Krylov subspace* of $\mathbf{A}$ and $\mathbf{b}$ [3, 16].

### 4.4.3 Bilinear transformation between continuous and discrete time systems

The *bilinear transformation* below is a *spectral transformation* $w : \mathbb{C} \to \mathbb{C}$ that maps the continuous time case to the discrete time case :

$$w : s \mapsto z = \frac{1+s}{1-s} \tag{4.41}$$

which maps the open left half plane onto the open unit disc because :

$$if \quad \mathcal{R}(s) < 0 \quad \Rightarrow \quad |z| = \left|\frac{1+s}{1-s}\right| < 1 \tag{4.42}$$

The *inverse bilinear transformation* of the Eq. (4.41) maps the discrete time case to the continuous time case :

$$w^{-1} : z \mapsto s = \frac{z-1}{z+1} \tag{4.43}$$

Both the bilinear transformation and the inverse one preserve the *stability* of the system.

The transition between the discrete time system $\mathbf{\Sigma}_d = \left[\begin{array}{c|c} \mathbf{A}_d & \mathbf{b}_d \\ \hline \mathbf{c}_d & d_d \end{array}\right]$ and the continuous time system $\mathbf{\Sigma}_c = \left[\begin{array}{c|c} \mathbf{A}_c & \mathbf{b}_c \\ \hline \mathbf{c}_c & d_c \end{array}\right]$ can be done with the above bilinear transformations with the following formulas [16] :

$$\mathbf{A}_c, \mathbf{b}_c, \mathbf{c}_c, d_c \xrightarrow{z=\frac{1+s}{1-s}} \begin{cases} \mathbf{A}_d = (\mathbf{I} + \mathbf{A}_c)(\mathbf{I} - \mathbf{A}_c)^{-1} \\ \mathbf{b}_d = \sqrt{2}(\mathbf{I} - \mathbf{A}_c)^{-1}\mathbf{b}_c \\ \mathbf{c}_d = \sqrt{2}\mathbf{c}_c(\mathbf{I} - \mathbf{A}_c)^{-1} \\ d_d = d_c + \mathbf{c}_c(\mathbf{I} - \mathbf{A}_c)^{-1}\mathbf{b}_c \end{cases} \tag{4.44}$$

$$\mathbf{A}_d, \mathbf{b}_d, \mathbf{c}_d, d_d \xrightarrow{s=\frac{z-1}{z+1}} \begin{cases} \mathbf{A}_c = (\mathbf{I} + \mathbf{A}_c)(\mathbf{I} - \mathbf{A}_c)^{-1} \\ \mathbf{b}_c = \sqrt{2}(\mathbf{I} - \mathbf{A}_c)^{-1}\mathbf{b}_c \\ \mathbf{c}_c = \sqrt{2}\mathbf{c}_c(\mathbf{I} - \mathbf{A}_c)^{-1} \\ d_c = d_c + \mathbf{c}_c(\mathbf{I} - \mathbf{A}_c)^{-1}\mathbf{b}_c \end{cases} \tag{4.45}$$

## 4.5 CSP method

The *CSP method* that is a multi time scale method of stiff Ordinary Differential Equations (ODEs) where both fast and slow time scales are encountered.The mathematical background has been analysed in chapter (2). The fast time scales are responsible for the development of low-dimensional manifolds on which the solution moves according to the slow time scales. As mentioned in chapter (2) this method can decouple the fast time scales from the slow ones.

For small systems the method can produce even analytic expressions of the solution. For large-scale systems the method can reduce the order to only the dimension of the *Slow Invariance Manifold* (SIM). Also, there are indexes that shows the participation of every time scale (see section (2.3)). The method has a lot more tools that can provide many more useful information about the solution. This way deeper results can be extracted from the resulting solution as it will be shown in chapter (5). The *CSP method* mathematical background has been extensively presented and applied in chapters (2, 5). Also in chapter (5) there is the comparison of the *CSP method* with the methods that are presented in this chapter.

## 4.6 Modal analysis

*Modal analysis* is the study of the dynamic properties of structures under *vibrational excitation*. In structural engineering, *modal analysis* uses the overall mass and stiffness of a structure to find the various periods at which it will naturally resonate. These periods of vibration are very important to note in earthquake engineering, as it is imperative that a building's natural frequency does not match the frequency of expected earthquakes in the region in which the building is to be constructed [5, 9, 20, 29, 31].

Although *modal analysis* is usually carried out by computers, it is possible to hand-calculate the period of vibration of any high-rise building through idealization as a fixed-ended cantilever with concentrated masses which is equivalent with the system shown in the Fig. (3.17). For a more detailed explanation see [10] as it provides an easy-to-follow approach to idealizing and solving complex structures by hand.

First the case without damping and external excitations will be examined. In this case the system of equations that describe the model that in the Eq. (4.1) becomes :

$$\mathbf{m\ddot{u}} + \mathbf{ku} = 0 \tag{4.46}$$

This problem is equivalent to the *eigenvalue problem* of this system. As mentioned in [8, 10, 19] the *natural frequency* $\omega_n$ and the *natural node mode* $\boldsymbol{\phi}_n$ which consists of the elements $\phi_{jn}$ that correspond to the DOF $j$. The *natural frequencies* of the problem are the square roots of the *eigenvalues* of the problem and the *modals* correspond to the *eigenvectors*. The *modal matrix* $\mathbf{\Phi}$ and the *spectral matrix* $\mathbf{\Omega}^2$ are :

$$\mathbf{\Phi} = \Big[\phi_{jn}\Big] = \begin{bmatrix} \phi_{11} & \phi_{12} & \cdots & \phi_{1N} \\ \phi_{21} & \phi_{22} & \cdots & \phi_{2N} \\ \vdots & \vdots & \ddots & \vdots \\ \phi_{N1} & \phi_{N2} & \cdots & \phi_{NN} \end{bmatrix} \qquad \mathbf{\Omega}^2 = \begin{bmatrix} \omega_1^2 & & & \\ & \omega_2^2 & & \\ & & \ddots & \\ & & & \omega_N^2 \end{bmatrix} \tag{4.47}$$

Each eigenvalue and eigenvector of the Eq. (4.46) can be written as follows:

$$\mathbf{k}\boldsymbol{\phi}_n = \mathbf{m}\boldsymbol{\phi}_n\omega_n^2 \tag{4.48}$$

Then by assembling the Eqs. (4.48) for $n = 1, 2, \ldots, n$ the following matrix relation can be created :

$$\mathbf{k\Phi} = \mathbf{m\Phi\Omega}^2 \tag{4.49}$$

It is proved in [8] that the following *orthogonality relations* are true for the eigenvectors $\phi_i$ and $\phi_j$

$$\boldsymbol{\phi}_i^T\mathbf{k}\boldsymbol{\phi}_j = 0 \qquad \textit{and} \qquad \boldsymbol{\phi}_i^T\mathbf{m}\boldsymbol{\phi}_j = 0 \qquad \forall\ i \neq j \tag{4.50}$$

The orthogonality of the natural nodes implies that the following square matrices are *diagonal* :

$$\mathbf{K} = \mathbf{\Phi}^T\mathbf{k}\mathbf{\Phi}^T \qquad \textit{and} \qquad \mathbf{M} = \mathbf{\Phi}^T\mathbf{m}\mathbf{\Phi}^T \tag{4.51}$$

Also the displacements $u$ can be expressed using the eigenvectors:

$$\mathbf{u} = \sum_{i=1}^{N} \boldsymbol{\phi}_i q_i = \mathbf{\Phi q} \tag{4.52}$$

then the velocities $\dot{u}$ and accelerations $\ddot{u}$ can be written in the following way:

$$\dot{\mathbf{u}} = \mathbf{\Phi}\dot{\mathbf{q}} \qquad \textit{and} \qquad \ddot{\mathbf{u}} = \mathbf{\Phi}\ddot{\mathbf{q}} \tag{4.53}$$

The Eq. (4.1) with respect to the basis $\mathbf{q}$ is :

$$\mathbf{m\Phi}\ddot{\mathbf{q}} + \mathbf{c\Phi}\dot{\mathbf{q}} + \mathbf{k\Phi q} = \mathbf{p}(t) \tag{4.54}$$

Then by multiplying with the matrix $\mathbf{\Phi}^T$ from the left and using the Eq. (4.51), an alternative expression of the Eq. (4.1) to the basis $\mathbf{q}$ is obtained :

$$\mathbf{\Phi}^T\mathbf{m\Phi}\ddot{\mathbf{q}} + \mathbf{\Phi}^T\mathbf{c\Phi}\dot{\mathbf{q}} + \mathbf{\Phi}^T\mathbf{k\Phi q} = \mathbf{\Phi}^T\mathbf{p}(t) \quad \Leftrightarrow \quad \mathbf{M}\ddot{\mathbf{q}} + \mathbf{C}\dot{\mathbf{q}} + \mathbf{Kq} = \mathbf{P}(t) \tag{4.55}$$

where $\mathbf{M} = \mathbf{\Phi}^T\mathbf{m\Phi}$ and $\mathbf{K} = \mathbf{\Phi}^T\mathbf{k\Phi}$ are diagonal and $\mathbf{C} = \mathbf{\Phi}^T\mathbf{c\Phi}$ and $\mathbf{P} = \mathbf{\Phi}^T\mathbf{p}$. In the special case where $\mathbf{C}$ is *diagonal* the equations can decouple [8,19]. For all the other cases there are methods to solve the system [8, 19]. One method that reduce the system is *Rayleigh-Ritz* method and it is based to the technique of modal analysis.

## 4.7 Rayleigh-Ritz method

In this method the displacements $\mathbf{u}$ are expressed with the help of the *Ritz vectors* $\boldsymbol{\psi}_i$ where $i = 1, 2, \ldots, r$:

$$\mathbf{u}(t) = \sum_{i=1}^{r} z_i(t)\boldsymbol{\psi}_i = \boldsymbol{\Psi}\mathbf{z}(t) \quad \Leftrightarrow \quad \dot{\mathbf{u}}(t) = \boldsymbol{\Psi}\dot{\mathbf{z}}(t) \quad \Leftrightarrow \quad \ddot{\mathbf{u}}(t) = \boldsymbol{\Psi}\ddot{\mathbf{z}}(t) \tag{4.56}$$

then similar to modal analysis the reduced system can be formed. The Eq. (4.1) with use the Eq. (4.56) is written to the basis that is created by the *Ritz vectors* $\psi_i$ :

$$\mathbf{m}\boldsymbol{\Psi}\ddot{\mathbf{z}} + \mathbf{c}\boldsymbol{\Psi}\dot{\mathbf{z}} + \mathbf{k}\boldsymbol{\Psi}\mathbf{z} = \mathbf{p}(t) \tag{4.57}$$

By multiplying with the matrix $\boldsymbol{\Psi}^T$ from the left the Eq. (4.57) becomes :

$$\boldsymbol{\Psi}^T\mathbf{m}\boldsymbol{\Psi}\ddot{\mathbf{z}} + \boldsymbol{\Psi}^T\mathbf{c}\boldsymbol{\Psi}\dot{\mathbf{z}} + \boldsymbol{\Psi}^T\mathbf{k}\boldsymbol{\Psi}\mathbf{z} = \boldsymbol{\Psi}^T\mathbf{p}(t) \quad \Leftrightarrow \quad \tilde{\mathbf{m}}\ddot{\mathbf{z}} + \tilde{\mathbf{c}}\dot{\mathbf{z}} + \tilde{\mathbf{k}}\mathbf{z} = \tilde{\mathbf{p}}(t) \tag{4.58}$$

where $\tilde{\mathbf{m}} = \boldsymbol{\Psi}^T\mathbf{m}\boldsymbol{\Psi}$,$\tilde{\mathbf{c}} = \boldsymbol{\Psi}^T\mathbf{c}\boldsymbol{\Psi}$,$\tilde{\mathbf{k}} = \boldsymbol{\Psi}^T\mathbf{k}\boldsymbol{\Psi}$ and $\tilde{\mathbf{p}} = \boldsymbol{\Psi}^T\mathbf{p}$. The resulting system in the Eq. (4.58) is consisted of $r$ differential equations. This way model reduction is achieved.

The *Ritz vectors* are like eigenvectors. The goal is to approximate the eigenmodes of the oscillation of the system with the *Ritz vectors*. So it is very important to choose appropriate *Ritz vectors*. In [8] there are many methods and two of them are:

- Physical insight natural mode shapes method
- Force dependent Ritz vectors

In building systems which are symmetrical and don't have complex geometries the important eigenmodes are very few (e.g 3-6) and they have expected shape [8, 37]. Then the *model reduction* is very successful because the method can approximate the eigenmodes that stimulate the system the most. The disadvantage though is when the building has a strange geometry then the method cannot predict the shape of the eigenmodes very good and the error of the method becomes unacceptable [8, 37].

# Chapter 5

# CSP analysis on a building model with damping

Buildings are the most common structures in the planet. It is very important to study their behaviour extensively for a wide variety of reasons. Accurate calculation of the buildings behaviour and response to different types of excitations and forces is crucial for safety, functionality, cost efficiency e.t.c. To achieve high accuracy models it requires the increase of the number of nodes and elements that describe the building. As we have seen in section (3.3) and in Fig. (3.12 a) for planar modelling each node has 3 DOFs (two translations and one rotation). Similarly, in 3D models each node has 6 DOFs (three translations and three rotations). In most cases there is the need of 3D modeling to create high accuracy models. For both cases it is shown below that for very dense modelling (high number of nodes) the number of degrees of freedom could get very high :

$$\text{number of DOFs} = (\text{number of nodes}) \times 3 \qquad \text{for} \qquad \text{2D models} \tag{5.1}$$

$$\text{number of DOFs} = (\text{number of nodes}) \times 6 \qquad \text{for} \qquad \text{3D models} \tag{5.2}$$

Consequently, high number of DOFs lead to large-scale systems. Many examples of large-scale systems are given in [7, 19, 37]. Due to the limitations of computer memory and computer power the solution of the above systems can be impossible or very time consuming. Also, direct numerical calculation of the solution creates big errors when the order of the system is large. In chapter (4) some techniques that can moderate the above problems were mentioned (e.g. like skyline storage integration, clever new algorithms that require less time, preconditioning e.t.c) [38, 39]. Although, those techniques can be very efficient , for really large-scale problems they are still not enough. For all the above reasons to reduce the order of the system is of crucial importance.

The dynamical equation of a building is given by the Eq. (3.63) for the linear - elastic building and by the Eq. (3.9) for the non linear - inelastic buildings. For the linear case the equation is :

$$\mathbf{m\ddot{u}} + \mathbf{c\dot{u}} + \mathbf{ku} = \mathbf{p}(t) \tag{5.3}$$

The mass matrix $\mathbf{m}$, the damping matrix $\mathbf{c}$, the stiffness matrix $\mathbf{k}$ and the force vector $\mathbf{p}(t)$ are required at each instant to calculate the solution of a building.

The discretization of a building and the calculation of $\mathbf{m}, \mathbf{c}, \mathbf{k}$ matrices and $\mathbf{p}(t)$ vector is not an easy task. The method for the proper discretization of a building is mentioned in section (3.3.1) and further information can be found in [8, 10, 19]. The easiest matrix to calculate is the mass matrix $\mathbf{m}$ and is described in section (3.3.4) and in [8, 10, 19]. The stiffness matrix $\mathbf{k}$ for systems with elastic behaviour is constant at every instant and in the inelastic case it changes every instant due to the deformation of the structure and material inelasticity and plasticity. For the linear case the method is described in section (3.3.2) and more information for both cases can be found in [8, 10, 19]. The damping matrix $\mathbf{c}$ is very difficult and nearly infeasible to calculate it exactly. The difficulties and methods to calculate an *equivalent damping* are explained in sections (3.1.4, 3.3.3) and more details in [1, 20, 29]. The difficulty in calculating the force vector $\mathbf{p}(t)$ is to identify values that represent critical real life loads or identify critical effective forces that are produced by various excitations (like earthquakes). This procedure is presented in sections (3.1.6, 3.3.5, 5.3) and analysed extensively in [5, 9, 20].

In this dissertation the CSP method will be applied to solve a building model of Los Angeles University Hospital found in [16]. This building model is solved in [16] by using : (i) *Balanced reduction method*, (ii) *Rational Krylov method* and (iii) *Least squares method*.

The following were achieved by solving this building model with CSP method :

- Find a reduced order system of the building model
- Understand building mechanisms and various phenomena appeared during building vibration
- Identify deformation pattern of buildings under different external loads and excitations
- Identify the contribution of every natural eigenmode at each instant
- Understand the evolution of the *SIM* under significant changes of external loadings and excitations
- Compare CSP method to other methods shown in chapter (4) and in [3, 16, 37]

In this chapter, the system in Eq. (5.3) will be transformed to an appropriate form to apply CSP method and determine the parameters of the model. Afterwards, the solutions for various loadings and excitations will be presented. Finally, there will be a comparison between the CSP method with the other model reduction methods analysed in chapter (4) and in [3, 16, 37].

## 5.1 Dynamical equations in CSP form

The equation that represent the physical problem of building vibrations is the harmonic damping oscillations equation. The system of these second order differential equations that gives the building model is given by Eq. (5.3). The system need to be transformed into an appropriate form in order to apply the CSP method. As it was shown in chapter (2) the CSP method can handle systems of the following form :

$$\frac{d\mathbf{y}}{dt} = \mathbf{g}(\mathbf{y}) \tag{5.4}$$

where $\mathbf{y}$ and $\mathbf{g}(\mathbf{y})$ are the $N$-dimensional column *state vector* and *vector field*, respectively and $\mathbf{g}$ is an algebraic function of $\mathbf{y}$.

The system of dynamical equations shown in the Eq. (5.3) can be written as follows :

$$\ddot{\mathbf{u}}(t) = \mathbf{m}^{-1}\mathbf{p}(t) - \mathbf{m}^{-1}\mathbf{c}\dot{\mathbf{u}}(t) - \mathbf{m}^{-1}\mathbf{k}\mathbf{u}(t) \tag{5.5}$$

This system of equation can be written in the form of the Eq. (5.4) in the following manner :

$$\begin{bmatrix} \dot{\mathbf{y}}_1(t) \\ \dot{\mathbf{y}}_2(t) \end{bmatrix} = \begin{bmatrix} \mathbf{0}_{n,n} & \mathbf{I}_{n,n} \\ -\mathbf{m}^{-1}\mathbf{k} & -\mathbf{m}^{-1}\mathbf{c} \end{bmatrix} \begin{bmatrix} \mathbf{y}_1(t) \\ \mathbf{y}_2(t) \end{bmatrix} + \begin{bmatrix} \mathbf{0}_{n,n} \\ \mathbf{m}^{-1} \end{bmatrix} \mathbf{p}(t) \tag{5.6}$$

$$\mathbf{y}(t) = \begin{bmatrix} \mathbf{y}_1(t) \\ \mathbf{y}_2(t) \end{bmatrix} \tag{5.7}$$

where the $\mathbf{y}_1(t)$ is the displacement vector which is the same as $\mathbf{u}(t)$, the $\mathbf{y}_2(t)$ is the velocities vector which is the same as $\dot{\mathbf{u}}(t)$and $\mathbf{y}(t)$ is a vector that contains the $n$ displacements of $\mathbf{y}_1(t)$ and $n$ velocities of $\mathbf{y}_2(t)$ where $n$ is the number of DOFs of the system in Eq. (5.5). In Eq. (5.4) the time $t$ is not included. This obstacle can be skipped by adding the equation $\dot{t} = 1$ in the Eqs. (5.6, 5.7) in the following way :

$$\begin{bmatrix} \dot{\mathbf{y}}_1(t) \\ \dot{\mathbf{y}}_2(t) \\ \dot{t} \end{bmatrix} = \begin{bmatrix} \mathbf{0}_{n,n} & \mathbf{I}_{n,n} & \mathbf{0}_{n,1} \\ -\mathbf{m}^{-1}\mathbf{k} & -\mathbf{m}^{-1}\mathbf{c} & \mathbf{0}_{n,1} \\ \mathbf{0}_{1,n} & \mathbf{0}_{1,n} & 0 \end{bmatrix} \begin{bmatrix} \mathbf{y}_1(t) \\ \mathbf{y}_2(t) \\ t \end{bmatrix} + \begin{bmatrix} \mathbf{0}_{n,n} & \mathbf{0}_{n,1} \\ \mathbf{m}^{-1} & \mathbf{0}_{n,1} \\ \mathbf{0}_{1,n} & 1 \end{bmatrix} \begin{bmatrix} \mathbf{p}(t) \\ 1 \end{bmatrix} \tag{5.8}$$

$$\widetilde{\mathbf{y}}(t) = \begin{bmatrix} \mathbf{y}_1(t) \\ \mathbf{y}_2(t) \\ t \end{bmatrix} \tag{5.9}$$

So the transformation of the system of dynamical equations shown in Eqs. (5.3, 5.5) to an appropriate CSP form was achieved. This form in shown in Eqs. (5.8, 5.9). Such a system is known to be a stiff one [2]. Also similar to the chapter (4.1.4) it can be shown that the system is observable and controllable.

The same trick is used to achieve state-space form or a suitable CSP form. To achieve the CSP form it was needed just one more simple change. All the methods (except when damping is neglected) use this trick to solve the system of second order differential equations in Eq. (5.3). Actually a system of $n$ second order differential equations is transformed to a system of $2n$ first order differential equations. So the system of equations that actually has to be solved has $2n$ equations and $2n+1$ when time was added. For simplicity the following matrices are denoted :

$$\mathbf{A} = \begin{bmatrix} \mathbf{0}_{n,n} & \mathbf{I}_{n,n} & \mathbf{0}_{n,1} \\ -\mathbf{m}^{-1}\mathbf{k} & -\mathbf{m}^{-1}\mathbf{c} & \mathbf{0}_{n,1} \\ \mathbf{0}_{1,n} & \mathbf{0}_{1,n} & 0 \end{bmatrix} \qquad \mathbf{B} = \begin{bmatrix} \mathbf{0}_{n,n} & \mathbf{0}_{n,1} \\ \mathbf{m}^{-1} & \mathbf{0}_{n,1} \\ \mathbf{0}_{1,n} & 1 \end{bmatrix} \qquad \widetilde{\mathbf{p}}(t) = \begin{bmatrix} \mathbf{p}(t) \\ 1 \end{bmatrix} \tag{5.10}$$

so by substituting the Eq. (5.10) and the Eq. (5.9) to the Eq. (5.8) it follows :

$$\frac{d\widetilde{\mathbf{y}}}{dt} = \mathbf{A}\widetilde{\mathbf{y}}(t) + \mathbf{B}\widetilde{\mathbf{p}}(t) \tag{5.11}$$

so $\widetilde{\mathbf{y}}$ is a $2n+1$ dimensional *state vector* and the RHS of the Eq. (5.11) is a $2n+1$ dimensional *vector field* according to the form of Eq. (5.4).

## 5.2 Steps of CSP algorithm

In the previous section the Eq. (5.3) has been transformed into the appropriate CSP form shown in the Eqs. (5.10, 5.11). The mathematical background of the CSP method is already extensively described in chapter (2). In this section the CSP algorithm will be described in steps.

*Step* 1: Set the initial values of $\mathbf{y}$ which are the initial displacements and initial velocities. Set $t_0$ the initial time, $t_{total}$ the total time and the time step $dt$.

*Step* 2: Calculate $\dot{\mathbf{y}}$ and the *Jacobian matrix* $\mathbf{J}$ for $t = 0$.

*Step* 3: Solve the whole system for one time step $dt$.

*Step* 4: Set the basis vectors $\mathbf{a}_i$ and $\mathbf{b}^i$ for $i = 1, \ldots, N$ where $N$ is the number of equations of the initial system $\dot{\mathbf{y}}(t) = \mathbf{g}(\mathbf{y})$.

*Step* 5: Set the number of *fast time scales* $M = k$. Then the *slow time scales* are $N - M = N - k$.

*Step* 6: Calculate *Jacobian matrix* $\mathbf{J}$ and its first $m$ derivatives $\frac{d^i\mathbf{J}}{dt^i}$ for $i = 1, \ldots, m$

*Step* 7: Apply CSP refinements ("$k_1$" $\mathbf{b}^r$-refinements and "$m_1$" $\mathbf{a}_r$-refinements). In *step* 6 the first $m = \max(k_1, m_1) - 1$ derivatives of Jacobian matrix $\mathbf{J}$ need to be calculated.

*Step* 8: Repeat *steps* 5 - 8, till find a value $k$ such that for $M = k$ fast time scales an *error criterion* is satisfied. Such *error criteria* can be found in section (2.2).

*Step* 9: Find the reduced order system for $N - M$ slow time scales . This is given by the equation $\dot{\mathbf{y}}(t) = \mathbf{a}_s \mathbf{f}^s$.

*Step* 10: Solve the reduced system of *step* 9 for time $t$.

*Step* 11: Repeat *steps* 4 - 11, till $t \geq t_{total}$ .

The above steps is the core of the CSP method. The above algorithm can be modified in various ways. Next the changes that have been done in different steps of the CSP algorithm will be described.

At *step* 4 the basis vectors $\mathbf{a}_i$ and $\mathbf{b}^i$ are selected. For the first time this can be at random. But because the system describes the dynamical behaviour of a building a better guess would be an approximation of the eigenmodes of the building. This can be done by calculating the natural eigenmodes of a cantilever with the same mass $m$ and the effective stiffness $k_{eff}$ which is a crude approximation of the actual stiffness of the building. This cantilever can be easily calculated and are shown in section (5.3). The formulas for the natural eigenmodes of the cantilever are given in [8,10]. After each iteration the CSP basis vectors $\mathbf{a}_r$ and $\mathbf{a}_s$, and their duals $\mathbf{b}^s$ and $\mathbf{b}^r$ that are produced after the CSP refinements at *step* 7 can be used. In this way, after some iterations the selection of the basis vectors $\mathbf{a}_i$ and $\mathbf{b}^i$ will be a very accurate approximation of the directions of the fast and slow time scales.

At *step* 8 the method checks if the selection of the number of fast time scales in *step* 5 is correct. But this selection might not be optimal. The *step* 8 can be modified such that the iteration process of *steps* 5-8 will continue until it finds $M$ fast time scales that satisfy the error criterion and the $M + 1$ fast time scales that don't satisfy the error criterion. The $M_{optimal}$ can change if the value of **AbsErr** in the error criterion change as well.

At *step* 5 the number of fast time scales was selected. It is known that the solution is attracted to an exponentially attracting Slow Invariance Manifold (SIM). This implies that if there are M fast time scales at time $t$ then there will be at least $M$ fast time scales at time $t + dt$ unless there is a dramatic change in the SIM. So after the first iteration the value of $M_{optimal}$ at time $t$ will be a good approximation of $M_{optimal}$ at time $t + dt$. In section (5.4) this is verified except from cases where there are significant changes to the external loads or excitations and the SIM differs.

*Steps* 3 and 10 can be done with the use of iterative methods to minimize the time and computations needed to acquire the solution.

At *step* 11 the criterion can be modified. After some time the solution approaches equilibrium state. When the solution is near equilibrium state it changes less after a time step $dt$. A criterion like $\|\mathbf{y}_{t+dt} - \mathbf{y}_t\| < \epsilon$ can be added and if that is satisfied the time step $dt$ can be increased. In that way the number of iterations and computations needed to achieve an accurate solution are drastically decreased.

By following the above recommendations, the modified CSP algorithm can extract more information of the problem and get the whole trajectory of the solution $\mathbf{y}$ in less time.

## 5.3 Determine problem parameters

The building model of Los Angeles Hospital shown in [16] is studied here. This building has 8 floors with 3 degrees of freedom for every floor. The idealized model of this building is shown in Fig (5.1). It easy to see that the number of DOFs are 24 by using the Eq. (5.1). To solve the system of 24 second order equations shown in Eq. (5.3) with the CSP method, the system need to be transformed to $49 = 2 \times 24 + 1$ first order equations shown in Eqs. (5.8-5.11).

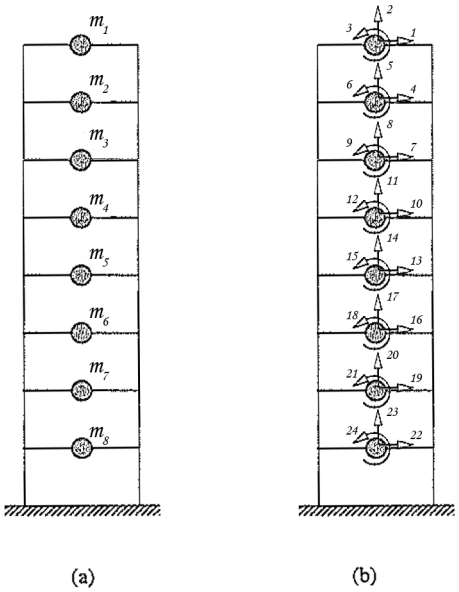


**Figure 5.1:** (a) Idealized 8 floor building (b) Degrees of freedom

The mass matrix $\mathbf{m}$, the damping matrix $\mathbf{c}$ and the stiffness matrix $\mathbf{k}$ of the Los Angeles Hospital was given by professor *Antoulas*. It is important to mention that the mass matrix $\mathbf{m}$ is diagonal. That is not surprising as it is a common phenomenon as it was shown in section (3.3.4). The other two matrices are dense. It is easy to calculate the matrices $A$ and $B$ with the use of the above matrices as the inverse of the mass matrix $\mathbf{m}$ can be easily calculated since $\mathbf{m}$ is diagonal.

The total mass of the building is $m \simeq tr(\mathbf{m})$, where trace of a matrix is the sum of the elements in the diagonal of the matrix. For guessing better the CSP basis vectors $\mathbf{a}_i$ and $\mathbf{b}^i$ in section (5.2), it is required to find a cantilever with $m$ and $k$ that can simulate the dynamical behaviour of the building. To achieve that a crude approximation of the effective stiffness of the building is required. In this case there is no information about the height of each floor or the material to calculate the Young's module. A crude approximation is $k_{eff} = \frac{1}{8}(k_{1,1} + k_{4,4} + \cdots + k_{22,22})$ which is a weighted sum of the stiffness terms correspond to the horizontal displacements of each mass. By using the total mass $m$ and an approximation of the effective stiffness $k_{eff}$ the step 4 of CSP method that is presented in section (5.2) can be modified.

In this dissertation the building model will be studied for various external forces and building excitations. The problem was solved for the following loading cases :

- free vibration with no external loads and an initial displacement and velocity
- static loading
- equally distributed effective earthquake forces
- triangular distributed effective earthquake forces

First the free vibration case will be examined. In free vibration, the system is moved from its equilibrium position and then oscillate. In this case the building is moved in the horizontal axis as shown in Fig. (5.2 a). The initial vertical displacements and rotations are set equal to zero. Also the initial velocities are set equal to zero. Obviously the initial time is equal to zero. The summary of the above is given below :

$$\mathbf{y}(0) = \begin{bmatrix} u_1(0) & 0 & 0 & u_4(0) & 0 & 0 & \dots & u_{22}(0) & 0 & 0 & \mathbf{0}_{24,1} & 0 \end{bmatrix}^T \tag{5.12}$$

$$\widetilde{\mathbf{p}}(t) = \mathbf{0}_{25,1} \tag{5.13}$$

at each instant $t$.

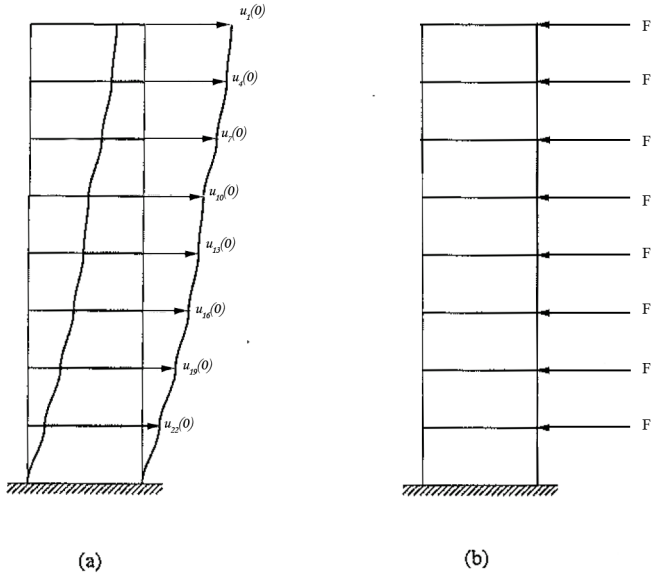


**Figure 5.2:** (a) Initial displacements for free vibration case (b) Static loading case

For the second case a static loading is applied at each mass in the horizontal direction. These loads that are applied, they will stay constant. The loads are shown in Fig. (5.2 b). The goal is to set an appropriate value to $F$ such that the static loading is critical for the structure. The solution for $F = 10kN$ is presented in section (5.4.2). The solution for other values of F are similar due to the linearity of the problem. For this case the solution is studied until $t_{total} = 50sec$.

For the following two cases the goal is to find a loading case that represent critical earthquake excitations. Two important characteristics for an earthquake are the *peak ground acceleration*(PGA) and *spectral acceleration*($Sa$) as shown in [9,20]. PGA is the most common instrumental measure of ground motion. It is a measure of ground motion amplitude, and represents the highest acceleration of the ground motion. PGA is measured relative to the acceleration of gravity. *Spectral Acceleration* is a relatively new instrumental measure of ground motion that includes building response. $Sa$ differentiates the response of structures by building height and structural type, both of which help to classify the buildings natural period, or its natural tendency to respond to wave motions of differing frequencies.

By searching the above characteristics and acceleration records for various earthquakes, it was found a range of values for most critical earthquakes in [9, 20]. The value range of spectral is $Sa = 0.2g - 0.4g$, of the frequency is $f = 0.1Hz - 1Hz$ and of the time $t = 10s - 30s$. For the following loading cases it was assumed that the ground motion is $\ddot{u}_g(t) = 0.3 \times \cos(20t)$ for $t = 0s - 20s$ and $\ddot{u}_g(t) = 0$ for $t > 20s$.

For the third case of effective earthquake forces, the formulas found in sections (3.1.6, 3.3.5) will be used. The forces that are applied in this case are shown in the Figs. (3.18, 5.3 a). For the ground motion the assumption that have been done above will be used.

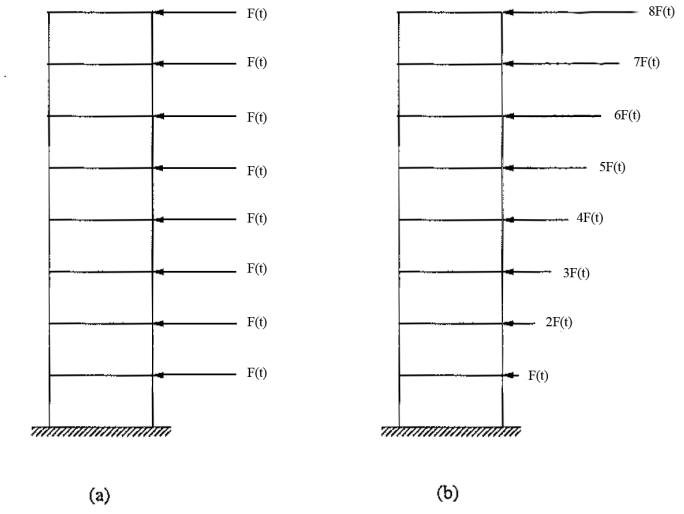


**Figure 5.3:** Effective earthquake forces (a) Equally distributed (b) Triangular distibuted

The assumption of concentrated masses in each floor was used to simulate the building response. That led to the third loading case. Instead of using this assumption for the effective earthquake forces they can be applied as in the Fig. (5.3 b). The triangular distribution is a more realistic approach and it is used in [9,20] and in various construction codes since the buildings are continuous structures. Actually the total horizontal force is the same as the one in the third case but its distribution is different. Because there is no information about the height of each floor it was assumed that all are equal and the force on the second floor is double the force of the first floor e.t.c.

## 5.4 Case study

In this section the solutions of the Los Angeles Hospital using the CSP method for the loadings described in section (5.3) will be presented. The solutions for other similar load cases can be obtained easily and with high accuracy. That is possible due to the linearity of the harmonic damping oscillation equations of the system.

### 5.4.1 Free vibration

The solution for the free vibration problem for SDF systems is given in Fig. (3.8). Here the diagrams of $u_1(t)$ and $\dot{u}_1(t)$ are presented.

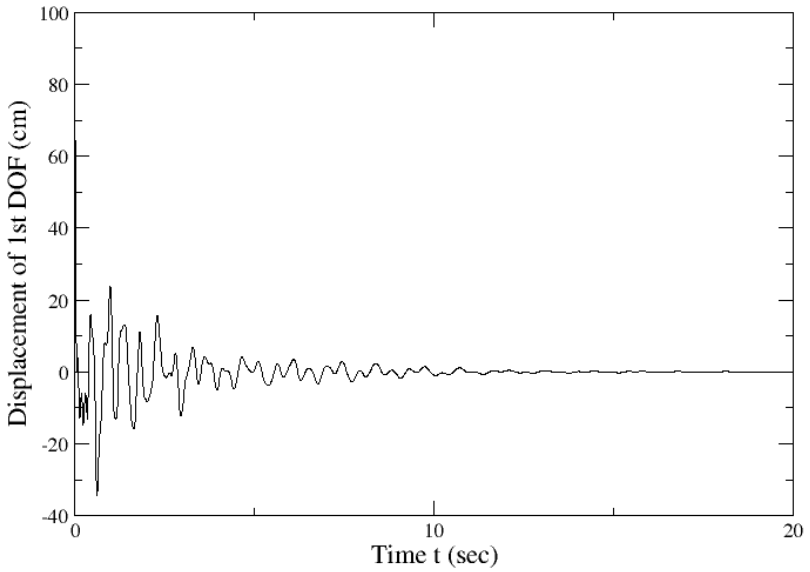


**Figure 5.4:** Displacement of the first DOF $u_1(t)$ over time

The Fig. (5.4) is showing the horizontal displacement $u_1(t)$ of the highest floor of the building and is similar to the Fig. (3.8). All the other horizontal movements are similar to this one but smaller in value. The building starts to oscillate and it reaches equilibrium state after 10-15 periods. This is expected as shown from the Fig. (3.9). That shows that the assumption for the *effective damping level* $\zeta = 5\%$ is accurate.

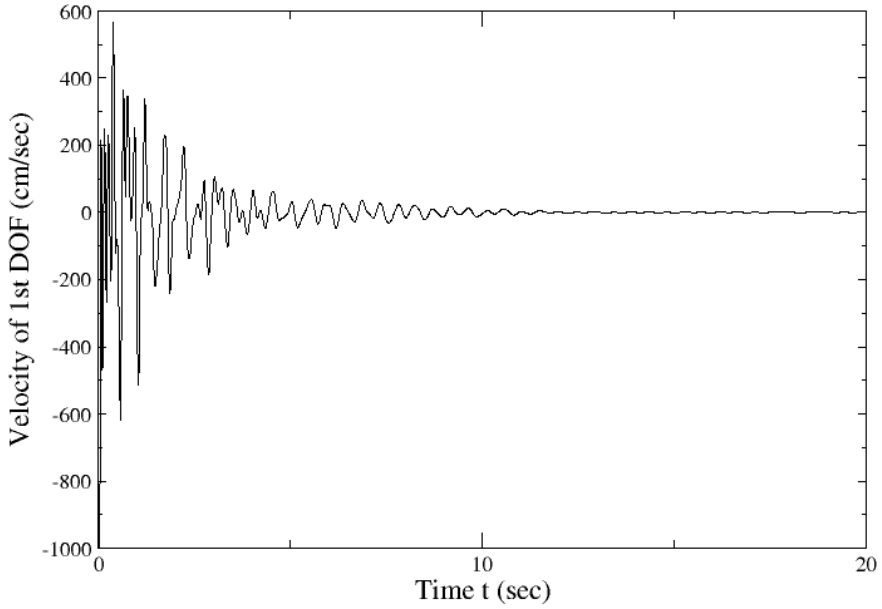


**Figure 5.5:** Velocity of the first DOF $\dot{u}_1(t)$ over time

The Fig. (5.5) is showing the velocity $\dot{u}_1(t)$ of the highest floor in the horizontal direction. All the other velocities on the horizontal direction are similar but smaller in value. The building starts to oscillate quickly, and the velocity decreases as the building starts to converge to the equilibrium state. After 10-15 oscillations as shown for the displacements the system reaches equilibrium state and the velocities become zero.

The eigenvalues of the problem are the eigenvalues of the matrix $\mathbf{A}$ shown in the Eq. (5.10). The eigenvalues are the same for each loading case since for the linear problems the matrices $\mathbf{m}, \mathbf{c}$ and $\mathbf{k}$ are constant at each instant and so the matrix $\mathbf{A}$. This is correct since they represent the natural eigenmodes of the structure and they don't depend on the loading. The eigenvalues are all *complex with negative real part*. This can be explained using the following found in [18]:

$$\frac{\mathbf{y}}{dt} = \mathbf{A}\mathbf{y}(t) \quad \Leftrightarrow \quad \mathbf{y}(t) = e^{\mathbf{A}t}\mathbf{y}_0 \tag{5.14}$$

where $\mathbf{A}$ is a $N \times N$ constant matrix.

Using the *Sylvester formula*:

$$\mathbf{y}(t) = e^{\mathbf{A}t}\mathbf{y}_0 = \sum_{k=1}^{N} e^{\lambda_i t}\mathbf{A}_i\mathbf{y}_0 \tag{5.15}$$

where $\mathbf{A}_i$ are the *Frobenious covariant* of $\mathbf{A}$.

As time $t$ passes the solution $\mathbf{y}(t)$ has to converge to zero and that is true only for complex eigenvalues with negative real parts $\lambda_i = -p \pm qi$ where $p, q > 0$. In a similar way it is shown in [18] that the eigenvalues are complex with negative real parts for the case $\frac{d\mathbf{y}}{dt} = \mathbf{A}\mathbf{y}(t) + \mathbf{B}\mathbf{u}(t)$.

The eigenvalues are equal for all the cases and are independent of the loadings. They are given in the table (5.1).

There is relation between the absolute value of the complex eigenvalues and the time scales that correspond is inversely proportional. In Fig. (5.6) there are shown the terms $\frac{1}{|\lambda_i|}$ that represent the time scales over time. Because the eigenvalues are in conjugate pairs each value $\frac{1}{|\lambda_i|}$ shown in the Fig. (5.6) corresponds to two eigenvalues. Each pair of complex eigenvalues correspond to a natural eigenmode of the starting system.

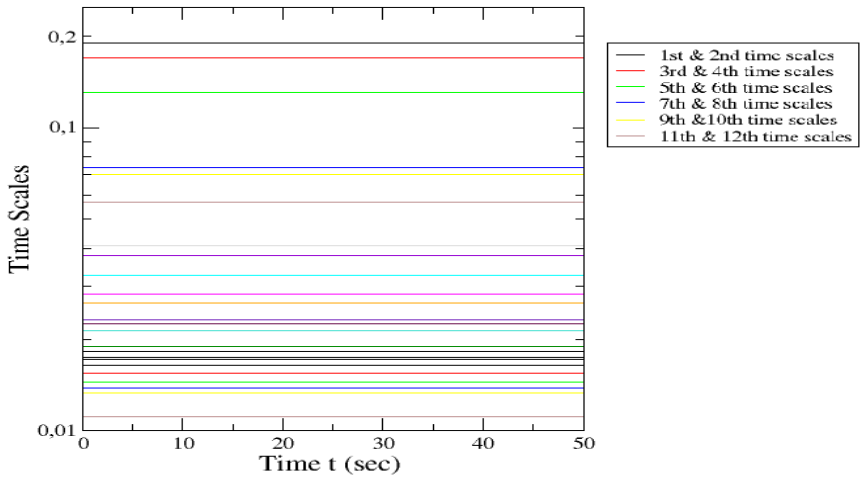


**Figure 5.6:** Time scales $\tau_i$ for $i = 1, 2, \ldots, 48$ over time

It is easy to observe from the Fig. (5.6) that the first 3-6 values are far greater than the other values. That values correspond to the first 3-6 natural eigenmodes. Because the eigenvalues are independent of the loading so the relation of the time scales that correspond to each pair of eigenvalues. The first 12 time scales are presented in the table (5.1). It is well known that the first 3-6 eigenmodes are mainly responsible for the building response under external loadings or excitations [8, 9, 19, 20].

**Table 5.1:** Eigenvalues, timescales and corresponding natural eigenmodes.

| Eigenvalues | Eigenvalues value $\lambda_i$ | Timescales | Timescales value $\tau_i$ | Natural eigenmodes |
|---|---|---|---|---|
| $1^{st}$ & $2^{nd}$ | $\lambda_1, \lambda_2 = -0.2618 \pm 5.2299i$ | $1^{st}$ & $2^{nd}$ | $\tau_1, \tau_2 = 0.1910$ | $1^{st}$ |
| $3^{rd}$ & $4^{th}$ | $\lambda_3, \lambda_4 = -0.2657 \pm 5.8923i$ | $3^{rd}$ & $4^{th}$ | $\tau_3, \tau_4 = 0.1694$ | $2^{nd}$ |
| $5^{th}$ & $6^{th}$ | $\lambda_5, \lambda_6 = -0.2781 \pm 7.6369i$ | $5^{th}$ & $6^{th}$ | $\tau_5, \tau_6 = 0.1309$ | $3^{rd}$ |
| $7^{th}$ & $8^{th}$ | $\lambda_7, \lambda_8 = -0.3431 \pm 13.479i$ | $7^{th}$ & $8^{th}$ | $\tau_7, \tau_8 = 0.0742$ | $4^{th}$ |
| $9^{th}$ & $10^{th}$ | $\lambda_9, \lambda_{10} = -0.3541 \pm 14.232i$ | $9^{th}$ & $10^{th}$ | $\tau_9, \tau_{10} = 0.0702$ | $5^{th}$ |
| $11^{th}$ & $12^{th}$ | $\lambda_{11}, \lambda_{12} = -0.4098 \pm 17.558i$ | $11^{th}$ & $12^{th}$ | $\tau_{11}, \tau_{12} = 0.0569$ | $6^{th}$ |
| $37^{th}$ & $38^{th}$ | $\lambda_{37}, \lambda_{38} = -2.2094 \pm 60.993i$ | $37^{th}$ & $38^{th}$ | $\tau_{37}, \tau_{38} = 0.0164$ | $19^{th}$ |
| $39^{th}$ & $40^{th}$ | $\lambda_{39}, \lambda_{40} = -2.4591 \pm 64.753i$ | $39^{th}$ & $40^{th}$ | $\tau_{39}, \tau_0 = 0.0154$ | $20^{th}$ |
| $41^{th}$ & $42^{th}$ | $\lambda_{41}, \lambda_{42} = -2.7662 \pm 69.096i$ | $41^{th}$ & $42^{th}$ | $\tau_{41}, \tau_{42} = 0.0147$ | $21^{th}$ |
| $43^{th}$ & $44^{th}$ | $\lambda_{43}, \lambda_{44} = -2.9995 \pm 72.222i$ | $43^{th}$ & $44^{th}$ | $\tau_{43}, \tau_{44} = 0.0138$ | $22^{th}$ |
| $45^{th}$ & $46^{th}$ | $\lambda_{45}, \lambda_{46} = -3.2102 \pm 74.936i$ | $45^{th}$ & $46^{th}$ | $\tau_{45}, \tau_{46} = 0.0133$ | $23^{th}$ |
| $47^{th}$ & $48^{th}$ | $\lambda_{47}, \lambda_{48} = -4.4849 \pm 89.582i$ | $47^{th}$ & $48^{th}$ | $\tau_{47}, \tau_{48} = 0.0115$ | $24^{th}$ |

As mentioned in chapter (2) when the trajectory evolves on the $(N - M)$-dimension *Slow Invariant Manifold* (*SIM*) the $M$ fast dissipative time scales $\tau_i$ $(i = 1, \ldots, M)$ are exhausted, so that the flow is characterized by the slow time scales $\tau_{M+1}, \ldots, \tau_N$. On the *SIM* the vector field $\mathbf{g}(\mathbf{y})$ has no component in the fast subspace; i.e., the amplitudes in Eq. (2.9) attain negligible values.

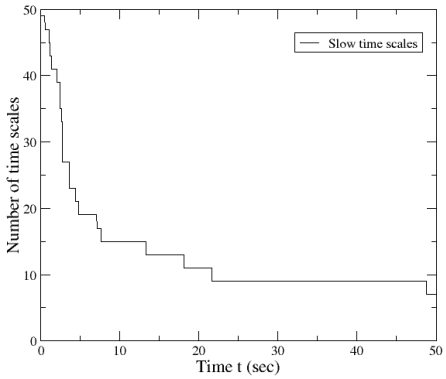


**Figure 5.7:** Number of slow time scales $N - M$ over time

The number of the slow time scales $N - M$ are shown in the Fig. (5.7). The system can be reduced to $N - M$ slow time scales and as it was mentioned before correspond to the first $\frac{N-M}{2}$ natural eigenmodes of the structure. It was shown in the Fig. (5.7) that the system is approaching the SIM quickly.

In the Fig. (5.7) it was shown that after $t \simeq 8sec$ there are 14,12,10,8,6 time scales. The eigenmodes that are stimulated are 7,6,5,4,3 respectively. The method manages to decrease the order of the system even further than other methods. In [16] the methods reduce the system to 12.

One more variable that can give important insight about the solution is the *CSP* amplitude $\mathbf{f}^s$ which is a projection of the vector field $\mathbf{g}(\mathbf{y})$ along the $N-M$ slow directions. The figure that shows the decrease of the principal slow time scales is shown in the Fig. (5.8). The rest CSP amplitudes are similar but they converge faster to zero. If a CSP amplitude $\mathbf{f}^s < \epsilon$ then is considered that this time scale becomes fast. It is known from Eq. (2.6) and Eq. (2.10) that the *CSP* amplitude $\mathbf{f}^s$ converge to zero as the system reaches equilibrium state.

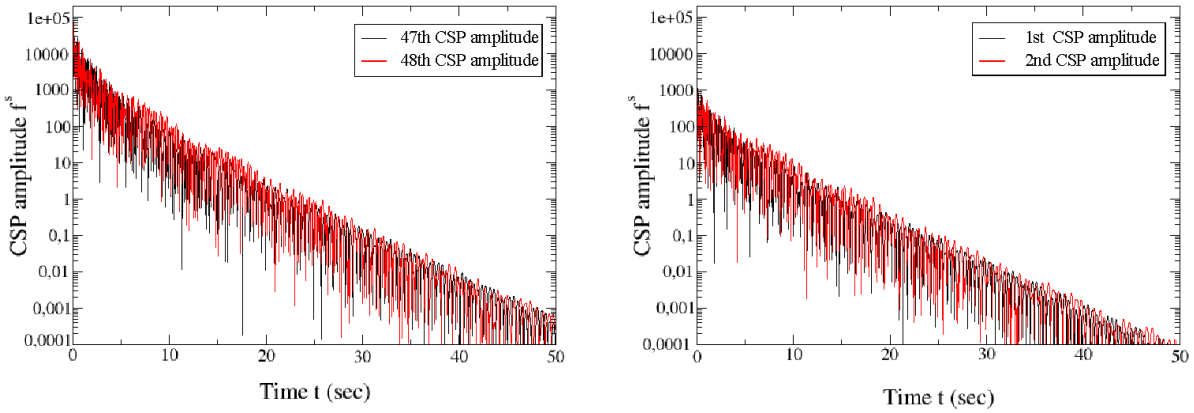


**(a)** **(b)**

**Figure 5.8:** The CSP amplitudes over time t: (a) the two slowest CSP amplitudes $\mathbf{f}^s$, (b) the two fastest CSP amplitudes $\mathbf{f}^r$

### 5.4.2 Static loading

The solution for the static loading problem is shown in the diagrams of $u_1(t)$ and $\dot{u}_1(t)$.

The Fig. (5.9) is showing the horizontal displacement $u_1(t)$ of the highest floor of the building. All the other horizontal movements are similar to this one but smaller in value. The building starts to move until it reaches its new equilibrium state. The oscillations of the system until reaching the new equillibrium state are similar to the Fig. (3.9) and are achieved after 10-15 periods. That shows that the assumption for the *effective damping level* $\zeta = 5\%$ is accurate.

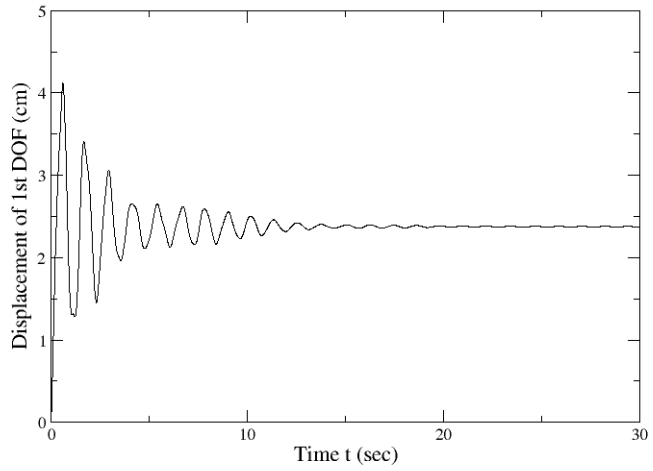


**Figure 5.9:** Displacement of the first DOF $u_1(t)$ over time

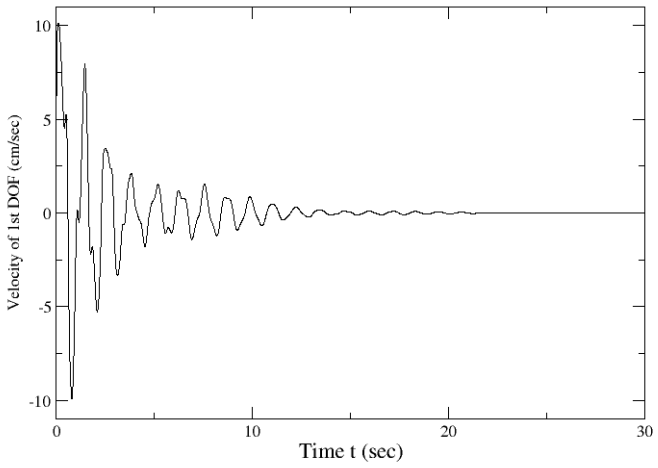


**Figure 5.10:** Velocity of the first DOF $\dot{u}_1(t)$ over time

Similar to the first case in section (5.4.1) the building starts to oscillate quickly and then the velocity decreases at a steady rate until reaching a new equilibrium state and the solution is shown in Fig. (5.10).

As mentioned in section (5.4.1) the eigenvalues of the matrix $A$ and the time scales are the same and independent of the loading case and are shown in table (5.1) and in Fig. (5.6).

In the Fig. (5.11) it was shown that after $t \simeq 4sec$ there are 8,6,4 time scales. The eigenmodes that are stimulated are 4,3,2 respectively. It was observed that the system reaches SIM slower in the case of free vibration by comparing the Figs. (5.7, 5.11).

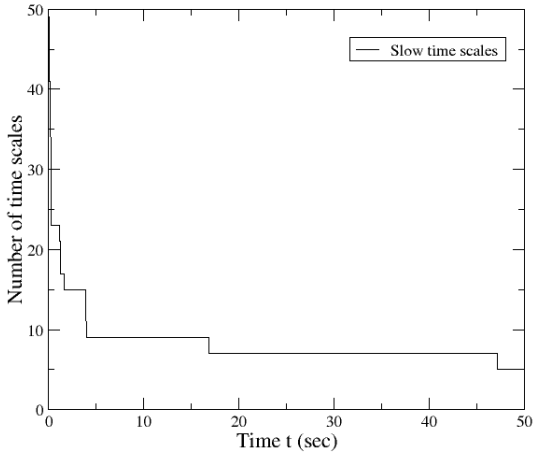


**Figure 5.11:** Number of slow time scales $N - M$ over time

In this case the *CSP* amplitudes $\mathbf{f}^s$ is shown in the Fig. (5.12). Similarly to the slow time scales the CSP amplitudes $\mathbf{f}^s$ have higher values for the case of free vibration.

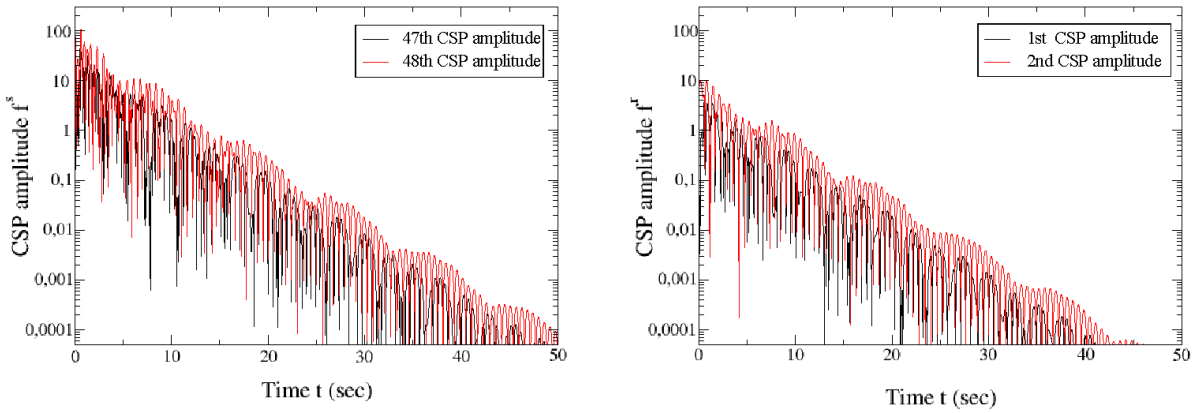


**(a)** **(b)**

**Figure 5.12:** The CSP amplitudes over time t: (a) the two slowest CSP amplitudes $\mathbf{f}^s$, (b) the two fastest CSP amplitudes $\mathbf{f}^r$

### 5.4.3 Equally distributed effective earthquake forces

The solution for the equally distributed effective earthquake forces problem which is described in section (5.3) is shown in the diagrams of $u_1(t)$ and $\dot{u}_1(t)$.

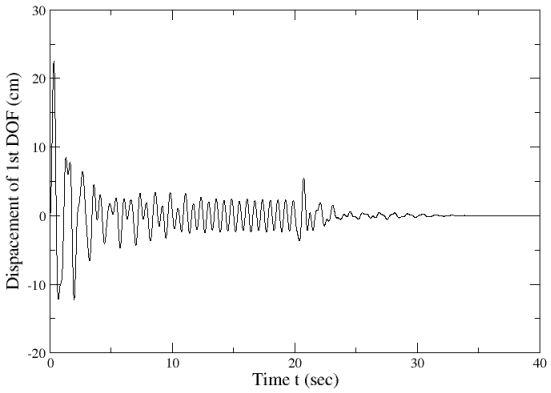


**Figure 5.13:** Displacement of the first DOF $u_1(t)$ over time

The Fig. (5.13) is showing the horizontal displacement $u_1(t)$ of the highest floor of the building. All the other horizontal movements are similar to this one but smaller in value. The building starts to oscillating according to earthquake excitation reaching a periodic state of movement and then after $t = 20s$ it steadily oscillates with reduced amplitude until reaching equillibrium state similar to the free vibration case. The oscillations of the system after $t = 20s$ until reaching the new equillibrium state are similar to the Fig. (3.9) and are achieved after 10-15 periods. That shows that the assumption for the *effective damping level* $\zeta = 5\%$ is accurate.

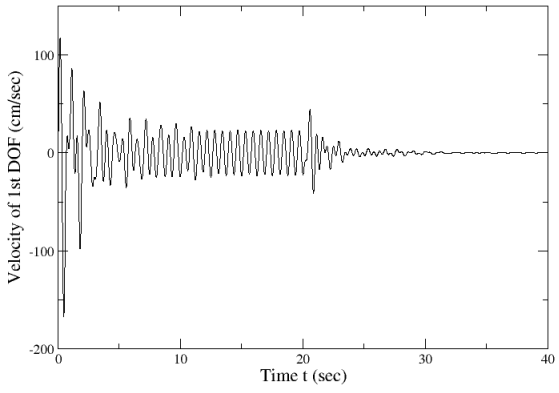


**Figure 5.14:** Velocity of the first DOF $\dot{u}_1(t)$ over time

Similar to the first case in section (5.4.1) the building starts to oscillate quickly and then the velocity decreases at a steady rate until reaching a new periodic state and then decreases even further until reaching the equilibrium state and the solution is shown in Fig. (5.14).

As mentioned in section (5.4.1) the eigenvalues of the matrix $A$ and the time scales are the same and independent of the loading case and are shown in table (5.1) and in Fig. (5.6).

In the Fig. (5.15) it was shown that after $t \simeq 4sec$ there are 10 time scales until $t = 20sec$. After the significant change in the loading the equilibrium state changes and some fast time scales can't be neglected for some iterations. Afterwards, the trajectory of the system is attracted to the new equilibrium state and after $t \simeq 24$ there are 8 time scales. The eigenmodes that are stimulated are 5 and 4 respectively.

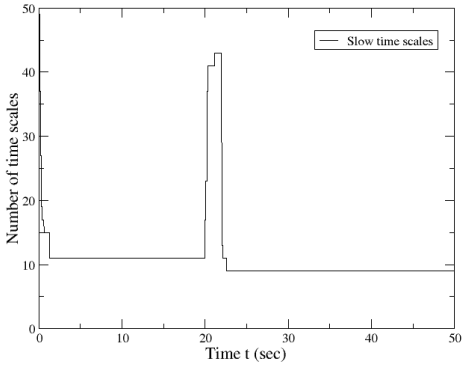


**Figure 5.15:** Number of slow time scales $N - M$ over time

In this case the *CSP* amplitudes $\mathbf{f}^s$ is shown in the Fig. (5.16). Similarly to the slow time scales the CSP amplitudes $\mathbf{f}^s$ have periodic behaviour when the system moves periodically and then they decreased similar to the free vibration case in Fig. (5.8).

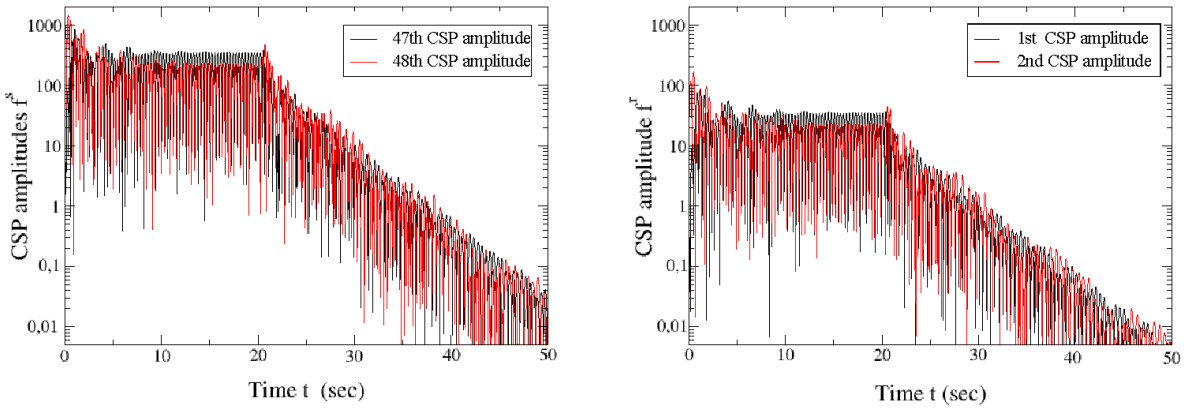


**(a)** **(b)**

**Figure 5.16:** The CSP amplitudes over time t: (a) the two slowest CSP amplitudes $\mathbf{f}^s$, (b) the two fastest CSP amplitudes $\mathbf{f}^r$

### 5.4.4 Triangular distributed effective earthquake forces

The solution for the triangular distributed effective earthquake forces problem which is described in section (5.3) is shown in the diagrams of $u_1(t)$ and $\dot{u}_1(t)$. It is shown that this case is more critical than the case in section (5.4.3). This is the reason why the construction codes use this approach. The logic behind this is that the assumptions about the modelling of the structure have to be made only when there are huge benefits. A more complex loading case doesn't affect the time of the calculations.

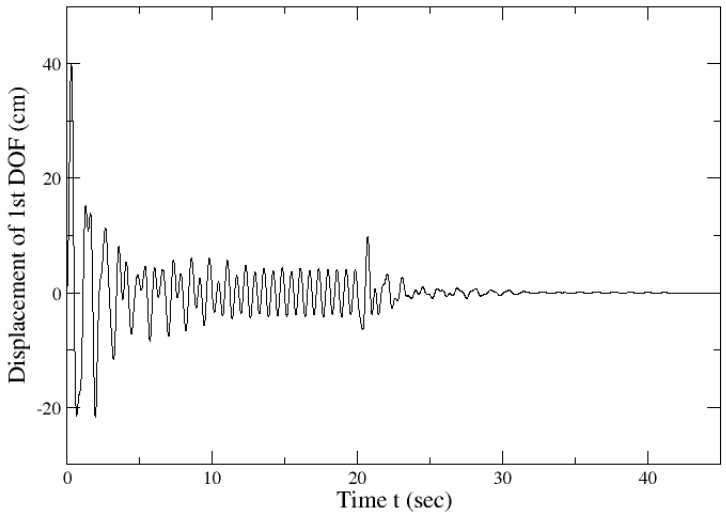


**Figure 5.17:** Displacement of the first DOF $u_1(t)$ over time

The Fig. (5.17) is showing the horizontal displacement $u_1(t)$ of the highest floor of the building. All the other horizontal movements are similar to this one but smaller in value. The building starts to oscillating according to earthquake excitation reaching a periodic state of movement and then after $t = 20s$ it steadily oscillates with reduced amplitude until reaching equillibrium state similar to the free vibration case. The oscillations of the system after $t = 20s$ until reaching the new equillibrium state are similar to the Fig. (3.9) and are achived after 10-15 periods. That shows that the assumption for the *effective damping level* $\zeta = 5\%$ is accurate. Also the result in this case is a little above acceptable limits on elastic buildings which is 3 cm per floor. In this case there are 8 floors and the safety threshold has been passed for a small time interval. It is worth mentioning that these are critical loading cases and the building has also plastic mechanisms in which it can absorb much more energy.

Similar to the first case in section (5.4.1) the building starts to oscillate quickly and then the velocity decreases at a steady rate until reaching a new periodic state and then decreases even further until reaching the equilibrium state and the solution is shown in Fig. (5.18).

As mentioned in section (5.4.1) the eigenvalues of the matrix $A$ and the time scales are the same and independent of the loading case and are shown in table (5.1) and in Fig. (5.6).

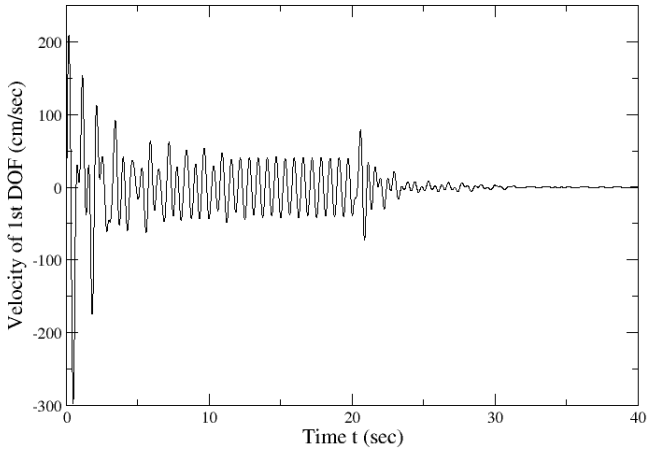


**Figure 5.18:** Velocity of the first DOF $\dot{u}_1(t)$ over time

In the Fig. (5.19) it was shown that after $t \simeq 3sec$ there are 10 time scales until $t = 20sec$. After the significant change in the loading the equilibrium state changes and some fast time scales can't be neglected for some iterations. Afterwards, the trajectory of the system is attracted to the new equilibrium state and after $t \simeq 23$ there are 8 time scales. The eigenmodes that are stimulated are 5 and 4 respectively.

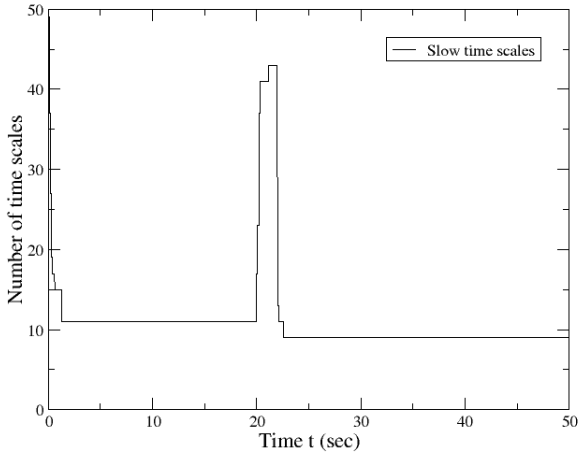


**Figure 5.19:** Number of slow time scales $N - M$ over time

In this case the CSP amplitudes $\mathbf{f}^s$ is shown in the Fig. (5.20). Similarly to the slow time scales the CSP amplitudes $\mathbf{f}^s$ have periodic behaviour when the system moves periodically and then they decreased similar to the free vibration case in Fig. (5.20).

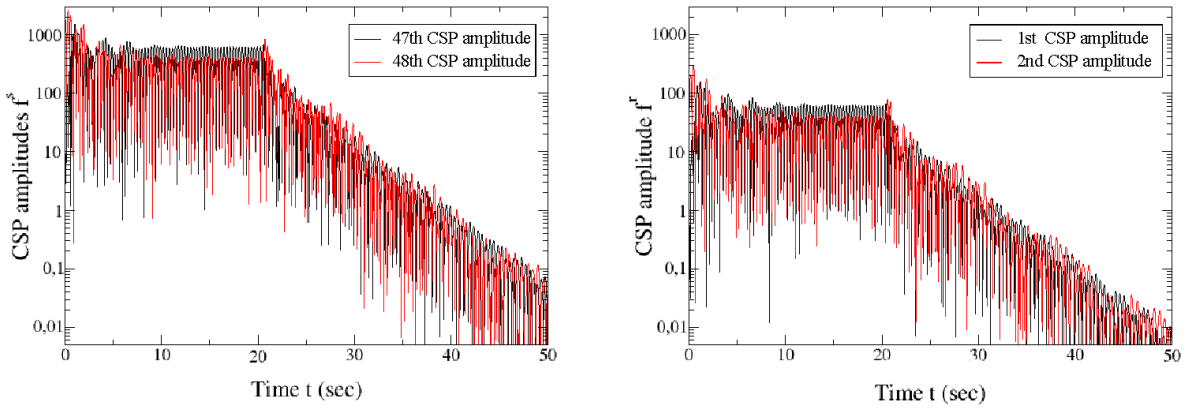


**(a)** **(b)**

**Figure 5.20:** The CSP amplitudes over time t: (a) the two slowest CSP amplitudes $\mathbf{f}^s$, (b) the two fastest CSP amplitudes $\mathbf{f}^r$

## 5.5 Comparison between CSP method and other model reduction methods

As it was shown in this chapter the CSP method can provide various tools and variables that gives the reader a better insight of the problem. Also, it was shown that the CSP method can decrease the order of the system much more than the other methods. In [16] there exist the results of the Balanced model reduction method, the rational Krylov method and the least squares based method.

All the methods in [16] result when analysing the building model of Los Angeles Hospital to a reduced system of order $r = 12$. The CSP method reduced the order of the system even further and the resulting $r = N - M = 8$ or 6 as shown in the Figs. (5.7, 5.11, 5.15, 5.19). In some cases shown in sections (5.4.3, 5.4.4), the method needs some more time to approach again the SIM after drastic changes in loadings.

The disadvantage is that the method has to solve once the system for the whole problem and then solve for some more iterations a system with higher order than r=12. This is the disadvantage comparing to other methods. It is worth mentioning that the error criteria mentioned in section 2.2 that are applied in the CSP algorithm for this dissertation use absolute error $\text{AbsErr}^i = 10^{-16}$ for all $i = 1, \ldots, N$. That is a serious threshold. If this threshold is relaxed then the system order can be reduced even further and faster but with less accuracy. The disadvantage though that can

be surpassed is that this method requires the solution of the starting system for the first iteration as shown in section (5.2).

The methods presented in the chapter (4) are compared with the CSP method. The advantages and disadvantages of each method are mentioned here using the informations presented in the chapters (2, 4, 5)

The Balanced reduction method has the following characteristics :

- High computational complexity due to the SVD factorization creates dense matrices and it requires calculations with those matrices
- Very accurate method
- Global and local error bounds
- The reduced order system is stable.

The rational Krylov method has the following characteristics :

- Low computational complexity
- Numerical reliable methods close to the interpolation points $\sigma$
- Require good selection of interpolation points $\sigma$ to have acceptable errors
- No local and globar error bounds

The least squares method has the following characteristics :

- Average computational complexity , by avoiding the explicit calculation of the matrices of the SVD factorization by using elements of the rational Krylov method
- Accurate method which uses global information from the system gramian and local information near the interpolation points $\sigma$
- Global and local error bounds but higher than the Balanced reduction method
- The reduced order system is minimal and computational stable

The Rayleigh-Ritz method has the following characteristics :

- The fastest model reduction method because it is based on the known fact that the buildings have 3-6 major eigenmodes that stimulate the system the most
- Can only be applied on building models without complex geometry
- Relied on the selection of the Ritz vector
- Higher error than the other methods
- Errors become unacceptable for buildings with strange and non symmetric geometry when the prediction of the shape of principal eigenmodes is not accurate

The CSP method has the following characteristics :

- Very fast method
- Gives great insight of the solution and the importance of different values because it has many tools to extract various important information.
- Could find a system with the optimal reduced order with respect to an desirable error bound
- Can identify the participation of different eigenmodes to the solution at each instant
- Very accurate method due to the error criteria that are set in each iteration and the most accurate for strict error bounds on the error criteria
- Requires the solution of the starting system at the first iteration
- Reduced system is non-stiff

By observing the following advantages and disadvantages it could be concluded that the CSP method is very fast and accurate at the same time and is computational reliable. Along with that it gives greater insight for the solution of the problem and the significance of the different variables and natural eigenmodes. Faster methods are the rational Krylov method and Rayleigh-Ritz method but they are not accurate and there don't have error bounds. The Balanced reduction method is very accurate but it has high computational complexity. The least squares method is a hybrid method that is both accurate, preserve stability and create a reduced model of order $r = 12$ with an average speed. This is comparable to the CSP method which is both accurate create reduced order models of order less than 12 for the most period of time but it requires the solution of the whole starting system in the first iteration.

# Chapter 6

# Conclusions

The building model of Los Angeles Hospital that is mentioned in [16] was considered here. The tools employed in this work to perform mode reduction were tools from *Computational Singular Perturbation (CSP)* analysis. The resulting reduced systems have smaller order than the systems that are produced with the methods in [16].

A description of how the building models are formed and solved is presented in chapter (3). The theory shows that for single degree of freedom (SDF) systems it is shown in sections (3.1, 3.2) that the solution has shape similar to a damped sinusoidal function. The same is true for every degree of freedom (DOF) for the multiple degree of freedom (MDF) system . The general picture that so far has emerged for the solution is as follows. The building starts to oscillate around the new equilibrium state. The amplitude of the oscillations is decreased according to the damping ratio $\zeta$ as shown in Figs. (5.4, 5.9, 5.13, 5.17). The velocity of each DOF of the system is decreased in the same manner and converge to zero as shown in the Figs. (5.5, 5.10, 5.14, 5.18). The diagrams of the displacements and the velocities have similar shape to the damped sinusoidal functions.

In order to get a better understanding of the building model of Los Angeles Hospital that is mentioned in [16], it was analysed further, on the basis of the multi-scale character of the model and for various external loadings and excitations as well. In [16] the model is reduced to a system of order $r = 12$. In this dissertation the order of the system was reduced even further as shown in Figs. (5.7, 5.11, 5.15, 5.19). The dynamics of the modified system were analysed in the present and it demonstrated that there are significant gaps among its time scales. This feature is validated with the use of the *algorithmic singular perturbation analysis* with the *CSP* method. Also it was observed that the *Slow Invariance Manifold* (SIM) can differ for different loadings and excitations that were applied in the structure. So extreme changes in loadings can differ the SIM such the trajectory of the solution will be further away and it will require some time to reach the new SIM as shown in Figs. (5.7, 5.11, 5.15, 5.19). During this phenomenon until the solution reaches the new SIM the number of slow time scales can get higher than before.

The building was analysed with the *CSP* algorithm for four different loading cases analysed in section (5.3) throughout the computational domain. At various points in time, the algorithm identified (i) the number of fast time scales, (ii) the eigenmodes that are stimulated by the building dynamical response, (iii) the contribution of each eigenmode to the vibration of the building, (v)

the eigenmodes that generate the exhausted fast time scales and (vi) the phenomena that drive the system to equilibrium.

It was shown that in the linear case building models the matrix $A$ in Eqs. (5.10, 5.11) is constant at each instant and obviously its eigenvalues and eigenvectors are constant at each instant. Because the eigenvalues are the same, the time scales are the same as shown in section (5.4).

It was observed and proved in chapter (5) the dissipative nature of all time scales since matrix $A$ correspond to a physical problem the solution can't go to infinity for every instant. In order that to be satisfied the eigenvalues have to complex and with a negative real part. That is also shown in Fig. (5.6) and Table (5.1).

It was found that the first 3-6 natural eigenmodes of the building are stimulated the most and dictate the trajectory of the solution. That is a generally true for most of the buildings and is mentioned in [8,10,19,20]. It was shown that each pair of complex eigenvalues (for each eigenvalue its conjugate is also an eigenvalue shown in section (5.4)) correspond to a natural eigenmode of the building. The SIM consisted of the time scales that correspond to the 3-6 principal eigenmodes of the structure. This is shown in Figs. (5.7, 5.11, 5.15, 5.19). The separation between fast and time scales is happened with the error criterion shown in section (2.2). All the results in this work are used error criteria with $\text{AbsErr}^i = 10^{-16}$ for all $i = 1, \ldots, N$. The number of fast time scales $M$ can be even bigger for a less strict selection of the **AbsErr**. But the number of fast time scales $M$ is optimal with respect the accuracy that was selected.

Studying the problem with multi time scale analysis it was found that the *Slow Invariance Manifold* can change dramatically due to extreme changes in loadings. The trajectory of solution that have been approaching the first SIM can be even further away from the new SIM and timescales and eigenmodes that are exhausted are stimulated again. But due to the dissipative nature of each time scale the trajectory of the solution is always attracted to the new SIM. That type of behaviour is shown if Figs. (5.7, 5.11, 5.15, 5.19).

Another tools of the CSP method that provides the crucial information about the solution is the *CSP amplitudes*. The *CSP amplitudes* $\mathbf{f}^r$ and $\mathbf{f}^s$ are the projections of the vector field $\mathbf{g}(\mathbf{y})$ along the $M$ fast and $N - M$ slow directions as mentioned in chapter (2). When the trajectory evolves on the $(N - M)$-dimension *Slow Invariant Manifold* (*SIM*) the $M$ fast dissipative time scales $\tau_i$ $(i = 1, \ldots, M)$ are exhausted, so that the flow is characterized by the slow time scales. For the systems that describe the dynamical response of the structures it was proved in section (5.4) that all the time scales are dissipative and they get exhausted over time. It was shown in Figs.(5.8, 5.12, 5.16, 5.20) the $\mathbf{f}^s$ are exhausted after some time. When the $\mathbf{f}^s$ is exhausted the slow time scale that corresponds to it, it becomes fast time scale. The system is reduced to 3-6 slow time scales due to the absolute error $\text{AbsErr}^i = 10^{-16}$ for all $i = 1, \ldots, N$ that was mentioned before.

Through searching the bibliography it was found a basic categorization of model reduction methods in [3, 4, 16]. The CSP method is belonging to another category of methods that are based in *asymptotic perturbation analysis* [11, 28, 45]. One more category that is found is the ones that are based in modal analysis of buildings and can only be applied on building equations. For each category a characteristic method is presented in chapter (4). The methods that are presented are the Balanced reduction method, rational Krylov method, least squares method, CSP method and Rayleigh-Ritz method that correspond to the categories SVD gramians based methods,

Krylov moment matching methods, SVD gramians - Krylov moment matching methods, asymptotic perturbation analysis methods and modal analysis methods respectively.

**Table 6.1:** Categories of models reduction methods, a method of each category and the advantages and disadvantages of these methods.

| Model reduction methods | | | |
|---|---|---|---|
| Categories | Methods | Advantages | Disadvantages |
| SVD gramians based methods | Balanced model reduction | • Very accurate method<br>• Global and local error bounds<br>• Reduced system is computationally stable | • High computational complexity<br>• High memory requirements |
| Krylov moment matching based methods | Rational Krylov method | • Low computational complexity | • Numerical reliable only close to the interpolation points $\sigma$<br>• Require good selection of interpolation points $\sigma$ to have acceptable errors<br>• No local and global error bounds |
| SVD gramians - Krylov moment matching based methods | Least squares method | • Accurate method which uses both global and local information<br>• The reduced order system is minimal and computational stable | • Average computational complexity<br>• Global and local error bounds but higher than the balanced reduction method |
| Modal analysis based methods | Rayleigh-Ritz method | • Lowest computational complexity | • Can only be applied on building models<br>• Relied on the selection of the Ritz vector<br>• Higher error than the other methods<br>• Errors are unacceptable for buildings with complex geometry |
| Asymptotic perturbation analysis based methods | CSP method | • Low computational complexity<br>• Provide great insight of the solution<br>• Could find a system with the optimal reduced order with respect to a desirable error bound<br>• Can identify the participation of different eigenmodes to the solution at each instant<br>• Very accurate method | • Requires the solution of the starting system at the first iteration |

In the table (6.1) there is a summary of the advantages and disadvantages of each method as shown in section (5.5). The CSP method gives the solution both fast and accurate. Studying the table (6.1), it is obviously that the CSP method has the best balance between accuracy and computational complexity. Furthermore, it provides various tools that give important information about the solution and the participation of different phenomena to the final solution of the system.

The building models have been studied extensively in [7–10, 19, 20]. Model reduction methods applied on buildings can be found in [3, 16, 37]. Model reduction in this work is achieved by applying CSP method. The multi scale analysis of the eigenmodes of the structure, could provide

the required insights on the significance of each behaviour and loading case to the solution of the system.

As a summary, it can be mentioned that this dissertation contains a bibliographic research of the model reduction methods that can be applied in a structure, the detailed application of the CSP method to simulate the damping response of a structure under various loadings and excitations with a reduced system. Further analysis of the dynamical problem with the CSP tools provide a deeper physical understanding about the damping oscillations in multi-storey structures.

# Bibliography


[1] S. Adhikari. *Damping models for structural vibration*. PhD thesis, University of Cambridge, 2001.

[2] R. C. Aiken. *Stiff computation*. Oxford University Press New York, Oxford, 1985.

[3] A. C. Antoulas. *Approximation of large-scale dynamical systems*, volume 6. Siam, 2005.

[4] A. C. Antoulas, D. C. Sorensen, and S. Gugercin. A survey of model reduction methods for large-scale systems. *Contemporary mathematics*, 280:193–220, 2001.

[5] E. Ashari. Calculating free and forced vibrations of multi-story shear buildings by modular method. *Research Journal of Recent Sciences*, 3(1):83–90, 2014.

[6] P. Benner, V. Mehrmann, and D. C. Sorensen. *Dimension reduction of large-scale systems*, volume 45. Springer, 2005.

[7] M. L. Bucalem and K.-J. Bathe. *The mechanics of solids and structures-hierarchical modeling and the finite element solution*. Springer Science & Business Media, 2011.

[8] A. K. Chopra et al. *Dynamics of structures*, volume 3. Prentice Hall New Jersey, 1995.

[9] A. Filiatrault. *Elements of earthquake engineering and structural dynamics*. Presses inter Polytechnique, 2013.

[10] A. Ghali, A. Neville, and T. G. Brown. *Structural analysis: a unified classical and matrix approach*. Crc Press, 2003.

[11] D. Goussis and S. Lam. A study of homogeneous methanol oxidation kinetics using csp. In *Symposium (International) on Combustion*, volume 24, pages 113–120. Elsevier, 1992.

[12] D. Goussis and G. Skevis. Nitrogen chemistry controlling steps in methane-air premixed flames. *Computational fluid and solid mechanics*, 1:650–653, 2005.

[13] D. A. Goussis. The role of slow system dynamics in predicting the degeneracy of slow invariant manifolds: the case of vdp relaxation–oscillations. *Physica D: Nonlinear Phenomena*, 248:16–32, 2013.

[14] D. A. Goussis and M. Valorani. An efficient iterative algorithm for the approximation of the fast and slow dynamics of stiff systems. *Journal of Computational Physics*, 214(1):316–346, 2006.

[15] S. Gugercin. An iterative svd-krylov based method for model reduction of large-scale dynamical systems. In *Proceedings of the 44th IEEE Conference on Decision and Control*, pages 5905–5910. IEEE, 2005.

[16] S. Gugercin and A. C. Antoulas. Model reduction of large-scale systems by least squares. *Linear algebra and its applications*, 415(2):290–321, 2006.

[17] M. W. Hirsch, S. Smale, and R. L. Devaney. *Differential equations, dynamical systems, and an introduction to chaos*. Academic press, 2012.

[18] R. A. Horn and C. R. Johnson. *Matrix analysis*. Cambridge university press, 2012.

[19] A. Kappos. *Dynamic loading and design of structures*. CRC Press, 2001.

[20] A. Kappos and G. Penelis. *Earthquake resistant concrete structures*. CRC Press, 2010.

[21] J. Kevorkian and J. D. Cole. *Multiple scale and singular perturbation methods*, volume 114. Springer Science & Business Media, 2012.

[22] J. Kevorkian and J. D. Cole. *Perturbation methods in applied mathematics*, volume 34. Springer Science & Business Media, 2013.

[23] P. D. Kourdis and D. A. Goussis. Glycolysis in saccharomyces cerevisiae: algorithmic exploration of robustness and origin of oscillations. *Mathematical biosciences*, 243(2):190–214, 2013.

[24] P. D. Kourdis, R. Steuer, and D. A. Goussis. Physical understanding of complex multiscale biochemical models via algorithmic simplification: Glycolysis in saccharomyces cerevisiae. *Physica D: Nonlinear Phenomena*, 239(18):1798–1817, 2010.

[25] S. Lam. Using csp to understand complex chemical kinetics. *Combustion Science and Technology*, 89(5-6):375–404, 1993.

[26] S. Lam and D. Coussis. Conventional asymptotics and computational singular perturbation for simplified kinetics modelling. In *Reduced kinetic mechanisms and asymptotic approximations for methane-air flames*, pages 227–242. Springer, 1991.

[27] S. Lam and D. Goussis. Understanding complex chemical kinetics with computational singular perturbation. In *Symposium (International) on Combustion*, volume 22, pages 931–941. Elsevier, 1989.

[28] S. Lam and D. Goussis. The csp method for simplifying kinetics. *International Journal of Chemical Kinetics*, 26(4):461–486, 1994.

[29] Z. Liang, G. C. Lee, G. F. Dargush, and J. Song. *Structural damping: applications in seismic response modification*, volume 3. CRC press, 2011.

[30] L. D. Lutes and S. Sarkani. *Random vibrations: analysis of structural and mechanical systems.* Butterworth-Heinemann, 2004.

[31] R. Marchand and T. J. McDevitt. Learning differential equations by exploring earthquake induced structural vibrations: A case study. *International Journal of Engineering Education*, 15(6):477–485, 1999.

[32] D. Maris. Asymptotic analysis of a Wnt$\beta$-catenin pathway model, 2014.

[33] J. Mohammadpour and K. M. Grigoriadis. *Efficient modeling and control of large-scale systems.* Springer Science & Business Media, 2010.

[34] A. H. Nayfeh. *Perturbation methods.* John Wiley & Sons, 2008.

[35] M. Paz. *Structural dynamics: theory and computation.* Springer Science & Business Media, 2012.

[36] T. Penzl. Algorithms for model reduction of large dynamical systems. *Linear Algebra and its Applications*, 415(2):322–343, 2006.

[37] Z.-Q. Qu. *Model order reduction techniques with applications in finite element analysis.* Springer Science & Business Media, 2013.

[38] Y. Saad. *Iterative methods for sparse linear systems.* Siam, 2003.

[39] Y. Saad. *Numerical Methods for Large Eigenvalue Problems: Revised Edition*, volume 66. Siam, 2011.

[40] M. Valorani, F. Creta, D. A. Goussis, J. C. Lee, and H. N. Najm. An automatic procedure for the simplification of chemical kinetic mechanisms based on csp. *Combustion and Flame*, 146(1):29–51, 2006.

[41] M. Valorani, D. A. Goussis, F. Creta, and H. N. Najm. Higher order corrections in the approximation of low-dimensional manifolds and the construction of simplified problems with the csp method. *Journal of Computational Physics*, 209(2):754–786, 2005.

[42] M. Valorani, H. N. Najm, and D. A. Goussis. Csp analysis of a transient flame-vortex interaction: time scales and manifolds. *Combustion and Flame*, 134(1):35–53, 2003.

[43] P. Van Dooren and B. Wyman. Linear algebra for control theory, volume 62 of the ima volumes in mathematics and its applications, 1994.

[44] F. Verhulst. *Methods and applications of singular perturbations: boundary layers and multiple timescale dynamics*, volume 50. Springer Science & Business Media, 2005.

[45] F. Verhulst. Periodic solutions and slow manifolds. *International Journal of Bifurcation and Chaos*, 17(08):2533–2540, 2007.

[46] D. C. Wilcox. *Perturbation methods in the computer age*. DCW Industries, 1995.

[47] A. Zagaris, H. G. Kaper, and T. J. Kaper. Analysis of the computational singular perturbation reduction method for chemical kinetics. *Journal of Nonlinear Science*, 14(1):59–91, 2004.

[48] A. Zingoni. *Vibration Analysis and Structural Dynamics for Civil Engineers: Essentials and Group-Theoretic Formulations*. CRC Press, 2014.